Drone-based spectral and 3D remote sensing applications for forestry and agriculture

BY Roope Näsi

NLS
FINNISH GEOSPATIAL RESEARCH INSTITUTE FGI

Drone-based spectral and 3D remote sensing applications for forestry and agriculture

Roope Näsi

A doctoral dissertation completed for the degree of Doctor of Science (Technology) to be defended, with the permission of the Aalto University School of Engineering, at a public examination held at the lecture hall M1 of the school on 14 December 2021 at 12.00.

Aalto University
School of Engineering
Department of Built Environment

Finnish Geospatial Research Institute
Department of Photogrammetry and Remote Sensing

Supervising professor
Prof. Miina Rautiainen, Aalto University, Finland

Thesis advisors
Prof. Eija Honkavaara, Finnish Geospatial Research Institute FGI
Prof. Juha Hyyppä, Finnish Geospatial Research Institute FG

Preliminary examiners
Dr. Jochem Verrelst, University of Valencia, Spain
Prof. Uwe Rascher, Forschungszentrum Jülich, Germany

Opponent
Dr. Zbynek Malenovski, University of Tasmania, Australia

NORDIC SWAN ECOLABEL

Printed matter
4041-0619

Author
Roope Näsi

Name of the doctoral dissertation
Drone-based spectral and 3D remote sensing applications for forestry and agriculture

Publisher School of Engineering

Unit Department of Built Environment

Series Aalto University publication series DOCTORAL DISSERTATIONS 168/2021

Field of research Geoinformatics

Manuscript submitted 4 November 2021	**Date of the defence** 14 December 2021

Permission for public defence granted (date) 10 November 2021	**Language** English

☐ **Monograph**	☒ **Article dissertation**	☐ **Essay dissertation**

Abstract

Practising sustainable agriculture and forestry requires information on the state of forests and crops to support management. In precision agriculture, crops are observed in order to treat them precisely in the right place and at the right time, saving both production costs and the environment. Similarly, in forests, information on the composition and state of forest health are crucial to enable their sustainable management. In particular, climate-change-driven insect pests have increased, but economic and ecological losses can be reduced by the right actions if up-to-date and precise information on the health of forests is available.

In recent years, drones with cameras have evolved into a flexible way to collect remote sensing data locally. Spectral cameras provide accurate information about the reflection properties of objects, and photogrammetric methods also provide a cost-effective way to collect three-dimensional (3D) data from an object. The objective of this work was to develop and assess drone-based 3D and spectral remote sensing techniques to classify the health status of individual trees and to estimate crop biomass, various biochemical parameters such as nitrogen content, and grass-feeding quality. The work developed a processing chain in which spectral and 3D features were extracted from remote sensing data. Then, combining the features with observations and reference measurements collected from plants, machine learning models were developed for tree health classification and estimation of crop-related parameters.

The effects of different factors related to data collection and processing on classification and estimation accuracies were studied in order to generate knowledge on optimal sensors and methods. In general, radiometric corrections, spectral resolution, and the combined use of spectral and 3D features improved classification and estimation accuracies. However, the optimal sensors as well as the data collection and processing methods depend on the different applications and their accuracy requirements. This work was the first to demonstrate the ability of drone hyperspectral data to map the health status of a forest by classifying individual trees infested by bark beetles. The results of the work also showed that drone-based mapping offers a great tool to estimate agricultural crop parameters which can be applied to the optimization of various precision agriculture tasks.

Tiivistelmä

Kestävän maa- ja metsätalouden harjoittaminen vaatii tietoa metsien ja viljelykasvien tilasta päätöksenteon tueksi. Täsmämaataloudessa viljelykasveja havainnoidaan, jotta viljelytoimenpiteet voidaan kohdistaa oikeaan paikkaan ja oikea-aikaisesti säästäen sekä tuotantokustannuksia että ympäristöä. Metsissä tieto metsien terveydentilasta on tärkeää, jotta voidaan hillitä metsätuhojen leviämistä. Erityisesti hyönteistuhot ovat lisääntyneet voimakkaasti ilmastonmuutoksen vauhdittamana, mutta taloudellisia ja ekologisia tappiota voidaan vähentää oikeilla toimenpiteillä, jos on olemassa ajantasaisesta tietoa metsien terveydentilasta.

Dronet ja niihin asennettavat kamerat ovat kehittyneet viime vuosina joustavaksi tavaksi kerätä kaukokartoitusaineistoa paikallisesti. Spektrikameroilla saadaan tarkkaa tietoa kohteen heijastusominaisuuksista, ja fotogrammetriset menetelmät mahdollistavat myös kustannustehokkaan tavan kerätä kohteesta kolmiulotteista (3D) tietoa. Tämän työn tavoitteena oli kehittää näihin aineistoihin nojautuen kaukokartoitusmenetelmiä yksittäisten puiden terveydentilan luokitteluun sekä viljelykasvien biomassan, erilaisten biokemiallisten parametrien, kuten typpipitoisuuden sekä nurmen ruokintalaadun, kuten D-arvon estimointiin. Työssä kehitettiin prosessointiketju, jossa kaukokartoitusaineistoista irrotettiin spektri- ja 3D-piirteitä, yhdistettiin ne kasveista kerättyihin havaintoihin ja mittauksiin sekä muodostettiin koneoppimismalleja puiden luokittelua ja viljelykasveihin liittyvien parametrien estimointia varten.

Työssä verrattiin useiden aineistonkeräykseen ja -prosessointiin liittyvien tekijöiden vaikutuksia luokittelu- ja estimointitulosten tarkkuuteen optimaalisten menetelmien löytämiseksi. Esimerkiksi spektri- ja 3D-piirteiden hyödyntäminen yhdessä sekä radiometriset korjaukset paransivat yleisesti luokittelu- ja estimointitarkkuuksia. Optimaaliset sensorit sekä aineistonkeräys- ja käsittelytavat riippuvat kuitenkin eri sovelluksista ja niiden tarkkuusvaatimuksista. Työssä osoitettiin ensimmäistä kertaa dronesta kerätyn hyperspektrisen aineiston kyvykkyys metsän terveydentilan havainnoinnissa luokittelemalla kuuset kolmeen luokkaan kirjanpainajan aiheuttaman tuhon perusteella. Työn tulokset myös osoittivat drone-pohjaisen kartoituksen kyvyn estimoida erilaisia viljelykasvien parametreja, joita voidaan edelleen soveltaa suunniteltaessa esimerkiksi lisälannoitusta tai säilörehun optimaalista korjuuaikaa.

Acknowledgements

The first steps towards this thesis were taken in 2014, when I had the chance to take my master advised by Prof. Eija Honkavaara at FGI, which was known as a Finnish Geodetic Institute. After completing my master, Eija offered me a work contract to continue as a researcher in her spectrophotogrammetry research group in the department of Photogrammetry and Remote Sensing at FGI. This has been renamed to Finnish Geospatial Research Institute FGI in 2015, after merging with National Land Survey of Finland. I would like to thank Prof. Henrik Haggren, whose introductory lectures on Photogrammetry and Remote Sensing, in the beginning of my studies in Aalto University, inspired me about the elegance of this field and who suggested that Prof. Miina Rautiainen could be my supervising professor in Aalto. In 2015 Autumn, I decided to apply for doctoral studies and Miina was happy to take me under her supervision. She has always helped and responded me fast about all my doctoral studies questions. I was also honoured to organize a special course about drone mapping in Aalto by Miina's idea. I am very grateful to Miina's support and valuable comments about the structure and suggestions to finalize this thesis. I want to thank also my advisor, Prof. Juha Hyyppä, for comments and ideas to finalize the thesis. Juha was also the person who answered my email about possible master thesis ideas and organized a meeting which led me to working with Eija and her group. I also want to thank Juha as the Head of the department and Prof. Jarkko Koskinen as the General Director of FGI for their efforts to create well-established research infrastructure. I would like the thank FGI, National Land Survey of Finland, Aalto University and School of Engineering as organizations to make this thesis possible.

All research and publications of this thesis have been carried out under Prof. Eija Honkavaara's supervision in FGI. I want to give my greatest thanks to her for everything she has done for my doctoral studies. I have been impressed on how dedicated to her work as a scientist and group leader she is. She has never given up and has been able to create a great research group, currently known as "Photogrammetry and Hyperspectral Imaging". Indeed, I want also to thank all previous and current team members for their support and helpful attitude. Namely, Niko, with whom I have shared the same table in Masala office since

I have also had a chance to get international contacts during my work at the FGI. In addition to conference trips, visits to São Paulo State University have been eye-opening experiences. I would like to thank Eija and Juha for these opportunities and especially Dr. Antonio Tommaselli and Dr. Nilton Imai for the friendly hospitality. I could never imagine how intensely these contacts could influence my life.

I never forget my roots in Alahärmä. Childhood and youth in the countryside offered the best possible foundation to my life. The primary school and the upper secondary school (Härmän lukio) provided me with an excellent base to continue studies at Aalto university, and I am grateful for all my teachers. As a son of a farmer, I could participate in farm work since my childhood. Still, it is important to me to take part of sowing, seeding, and planting in every spring. Forest is also special to me, not least because of my orienteering hobby. Besides, considering my passion for maps, I can tell that I have been lucky with the topic of my thesis, since it combines many important things to me.

Finally, I would like to thank my friends and family. I have been sharing similar interests with Eero since our childhood, which has made us to be lifelong friends. Lately, I have been spending my free time especially with Aimad, Karla, Mariana, Fabricio, Luiz and Ziyi. Thanks for all nice dinners and social evenings. I do not have enough words to thank my parents Ritva and Raimo for what they have done for me. Together with my siblings Riikka and Raine, they have provided me always with a safe and warm family to be a part of. Kiitos. Thanks also to many relatives who have encouraged me in my studies and in my life in general. To Raquel, my dear wife: thank you for everything. Muito obrigado por tudo.

Alahärmä, November 2021

Contents

List of Abbreviations

ALS	Airborne Laser Scanning
BVLOS	Beyond-Visual-Line-Of-Sight
BBA	Bundle Block Adjustment
BRDF	Bidirectional Reflection Distribution Function
CHM	Canopy Height Model
CNN	Convolutional Neural Network
DM	Dry Matter
DMY	Dry Matter Yield
DN	Digital Number
DSM	Digital Surface Model
DTM	Digital Terrain Model
EBV	Essential Biodiversity Variable
EOP	Exterior Orientation Parameters
ESC	Electronic Speed Controls
FCU	Flight Controller Unit
FGI	Finnish Geospatial Research Institute
FPI	Fabry-Pérot Interferometer
FWHM	Full Width at Half Maximum
FY	Fresh Dield
GCP	Ground Control Point
GNSS	Global Navigation Satellite Systems
GSD	Ground Sampling Distance
HDRF	Hemispherical Directional Reflectance Factor
IMU	Inertial Measurement Unit

iNDF	Indigestible Neutral Detergent Fibre
IOP	Interior Orientation Parameters
k-NN	k-Nearest Neighbours algorithm
LAI	Leaf area index (LAI)
LiDAR	Light Detection and Ranging
LiPo	Lithium Polymer
LOOCV	Leave-one-out Cross-Validation
ME	Metabolized Energy
MLR	Multilinear Regression
MSI	MultiSpectral Imager
Ncont	Nitrogen concentration
NDF	Neutral Detergent Fibre
NDVI	Normalized Difference Vegetation Index
NIR	Near InfraRed
NIRS	Near-Infrared Reflectance Spectroscopy
NU	Nitrogen Uptake
PCC	Pearson Correlation Coefficient
PLSR	Partial Least Squares Regression
RF	Random Forest algorithm
RGB	Red, Green, Blue bands
RMSE	Root Mean Square Error
RMSE%	Normalized Root Mean Square Error
SLR	Simple Linear Regression
RPAS	Remotely Piloted Aerial Systems
SAR	Synthetic Aperture Radar
SfM	Structure from Motion
SVM	Support Vector Machines
SWIR	Short-wavelength InfraRed
UAS	Unmanned Aerial System
UAV	Unmanned Aerial Vehicle
VNIR	Visible Near InfraRed

WSC   Water Soluble Carbohydrates

List of Publications

This thesis is based on the following research articles, which are referred to in the text by their Roman numerals. Articles are reprinted with the permission of the publishers.

I Näsi, R., Honkavaara, E., Lyytikäinen-Saarenmaa, P., Blomqvist, M., Litkey, P., Hakala, T., Viljanen, N., Kantola, T., Tanhuanpää, T. & Holopainen, M. (2015). Using UAV-based photogrammetry and hyperspectral imaging for mapping bark beetle damage at tree-level. Remote Sensing, 7(11), 15467-15493.

II Näsi, R., Honkavaara, E., Blomqvist, M., Lyytikäinen-Saarenmaa, P., Hakala, T., Viljanen, N., Kantola, T. & Holopainen, M. (2018). Remote sensing of bark beetle damage in urban forests at individual tree level using a novel hyperspectral camera from UAV and aircraft. Urban Forestry & Urban Greening, 30, 72-83.

III Näsi, R., Viljanen, N., Kaivosoja, J., Alhonoja, K., Hakala, T., Markelin, L., & Honkavaara, E. (2018). Estimating biomass and nitrogen amount of barley and grass using UAV and aircraft based spectral and photogrammetric 3D features. Remote Sensing, 10(7), 1082.

IV Oliveira, R. A., Näsi, R., Niemeläinen, O., Nyholm, L., Alhonoja, K., Kaivosoja, J., Jauhiainen, L., Viljanen, N., Nezami, S., Markelin, L., Hakala, T & Honkavaara, E. (2020). Machine learning estimators for the quantity and quality of grass swards used for silage production using drone-based imaging spectrometry and photogrammetry. Remote Sensing of Environment, 246, 111830.

V Tuominen, S., Näsi, R., Honkavaara, E., Balazs, A., Hakala, T., Viljanen, N., Pölönen, I., Saari, H. & Ojanen, H. (2018). Assessment of classifiers and remote sensing features of hyperspectral imagery and stereo-photogrammetric point clouds for recognition of tree species in a forest area of high species diversity. Remote Sensing, 10(5), 714.

Author's Contribution

Publication I: Using UAV-based photogrammetry and hyperspectral imaging for mapping bark beetle damage at tree-level

Näsi processed radiometric datasets, developed classification methods and analysed the results. Lyytikäinen-Saarenmaa, Blomqvist and Kantola provided ground truth concerning the forest measurements. Hakala conducted the drone data capture. Viljanen carried out the photogrammetric processing. Litkey developed the analysis method of DSMs. Tanhuanpää delineated the tree crowns from the point clouds. Näsi, Honkavaara and Lyytikäinen-Saarenmaa wrote the first draft of the manuscript, and all others assisted in writing and revising. Honkavaara supervised the photogrammetric and remote sensing development and analysis and arranged required resources.

Publication II: Remote sensing of bark beetle damage in urban forests at individual tree level using a novel hyperspectral camera from UAV and aircraft

Näsi processed radiometric datasets, carried out the photogrammetric processing of aircraft data, developed an image-based method to identify individual trees, developed classification methods and analysed the results. Lyytikäinen-Saarenmaa, Blomqvist and Kantola provided ground truth concerning the forest measurements. Hakala conducted the drone data capture. Viljanen carried out the photogrammetric processing of drone-based datasets. Näsi, Honkavaara and Blomqvist wrote the first draft of the manuscript, and all others assisted in writing and revising. Honkavaara supervised the photogrammetric and remote sensing development and analysis and arranged required resources.

Publication III: Estimating biomass and nitrogen amount of barley and grass using UAV and aircraft based spectral and photogrammetric 3D features

Näsi contributed to the remote sensing data collection, processed drone-based radiometric datasets, developed estimation methods and analysed the results. Kaivosoja and Alhonoja provided the agricultural ground truth. Hakala built the drone system and contributed to drone data collection. Viljanen carried out all geometric processing steps and the analyses of them and contributed to drone data collection. Markelin processed radiometric datasets collected by aircraft. Näsi had a leading role in writing

the paper. Honkavaara and Viljanen participated in writing the paper with the assistance of all other authors. Honkavaara supervised the study and contributed to analysing the results. Honkavaara and Kaivosoja arranged all the required resources and designed the experiments.

Publication IV: Machine learning estimators for the quantity and quality of grass swards used for silage production using drone-based imaging spectrometry and photogrammetry

Näsi contributed to remote sensing data collection, developed estimation methods, and participated in data analysis and writing. Oliveira contributed to geometric and radiometric data processing, analysing the results and writing. Niemeläinen, Nyholm, Kaivosoja, Alhonoja and Jauhiainen provided the agricultural ground truth. Viljanen contributed to geometric processing and remote sensing data collection. Hakala built the drone system and contributed to remote sensing data collection. Nezami and Markelin contributed to radiometric processing. Oliveira, Näsi, Niemeläinen and Honkavaara wrote the manuscript with the assistance of all other authors. The experiments were planned by Honkavaara, Niemeläinen and Kaivosoja. Honkavaara and Kaivosoja acquired the funding.

Publication V: Assessment of classifiers and remote sensing features of hyperspectral imagery and stereo-photogrammetric point clouds for recognition of tree species in a forest area of high species diversity

Näsi contributed to remote sensing and ground truth data collection and geometric processing of spectral cameras, and performed radiometric processing and preliminary analysis of individual tree spectra. Tuominen provided the ground truth considering the tree species and genus. Saari and Ojanen corresponded about the sensor development and calibration. Hakala built the drone system and conducted the data capture. Viljanen contributed to remote sensing data collection and geometric processing. Balazs and Tuominen extracted the remote sensing features and performed the classification experiments. Tuominen, Näsi and Honkavaara wrote the manuscript with the assistance of other authors. The experimental layout was designed by Tuominen, Pölönen, Honkavaara and Saari.

1. Introduction

1.1 Motivation and background

Human life, economy and well-being rely on nature. Biodiversity is the key factor in enabling nature to be productive (Dasgupta, 2021). In this context, the need to further develop sustainable agriculture and forestry has been widely addressed.

Agriculture is the base for global food production, but it is also a significant driver of biodiversity loss. The urgent claim for achieving smart and innovative solutions for ensuring the sustainability of agriculture has been addressed in the Farm to Fork Strategy presented by the European Commission as part of the European Green Deal initiative, which aims at 'making the entire food chain from production to consumption more sustainable and neutral in its impact on the environment' (EC, 2020). In the concept of precision agriculture or smart farming, the main aim is that plants get the precise treatment at the right time and the right place, based on their observed and measured requirements in order to boost ecological and economically sustainable food production.

Sustainable forestry relies on healthy forests. However, forest disturbances, particularly by insect pests, are increasing in frequency, intensity and spatial extent due to drivers related to climate change (Sommerfeld et al., 2018). In Europe, the European spruce bark beetle (*Ips typographus*) has become a force that is changing forest landscapes across Europe, causing significant ecological and economic losses (Hlasny et al., 2019). For example, the bark beetle situation in the Czech Republic is disastrous. Approximately 30 million cubic metres were affected by bark beetles in 2019, which is five times more than in 2017. The number of damaged trees is larger than what the logistics can handle, and the economic loss is estimated to be 1.12 billion € (Toth et al., 2020). Early detection of bark beetle outbreaks is needed to plan management action to prevent further expansion of the outbreaks.

Drone technology has developed rapidly in the last decade, providing an alternative platform to traditional remote sensing platforms such as aircraft and satellites (Manfreda et al., 2018). Furthermore, multi- and hyperspectral cameras have been miniaturized, allowing them to be carried by even small drones (Aasen et al., 2018). Great developments in photogrammetric and computer-vision algorithms have taken image-based dense 3D reconstruction to the next level (Wu et al., 2013). These developments have revolutionized spectral and structural measurements, making them flexible and low-cost, and they have opened new prospects to monitor agricultural crops and forest health.

1.2 Objectives and overview of the thesis

The general objective of the thesis is to develop drone-based 3D and spectral remote sensing techniques for forestry and agriculture. In all of the publications in this thesis, drones were the main platform for remote sensing data acquisition, where different camera systems were mounted. The main sensor to collect spectral data was a frame-based hyperspectral camera, which also enables the use of photogrammetry and structure-from-motion techniques to solve georeferencing parameters and the generation of the 3D point cloud data. However, in order to achieve a higher level of spatial accuracy and density, the 3D data were also generated based on RGB cameras. Besides, in all publications, the potential of drone-based remote sensing data was demonstrated in real forestry and agriculture-related applications. Mapping of forest damage caused by bark beetles has been investigated in publications I and II, whereas tree species and genus classification were addressed in Publication V. Regarding agricultural applications, estimation of various biophysical, biochemical and feeding quality crop parameters were investigated. Biomass and nitrogen content were estimated in Publication III, targeting additional fertilization application. In Publication IV, biomass and various feeding quality parameters were estimated to optimize the harvesting time of silage grass, aiming to maximize the quantity and quality of the yield.

The conceptual framework of the thesis, including its main contributions and objectives, are summarized in Figure 1. The specific objectives of the thesis are defined as follows:

Objective 1: To develop drone-based 3D and spectral remote sensing techniques for classifying the health status and species of an individual tree (Publications I, II, V)

Objective 2: To develop drone-based 3D and spectral remote sensing and machine learning methods for agricultural crop parameter estimation (Publications III and IV)

Objective 3: To assess the effects of different measurement parameters—such as radiometric processing levels, selection of spectral sensor, spatial resolution and integration of spectral and 3D data for classification and estimation accuracy (Publications II–V).
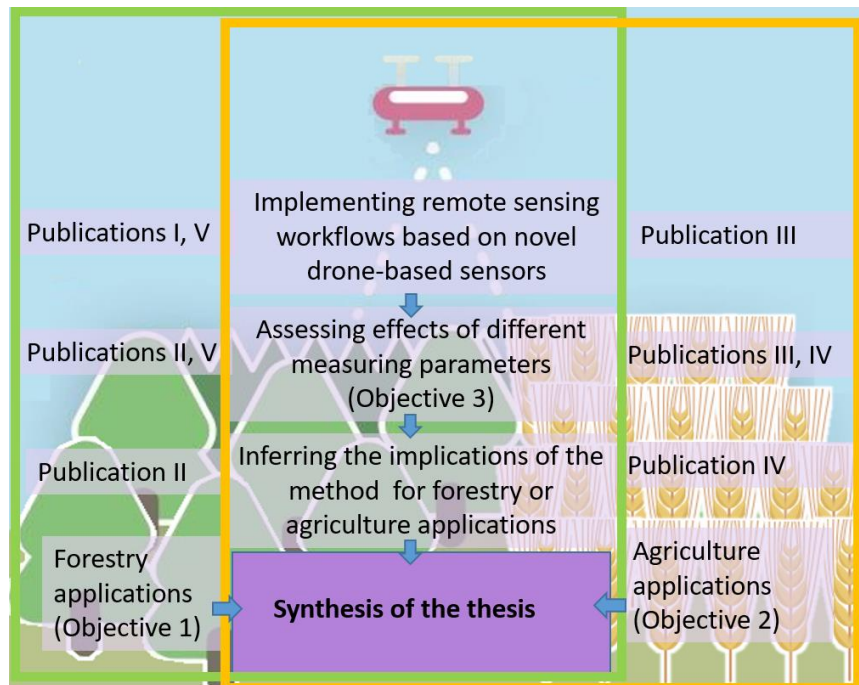
Figure 1. A conceptual framework, representing the components of the thesis, scientific objectives and links among them and the publications. The green box represents the forestry and the yellow box represents agriculture-related publications, components and objectives. (Picture in the background has been modified from the picture, which National Land Survey of Finland has the copyright)

All publications have a similar basic structure. Remote sensing workflows were implemented, based on spectral and 3D data collected by a drone. The main parts of the workflow include geometric and radiometric processing and feature extraction followed by estimation or classification of the interest variables using machine learning methods. Different settings during data collection and data processing affect the data to be used in the analysis phase. For example, the sensor itself affect the spectral response and—together with the flying height—the spatial resolutions. Also, atmospheric effects and variable weather conditions can influence the measured spectral values. Radiometric processing aims to reduce these effects, and it can be performed using various approaches. Furthermore, several features can be calculated from spectral and 3D data, and they can be divided or integrated into various feature sets. All of the above-mentioned different settings (the 'measurement parameters') have affected the final estimation or classification accuracy. Consequently, comparing these parameters is key to finding optimal sensors, data collection and processing methods for different applications. All publications include an assessment of these parameters, but publications II–V focus on more of them. Similarly, in all publications, remote sensing workflows were implemented, but their significance is highlighted in publications where they have been first implemented considering novel sensors in forestry (I, V) or agricultural applications (III). It is worth noting that although in all publications an application has been demonstrated, the implications for bark beetle damage mapping (in Publication II) and grass quality and quantity parameters (in Publication IV) have been analysed more deeply than in other publications where the focus has been more technically oriented.

An overview of the publications in this thesis and the research links between the publications are given below:

In Publication I, forest health was monitored for the first time using drone-based hyperspectral imaging. An entire drone-based remote sensing workflow to detect and classify individual trees from the novel drone-based hyperspectral imaging system was implemented. Norway spruces (*Picea abies*) were classified successfully into 2 or 3 classes based on symptoms caused by a bark beetle attack.

In Publication II, bark beetle damage mapping based on airborne spectral information is further developed and extended to larger areas. The study assesses the effect of spatial resolution and training data size on the accuracy of the classification process. Additionally, the study demonstrated spruce health maps for forest management purposes.

In Publication III, the workflow was developed for estimating agricultural crop parameters using machine learning and drone-based remote sensing. Both 3D and spectral features were employed and their performance to estimation accuracy was compared. The study also assessed the effects of different spatial resolution and radiometric processing on the estimation accuracy.

In Publication IV, the quantity and quality parameters of grass swards were estimated based on machine learning, drone-based spectral imaging and photogrammetry. Both spectral and 3D features were employed, and the performance of different sensors (RGB, multi- and hyperspectral) was compared. The workflow, developed in Publication III, was extended and assessed more completely. The assessment of developed estimators was also tested in independent test fields with suitable accuracy, verifying that the estimators were not only specific to training data.

In Publication V, drone-based photogrammetric 3D and spectral data from two novel cameras in VNIR and SWIR spectral ranges were used for tree species recognition in an arboretum. Data from both sensors and 3D features were integrated, and their performance accuracy was compared. The study also evaluated the level of radiometric processing for estimation accuracy.

The development of the remote sensing workflow was a continuous process, which is visible in Publications I–V. In Publication I, only spectral features and a simple classifier were employed. The results were not assessed with independent test areas, and different measurement parameters were not optimized. In contrast, in Publication IV, 3D and spectral features and more developed machine learning algorithms were employed, various measurement parameters were optimized, and the results were assessed with independent test fields.

2. Literature review

This chapter aims to provide background information about the concepts, terms and previous research related to the topic of the thesis in order to understand the research work that was done. First, drones and sensors as tools for optical remote sensing are described. Secondly, forestry and agricultural applications related to the topic are briefly described with a review of how remote sensing had been applied previously.

2.1 Drone-based remote sensing systems

2.1.1 Platforms

The history of drones dates back more than a hundred years, but their use for a long time was mostly limited to military applications (Colomina and Molina 2014). Drones are referred to by many different names and abbreviations, such as UAV, UAS and RPAS. Unmanned aerial vehicle (UAV) refers specifically to the flying vehicle itself. In addition to the vehicle, the Remotely Piloted Aerial System (RPAS) and Unmanned Aerial System (UAS) emphasize the entire system, including other components necessary for operation, such as the ground control station and the communication data link between the vehicle and the ground station. Being a simple term, 'drone' has become popular in public use, and it is used in this study, even though the aforementioned terms are technically more precise.

Technological developments led to price reduction and miniaturization of components related to drones, such as batteries, in particular LiPo (Lithium Polymer), Global Navigation Satellite System (GNSS) receivers, inertial measurement units (IMU) and electronic speed controls (ESC), which were driving the adoption of rotary and fixed-wing drones for civilian applications (Siebert and Teizer, 2014; González-Jorge et al., 2017). Lightweight components and higher-capacity batteries enabled longer flight times without additional fuel. Drones with two or more rotors (multicopters) especially benefitted from the development of ESCs for brushless motors, and these have replaced conventional single- and double-rotor helicopters. Multicopters, such as quadcopters with four rotors and hexacopters with six rotors are controlled by changing the speed of the rotors via ESCs, which makes flight control simpler than with helicopters, which require controlling the blade rotations. Due to sophisticated au-

topilot, i.e. the Flight Controller Unit (FCU), the control of multicopters is flexible and user-friendly, which has increased their popularity (Siebert and Teizer, 2014).

Aerial imaging is one of the most famous civilian applications of modern drones (González-Jorge et al., 2017). The popularity of drones as a platform for the remote sensing sensors increased dramatically after 2010 (Nex and Remondino, 2014; Pajares, 2015). In environmental monitoring, the popularity mainly relies on drones as having bridged the gap between space and other airborne and terrestrial platforms (Pajares, 2015; Toth and Jóźków, 2016; Manfreda et al., 2018). Compared to other airborne remote sensing platforms (such as manned aircraft and satellites), drones are low-cost and flexible to operate, but they are limited to smaller mapping coverage. Static or mobile platforms used at ground level (often referred to as proximal sensing or terrestrial approaches) are even more flexible, but the spatial coverage is more limited than with drones (Figure 2). The potential of different remote sensing platforms in their spatial coverage and flexibility for environmental mapping is illustrated in Figure 2. The term 'flexibility' in this context refers, firstly, to the amount of required effort to start the data collection, and secondly to the possibilities of influencing the data collection during its execution (e.g., changing the flight plan). High flexibility also means that data collection can be repeated often, i.e. the temporal resolution can be selected more freely. Besides, the drone types (such as fixed-wing and multicopters) differ in their features as a remote sensing platform. Fixed-wing drones are faster than multicopters and benefit from their spatial coverage. On the other hand, the ability of multicopters to fly slowly or even stop in the air benefits flight operations for certain applications. Furthermore, multicopters are more flexible in mounting payloads.
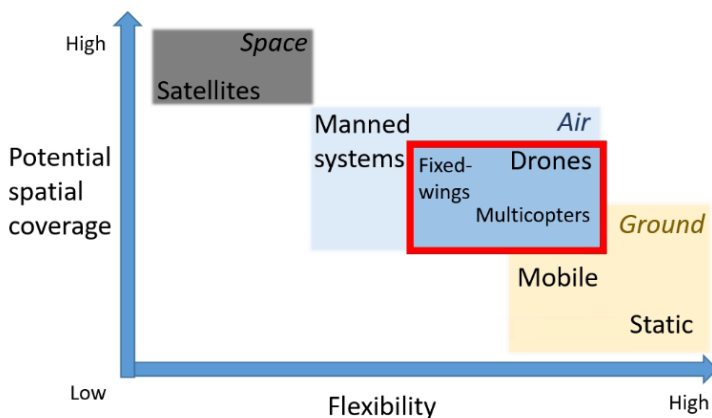
Figure 2. The potential spatial coverage and flexibility of different remote sensing platforms for environmental mapping.

2.1.2 Sensors

In the science of photogrammetry and remote sensing, modern drones were first applied in photogrammetry and after Eisenbeiss (2009) introduced the term 'UAV Photogrammetry', the 3D reconstruction based on drone imaging in-

creased dramatically (Nex and Remondino, 2014). Small off-the-self RGB digital cameras were used for photogrammetric 3D reconstruction. In the early 2000s, spectral remote sensing sensors were too heavy to be mounted on drones. However, since the importance of spectral areas outside the visible range is known (especially in vegetation remote sensing), the development of lightweight spectral cameras suitable for drones was started. According to Aasen et al. (2018), the first drone-based spectral sensor was an RGB camera modified by removing filters to collect near-infrared (NIR) information in addition to three bands in the visible range, as presented by Lelong et al. (2008). Afterwards, various miniaturized spectral sensors with multiple working principles were presented. They can be divided into three main groups: point spectrometers (e.g. Burkart et al., 2013) that records the spectral signature in one point, pushbroom spectrometers (e.g. Zarco-Tejada et al., 2012) that record spectral information in one spatial dimension, and 2D imagers that record the spectral information in two spatial dimensions. Among the 2D imagers, there are still various sensor approaches. For instance, multiple cameras can be combined (multi-camera 2D imagers) as the one presented in Berni et al. (2009) which was able to collect six bands. The first miniaturized 2D imager, which was described as a hyperspectral sensor with more than 30 spectral bands, was introduced by Saari et al. (2011). This sensor records the spectral bands sequentially in time (sequential 2D imager). Consequently, the spectral bands need to be aligned when captured from a mobile platform such as a drone. Several types of snapshot 2D imagers, which collect spectral and spatial information simultaneously, have also been introduced (Aasen et al., 2018).

All of these sensors have advantages and disadvantages, considering their usability as a remote sensing sensor, since the building of spectral sensors is always a tradeoff between spatial aspects (resolution and coverage), spectral aspects (spectral resolution and range) and radiometric resolution. Concerning the spectral aspects, the spectral range defines the possible range in the electromagnetic spectrum where the observations are made. Drone-based sensors mostly operate from visible to near-infrared (350-1000 nm, VNIR), but a few sensors operating in shortwave infrared (1000-1600 nm, SWIR) have been presented (Honkavaara et al., 2016; Jenal et al., 2019). Spectral resolution is primarily referred to as a measure of the ability to separate different wavelengths in the electromagnetic spectrum. This is commonly measured as FWHM (Full Width at Half Maximum), which means the distance between points on opposite sides of the maximum value of a function where the function gets half of its maximum value (Figure 3). The spectral resolution is also closely related to the number of collected bands. Radiometric resolution describes how many levels the intensity of the received signal can be divided (bit depth), but it is also related to the signal-to-noise ratio. A comparison of different spectral sensors concerning these aspects can be found in the review by Aasen et al. (2018).
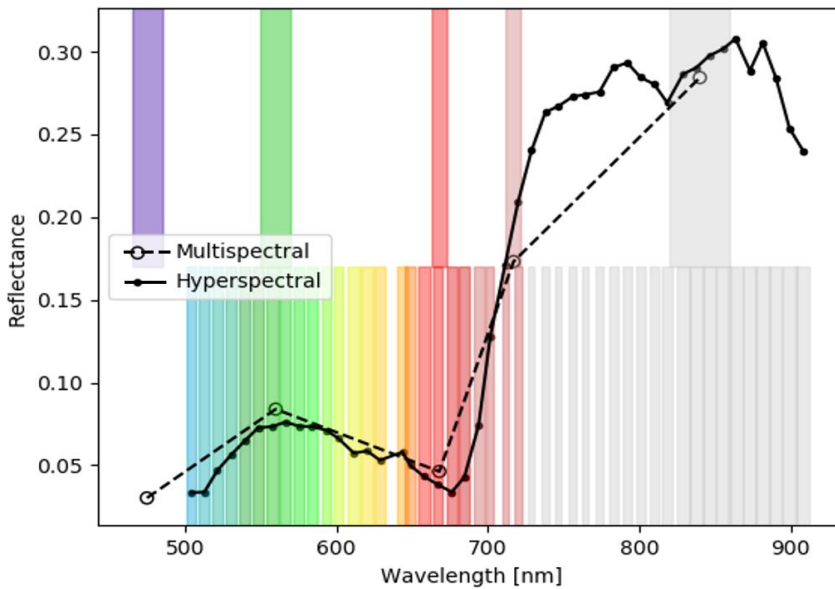
Figure 3. Typical spectral response of vegetation measured by a hyperspectral (Rikola model 2018, manufactured by Senop) and a multispectral (RedEdge, manufactured by MicaSense) camera, operating in VNIR range for drone-based remote sensing. The location of the bars marks the central wavelength of the spectral bands and width of the bars marks the FWHM at the top of the chart for multispectral and at the bottom of the chart for hyperspectral camera.

2.2 Optical remote sensing of vegetation

Optical remote sensing is based on measurements of the interaction between electromagnetic radiation and the vegetation. The incident electromagnetic radiation can be absorbed, reflected or transmitted by the object. Different objects react to this radiation in different ways, forming the characteristic reflection spectrum of each object. Green plants absorb almost all visible light due to chlorophylls but reflect much of the radiation when visible light changes to infrared radiation (Knipling, 1970). Various biophysical and biochemical properties of vegetation influence the reflectance spectrum (Curran, 1980). This has made optical remote sensing a tool for various vegetation-related applications. This section briefly describes applications and remote sensing methods related to this thesis.

2.2.1 Forestry: tree health and tree species classification

The composition and health of tree species is fundamental information when describing forest ecosystems. Information on tree species is considered an essential biodiversity variable (EBV) in the context of worldwide biodiversity monitoring (Pereira et al. 2013; Vihervaara et al., 2017; Jetz et al., 2019). Also, information on tree species is crucial for forest inventories since it is used for species-specific yield and growth models (Laasasenaho, 1982; Korpela and Tokola, 2006). Information on tree species is also important in forest health mapping since many disturbances, particularly those caused by insect pests, are mostly tree-species-specific.

Forests can face both biotic stresses (such as insect pests and pathogens) and abiotic stresses (such as wind, storms, floods and fires) (Lindner et al., 2010; Seidl, 2017). Many of these stresses appear as discolouration and defoliation of canopy, which remote sensing technologies can detect. Remote sensing has been employed especially for insect pest damage mapping, and conifer bark beetles have been one of the most-studied damage agents (Senf et al., 2017). In Europe, the European spruce bark beetle has been causing significant damage to Norway spruce forests. The infestation by bark beetle is typically divided into four phases: green, yellow, red and grey attacks (Wermelinger, 2004; Blomqvist et al., 2018; Abdullah et al., 2018a). In the green-attack phase, the canopy is still green, but visible symptoms are located only in tree trunks as entrance holes of beetles and as fresh resin flows. In the next phases, the canopy colour changes to yellow and red before needles fall off and the tree dies (grey attack) (Wulder et al., 2006). Detecting bark beetle damage as early as possible enables the planning of actions to prevent the spread of outbreaks.

Forest health has been observed in the VNIR range since World War II and from a wider spectral range since the 1960s (Carneggie and Lauer, 1966; Ustin and Gamon, 2010). However, remote sensing technologies have developed enormously after these years, presenting new solutions for forest health monitoring (Torresan et al., 2017; White et al., 2016). Various remote sensing methods with different spatial, spectral and temporal resolutions exist (Fassnacht et al., 2016; Hall et al., 2016; Senf et al., 2017). For instance, satellites (such as the Landsat series) collect forest information on a global scale but are limited to low spatial resolution (Landsat-8 Ground Sample Distance (GSD) of 30 m). Therefore, forest inventories using satellite data have typically been carried out at the forest-stand or sample-plot levels, not at the individual tree level. Landsat-8 has been applied especially in forest health monitoring studies (Rock, 1986; Foster et al., 2017) and for mapping the diversity of tree species (Walsh, 1980). After launching the Sentinel-2 satellites (GSD 10-60m), their MultiSpectral Imager (MSI) has been used in various studies in forest health monitoring (Zarco-Tejada et al., 2018; Abdullah et al., 2018b; Huo et al., 2021; Fernandez-Carrillo et al., 2020) and tree species classification (Immitzer et al., 2016; Persson et al., 2018). Abdullah et al. (2018b) were the first to show that the early phase of bark beetle outbreak, the green attack stage, could be detected from Sentinel-2 data.

Aircraft enables high spatial and spectral resolution when applied as a platform for spectral sensors. For example, Lausch et al. (2013) and Fassnacht et al. (2014) used aerial imagery with 4-7m of GSD, collected by a Hyperspectral Mapper (HyMAP) instrument (125 bands; 450−2480nm), to detect a bark beetle infestation in Germany. They found that spectral bands in the VNIR range, and especially the red edge (690 nm), contributed to classification accuracies, but they stated that their pixel-based method led to misclassifications between tree health and soil classes. Recently, Potterf et al. (2019) stated that airborne colour-infrared images from 2007 to 2015 with GSD of 20-30 cm were accurate enough to manually digitize the spread of beetle infestations from windthrown, which allowed the modelling of the infestation gradient. Laser scanning from aircraft (ALS; airborne laser scanning) has also been widely and successfully used for tree species classification (Holmgren et al., 2004; Suratno et al., 2009; Korpela et al., 2010; Hovi et al., 2016). In forest health monitoring (e.g. Kantola et al., 2010), ALS (Airbrone Laser Scanning) point clouds have been employed less often than spectral images.

Since the developments in drone and lightweight sensor technologies, they have been employed in forest health monitoring and tree species classification, enabling mapping with very high spatial and temporal resolution. The first studies to classify tree species from drone-based VNIR range measurements were conducted with multispectral sensors, e.g. by Lisien et al. (2015) and Michez et al. (2016) in Belgium. They concluded that multitemporal and high spatial resolution are efficient ways to classify broadleaved tree species, and the combination of RGB and NIR features provide better classification accuracy than the use of only one of them. Nevalainen et al. (2017) showed for the first time that the combination of photogrammetric point clouds and hyperspectral data in the VNIR range is a sufficient tool to detect and classify tree species in boreal forests. Prior to the Publication V, the drone-based spectral sensors operating in the SWIR range were not studied in a forest environment.

In the study by Lehmann et al. (2015), the feasibility of drone-based imaging to monitor forest damage caused by insect pests were shown using multispectral data. Hyperspectral drone imaging in insect pest monitoring was studied for the first time in Publication I, where individual Norway spruces infested by the European spruce bark beetle were classified into three classes. Recently, monitoring damage by the same bark beetle, using multispectral imaging from drone, has been studied by Klouček et al. (2019) and Brovkina et al. (2018). Klouček et al. (2019) concluded that a low-cost multispectral sensor was also able to classify infested trees with promising accuracy. Brovkina et al. (2018) classified the first tree species and then stated that Normalized Difference Vegetation Index (NDVI; Rouse, 1974) values of spruces with fungal pathogens and bark beetles differed statistically from healthy spruces. Drone imaging has also been employed successfully to mapping insect damage in other tree species, such as *Pinus radiata* (Dash et al. (2017), *Abies sibirica* (Safonova et al., 2019) and *Pinus yunnanensis* (Lin et al., 2019; Liu et al., 2020).

The common approach to classifying spectral remote sensing data has been pixel-based, especially for satellite imaging. The high spatial resolution of drone-based imaging has enabled the move from pixel-based methods to object-based methods, and particularly to the individual tree level. In the object-based method, pixels are first segmented into similar groups before classification (Blaschke, 2010). For instance, Lehman et al. (2015), Michez et al. (2016) and Franklin (2018) have applied this approach to drone-based data. Franklin (2018) concluded that object-based methods outperformed pixel-based methods in the tree species classification. Michez et al. (2016) concluded that their smallest scale in the object-based analysis ($1m^2$) outperformed the analysis with a higher scale. In the forest, object-based approaches typically led to irrelevant classes, such as canopy gaps as in the study by Lehman et al. (2015). In individual tree approaches, the trees are first detected in order to target the analysis only to them. Photogrammetric point clouds have been widely employed and proved to be efficient in detecting individual trees from drone-based imaging data, especially in forests where the forest floor is visible (Puliti et al., 2015; Nevalainen et al., 2017; Minarik et al., 2020).

Various machine learning algorithms—such as k-Nearest Neighbours (k-NN), Multilayer Perceptron, Support vector machines (SVM) and Random Forest (RF)—have been applied to classify tree species and health status. None of these classifiers have been found to be the best for all use cases (Maxwell et al., 2018). In addition to classification performance, the algorithms differ regarding the

requirements of training data and the number of parameters to be optimized (Kotsiantis et al., 2007). Recently, the popularity of deep learning methods, particularly convolutional neural networks (CNN), have gotten them more attention, and they have resulted in high classification accuracies when drone data has been employed to classify tree species (Sothe et al., 2020; Nezami et al., 2020; Miyoshi et al., 2020b) and health status (Safonova et al., 2019).

2.2.2   Agriculture: crop parameter estimation

As defined by the International Society of Precision Agriculture, 'Precision agriculture is a management strategy that gathers, processes and analyses temporal, spatial and individual data and combines it with other information to support management decisions according to estimated variability for improved resource use efficiency, productivity, quality, profitability and sustainability of agricultural production.' (ISPA, 2019). In this context, timely information about the properties of agricultural crops, i.e. crop parameters, is highly relevant. Depending on the agricultural task, different kinds of crop parameters are of interest, such as biophysical, biochemical and feeding-quality parameters. Biophysical parameters such as biomass, Leaf area index (LAI) and plant height are related in the agricultural context to the quantity of the yield. Above-ground biomass, often referred to as biomass, is the fundamental parameter to be estimated in precision agriculture and, in the case of grass crops, it directly defines the quantity of grass, i.e., the yield of grass. Beyond the agricultural context, biophysical parameters provide insight into the structure and function of ecosystems (van Cleemput et al., 2018). Biochemical parameters, such as nitrogen and phosphorus content, define the general nutritional status and identify specific nutritional deficiencies of the plant. Feeding quality parameters consist of a group of parameters that define the nutritional value of a specific plant or group of plants for the specified animal species. For instance, digestibility is commonly evaluated with the D-value parameter, which is directly related to metabolized energy (ME) and, in the case of grass silage for a ruminant, the D-value multiplied by 0.016 provides ME (MAFF, 1975). Another important parameter called crude protein is directly related to nitrogen content (Jones, 1931).

Remote sensing has been offering tools to provide information about crop parameters for decades (Bauer and Cipra, 1973; Curran, 1980; Weiss et al., 2020). In the context of precision agriculture, the first applications were conducted from satellites and various terrestrial platforms (Bhatti et al. 1991; Mulla et al., 2013). From satellites, optical data has been collected from Landsat TM (Bhatti et al. 1991; Thenkabail, 2003) and Sentinel-2 (Clevers et al., 2017; Delloye et al., 2018), and active data from synthetic-aperture radar (SAR) (Karjalainen et al., 2008). Terrestrial approaches include crop height measurement using laser scanning (Lumme et al., 2008; Hoffmeister et al., 2013; Tilly et al., 2014), tractor-mounted sensors for nitrogen and biomass estimation (Tremblay et al., 2009) and field spectrometers for feeding quality parameter estimation (Pullanagari et al., 2012, Smith et al., 2020). However, these approaches do not meet the requirements for precision agriculture in terms of flexibility, high spatial accuracy and cost-efficiency. Developments in drones, sensors and photogrammetry have raised crop monitoring for precision agriculture to a new level (Tsouros et al., 2019). Drones offer flexible and low-cost platforms for spectral

cameras to collect multi- or even hyperspectral data. In addition, photogrammetric 3D reconstruction based on structure from motion (SfM) and dense image matching algorithms (Wu, 2013; Hirschmüller, 2008) enables a cost-efficient 3D data collection of crops.

Biophysical parameters, in particular (above-ground) biomass, are the most common crop parameter to be estimated using drone-based imaging. Both photogrammetric 3D (Bendig et al, 2014; Li et al., 2016) and spectral data from multispectral (Berni et al., 2009; Hunt et al., 2010; Candiago et al., 2015; Liu et al., 2019) and hyperspectral sensors (Honkavaara et al., 2013; Aasen et al., 2015; Barnetson et al., 2020) have been adopted to estimate the biomass of various crops. Furthermore, the combination of 3D and spectral has been claimed to be a feasible approach in the context of biomass estimation (Bendig et al., 2015; Yue et al., 2017; Viljanen et al., 2018). Nitrogen is the most important nutrient to boost crop growth and it can also affect to the structure of a plant such as to the stem/ leaf ratio of the grass swards (Van Soest, 1994). Therefore, nitrogen (such as, nitrogen concentration or nitrogen uptake) has been a widely estimated biochemical parameter in the remote sensing literature (Berger et al., 2020a), and only a few studies spectral data have been collected from drones. Prior to Publication III, drone-based methods were mainly conducted by multispectral sensors (Geipel et al., 2016; Liu et al., 2016). Feeding quality parameters have been estimated especially for different grass swards used for forage production for ruminants directly by pasturing or by harvesting and preserving it to silage. One of the first studies to estimate those parameters applying drones was done by Capolupo et al. (2015), where hyperspectral vegetation indices and partial least squares regression models were used to estimate ME and crude protein. Linear regression models have been used by Barnetson et al. (2020) with hyperspectral data and Michez et al. (2020) with multispectral data.

Machine learning methods have been adopted for agricultural crop parameter estimation mainly due to their ability to handle a large number of data and nonlinear tasks (Chlingaryan et al., 2018). In contrast to physically based methods, they are variable-driven approaches. They are also often considered as non-parametric and nonlinear methods in contrast to parametric and linear regression methods (Verrelst et al., 2019). Parametric regression methods are typically built by fitting the model between a crop parameter and a single vegetation index or another metric that has been selected based on physical knowledge of plant properties. Considering the drone-based crop parameter estimation, the first approaches were typically in this category, such as biomass estimation based on the correlation with the NDVI index (Swain et al., 2010) or the photogrammetric surface model (Bendig et al., 2014). Non-parametric linear methods, such as partial-least-squares-regression (PLSR), have been adopted, especially with hyperspectral data (Capolupo et al., 2015). The high performance of machine learning methods in various remote sensing tasks (Lary et al., 2016; Chlingaryan et al., 2018) inspired the employment of them for drone-based crop estimation, such as the use of the random forest algorithm (RF) to estimate biomass (Viljanen et al., 2018) and feeding quality parameters of grass in Publication IV. The latest rising trend, considering the machine learning methods in remote sensing, has been deep learning algorithms, in particular CNN (Kattenborn et al., 2021). For instance, Castro et al. (2020) presented promising results when they estimated the biomass of grass based on RGB images collected from drones using such an approach.

3. Material

3.1 Study areas and biophysical ground truth

All study areas were located in southern Finland. The size of the areas ranged from 2.5 ha to 3000 ha (Table 1). In publications I and II, the study was done in the city of Lahti, where European Spruce Bark beetles had been causing serious damage to Norway spruces. In Publication V, the study was done in in Kouvola, in the Mustila Arboretum, where there is an exceptionally large variety of coni-fer and broad-leaved tree species related to boreal forests. The study area in Publication III was in the city of Vihti, in an agricultural remote sensing test field that included malt barley parcel and an experimental site of grass silage. Experimental grass sites were also used as a study area in Publication IV. The areas were located in Jokioinen with four different experiments established in two different parcels, including timothy meadow fescue grass crops.

Table 1. Summary of study areas.

	Location (Municipal-ity in Finland)	Size	Description
Publication I	Lahti	8 ha	Norway spruce dominated urban forest
Publication II	Lahti	3000 ha	Norway spruce dominated urban forest
Publication III	Vihti	35 ha	Agricultural test site with barley and grass parcels
Publication IV	Jokioinen	2.5 ha	Experimental site of grass silage (primary and regrowth)
Publication V	Kouvola	40 ha	Arboretum with a large variety of tree species

Biophysical ground truth refers here to observations or measurements of trees in forest and crops in agricultural fields. Remote sensing techniques are not able to directly measure the biophysical properties of a plant, so accurate reference observations and measurements of variables (such as the health status of the spruce and biomass in a barley field) were essential in developing these tech-niques. The variables were either categorical or continuous. Information on the variables used as input data to train and validate the machine learning models (Section 4.4) is summarized in Table 2.

In the forest-related studies (I, II and V), ground truth variables were categor-ical, and observations were made by experts in the field. In publications I and II, ground truth was related to the health status of Norway spruces, considering bark beetle infestation. Various symptoms were assessed in trunks and crowns at the individual tree level. The method of observing symptoms is described in more detail in a study by Blomqvist et al. (2018). In publications I and II, the

observations of crown colour were selected to indicate the health status of spruces. Symptoms were initially categorized into four classes, but due to the low number of observations in one class, three were used in the final analysis. Consequently, health status was a categorical variable that included three classes (healthy, infested and dead). In Publication V, ground truth included the species and genus of 673 test trees. Test trees had 26 different species from 14 genera, defining two categorical variables.

In the agricultural studies (III and IV), all ground truth variables were continuous and were measured using direct and indirect methods (Table 2). Biomass (fresh and dry) was measured with a common method in agricultural research called 'cut and dry' (Ali et al., 2016). This method involves first cutting a sample of a fresh crop from a specified area and then weighing it before and afterwards drying in order to determine fresh and dry biomass, respectively. This method produces information about above-ground biomass and, in the case of grass, it directly defines the quantity of the grass, i.e. the yield of the grass. In publications III and IV, biochemical variables (such as nitrogen content) and the feeding quality variables of grass (such as digestibility (D-value)) were measured in the laboratory from dried samples. In Publication IV, the state-of-art method in feeding quality analysis—the near-infrared reflectance spectroscopy (NIRS) technique (Decruyenaere et al., 2009)—was used as a ground truth that provided mass-based measures for the biochemical variables of the leaf.

Table 2. Summary of ground truth information used as an input in the classification and estimation phases. The number of samples refers to the number of individual trees in publications I, II and V and the number of test plots in publications III and IV. In Publication III, 36 samples of barley crop were analysed separately from 8 samples of grass. In Publication IV, 104 samples were collected during the primary growth and 117 samples during regrowth. These samples were analysed separately. FY: Fresh yield and DMY: Dry Matter Yield (kg/m^2 in Publication III, (kg/ha in Publication IV); Nitrogen content: D-value: digestible organic matter in dry matter (g/kg DM); iNDF: indigestible neutral detergent fibre (g/kg DM); NDF: neutral detergent fibre (g/kg DM); WSC: water-soluble carbohydrates (g/kg DM); Ncont: nitrogen concentration (referred to as Nitrogen % in Publication III: 10g/kg DM and g/kg DM in Publication IV); NU: nitrogen uptake (referred to as Nitrogen content in Publication III: kg/m^2 and kg/ha in Publication IV).

	Plant	Number of samples	Type of the variables	Variables
Publication I	*Picea abies*	78	categorical	Health status
Publication II	*Picea abies*	330	categorical	Health status
Publication III	*Phleum pratence, Festuca Partensis, Hordeum vulgare*	36+8	continuous	Biomass (fresh and dry; FY, DMY), Nitrogen (uptake and concentration)
Publication IV	*Phleum pratence, Festuca Partensis*	104+117	continuous	Biomass (fresh and dry; FY, DMY), Feeding quality (D-value, iNDF, NDF, WSC, Ncont, NU)
Publication V	26 different tree species	673	categorical	Species, Genus

The geospatial location of the ground truth is also an important observation for matching the remote sensing data to it. GNSS were utilized to locate the ground truth in publications I–IV. In the forest, the accuracy of the GNSS measurements was not sufficient to precisely locate the test trees in the area; thus the coordinates were matched visually to treetops based on collected high-resolution orthophotos. Ground truth included more supporting information that was utilized during the analysis. For instance, based on the measured diameter-breast-height, small trees were eliminated from the analysis in publications I and II. The clear-bounded plots of experimental grass sites were digitized directly to the orthophotos.

The collection of biophysical ground truth was carried out by collaborating forestry and agricultural researchers from the University of Helsinki, in Publications I and II, and the Natural Resources Institute Finland, in Publications III–V.

3.2   Remote sensing data

Remote sensing data were collected mainly using drones as a platform. All drones used in the data collection were multicopters with varying numbers of rotors. They built at the Finnish Geospatial Research Institute (FGI) for research purposes. The drone used in publications I and II had relatively limited operational parameters, but the drones used in publications III–V were significantly more developed (Table 3). The relatively low payload of the octocopter did not enable to mount the spectral and RGB cameras simultaneously to the drone. Instead, the hexa- and quadrocopters were able to carry multiple cameras at the same time making the data collection more efficient. A single-board computer and GNSS receiver were installed in drones in publications III–V to record the trajectory of the drone and the timing data for all devices. In publications II and III, a small, manned aircraft (Cessna) was operated as well. Compared to drones, the payload capacity and flight time of small aircraft are significantly higher, but they are not as flexible as drones to operate, especially when mapping relatively small areas.

Table 3. Summary of drones used.

| Type | Frame | Autopilot | Typical operational: | | Additional supporting equipment | | Publication |
			Payload	Flight time	Single-board computer	GNSS receiver	
Octocopter	Droidworx AD-8 frame	MikroKopter	1.5 kg	7 min	-	-	I, II
Hexacopter	Tarot 960	Pixhawk 1, with Arducoper 3.15 firmware	4 kg	20 min	Rasper-ryPi2	NV08C-CSM L1	III, V
Quadrocopter	Gryphon dynamics	Pixhawk 1, with ArduPilot APM Copter 3.4 firmware	4 kg	25 min	Rasper-ryPi3	NV08C-CSM L1	IV

The entire study was carried out using a Fabry-Pérot interferometer (FPI) – based spectral camera as the main sensor. The FPI camera technology was developed by the VTT Technical Research Centre of Finland (Mäkynen et al., 2011; Saari et al., 2011). The FPI consists of two parallel reflective surfaces. By changing the gap between them, it is possible to collect different wavelengths in frame format. Due to this basic principle of FPI technology, the acquisition of spectral bands is sequential in time, which needs to be considered in data processing when the camera is used in a mobile platform such as a drone (Honkavaara et al., 2013, 2017; Oliveira et al., 2016). All versions of the FPI camera were prototypes and allowed for the configuration of a certain group of spectral bands within the camera's spectral range before data acquisition. Overall, 32 to 36 spectral bands were acquired for each study area. Summary information on the FPI spectral imagers used is shown in Table 4.

Table 4. Summary of FPI-based spectral cameras. 'No. bands' refers to the number of originally acquired spectral bands in these studies. 'FWHM' refers to full width at half maximum, presenting the range of wavelengths covered by a single band.

Spectral camera	Spectral range	No. bands	FWHM	Image size (pix)	Pixel size	Focal length	Publications
FPI2012b	500-900 nm	36	15-30 nm	1024 x 648	0.011mm	10.9mm	I–IV
FPI Rikola VNIR	400-1000 nm	36	10-15 nm	1010 x 1010	0.02mm	9.0mm	V
FPI SWIR	1100-1600 nm	32	20-30 nm	320 x 256	0.005mm	12.2mm	V

In addition to spectral cameras, regular consumer digital cameras (RGB) were mounted to drones. The purpose of the RGB cameras was to collect data at a high spatial resolution. As a result of applying different RGB camera systems, GSDs of the RGB cameras were 10−40% of the spectral camera GSD (Table 5). Consequently, RGB cameras were the main technique used for 3D data production. In addition, images from RGB cameras were employed to support the georeferencing of the spectral images (see Section 4.1). In publications III and IV, the RGB images' digital values (DN) were converted to reflectance to represent a three-band spectral sensor.

Remote sensing data was acquired in extensive flight campaigns (Table 5). Flight campaigns were planned separately for each test area to meet the requirements of the study. In publications II and III, one objective was to compare the effects of different spatial resolutions in applications. Therefore, in Lahti and Vihti, data were collected with various flying heights and also with small manned aircraft at 450 m to 900 m flying height. In addition, the Vihti study area consisted of two different targets—grass and barley—where flights were planned separately. Multitemporal data collection was carried out in the Jokioinen study area, where primary growth at the grass site was imaged four times and regrowth three times. In Publication V, data was collected with two different spectral sensors, but they were not possible to collect simultaneously due to the maximum payload capacity of the drone.

In addition to the general data acquisition plans, flight parameters (such as flying height and speed) should be planned carefully to confirm that the quality of data meets the set requirements and expectations. All sensors were central-projection cameras that collected vertical aerial images. Thus, classic photogrammetric models and formulas starting from collinearity equations were applied in flight planning (see, e.g., Mikhail, 2001). Flying height is an important flight parameter because, along with sensor properties, it defines the GSD and image coverage. By increasing the flying height, the image coverage increases, which increases the speed of data collection. Decreasing the flying height improves the spatial resolution, enabling observation of smaller details. Also, regulations need to be taken into account when selecting the flying height. When the data campaigns in test areas were done, Finnish regulation allowed drone flights with a visual-line-of-sight and a maximum 150 m flying height without specific permission procedures. Considering all of the abovementioned aspects, flying heights of drone campaigns were selected from 50 m to 140 m (Table 5). Flying heights over 90 m were mainly used. But when the GSD requirements were small targets, especially in grass-related studies (III, IV), 50 m was also used. Overlaps between images should also be enough that the same point can

be observed in multiple images, which is the core idea of stereoscopic photogrammetry and SfM techniques. For SfM software, such as Agisoft Photoscan, the 60% side and 80% forward overlaps are recommended at the minimum (Agisoft, 2019), and they also exceeded in all of the spectral datasets in Publication I. When flying height and sensor properties were known, the flight speed and distance between flight lines were calculated to achieve the recommended overlaps.

Table 5. An overview of flight campaigns considering the study area, campaign description, platforms and sensors. Multitemporal (no. campaigns): 'Yes' if the campaign was multitemporal and number of flight campaigns. No. flights: Number of individual flights to cover the study area. *In Vihti, aircraft data was collected in a single flight but changing the sensors and flying height during the flight.

Publi-cation	Study area	Campaign			Platform	Sensors			
	Location (target)	Mul-titem-poral (no. cam-paigns)	No. flig hts	Flying height (m)	UAV/aircraft (type)	Spectral	GSD of the spec-tral cam-era (cm)	RGB	GSD of RGB (cm)
I-II	Lahti	No	2	90	UAV (Octo)	FPI2012b	9	Samsung NX1000	2
II	Lahti	No	1	500	Aircraft	FPI2012b	50	-	
III	Vihti (grass)	No	1	140	UAV (Hexa)	FPI2012b	14	Samsung NX500	3.7
III	Vihti (grass)	No	1	50	UAV (Hexa)	FPI2012b	5	Samsung NX500	1.3
III	Vihti (barley)	No	4	140	UAV (Hexa)	FPI2012b	14	Samsung NX500	3.7
III	Vihti (barley)	No	1*	450	Aircraft	FPI2012b	62	-	
III	Vihti (barley)	No	1*	700	Aircraft	-		Nikon D3X	5
III	Vihti (barley)	No	1*	900	Aircraft	-		Nikon D3X	10
IV	Jokioinen (primary growth)	Yes (4)	2	50	UAV (Quadro)	FPI2012b	5	Sony A7R	0.64
IV	Jokioinen (regrowth)	Yes (3)	1	50	UAV (Quadro)	FPI2012b	5	Sony A7R	0.64
V	Kouvola	No	3	120	UAV (Hexa)	FPI Rikola VNIR	8	Samsung NX300	3
V	Kouvola	No	3	120	UAV (Hexa)	FPI SWIR	20	Samsung NX300	3

In addition to data collected by drones, supporting remote sensing data was also collected during field campaigns. Ground control points (GCP) were installed and their coordinates measured with the virtual reference station real-time kinematic GNSS devices in publications III–V to support geometric processing. In publications I–III and V, ASD Field Spec Pro spectrometer measured irradiance data during the data collection to support radiometric processing. Furthermore, in all studies, reference reflectance panels were installed, measuring 1 m × 1 m for drone campaigns and 5 m x 5 m for aircraft campaigns were installed. Their reflectance was measured with an ASD spectrometer, as they were used as a reference in reflectance transformation (Section 4.2).

4. Methods

This chapter introduces the methodology of developed remote sensing work-flows, from collecting remote sensing and biophysical ground materials to esti-mating and classifying the results. The summarized methodology of all publica-tions is presented in Figure 4. The method workflow can be divided into four main steps, starting from geometric and radiometric processing and ending on feature-extraction to estimation and classification, using machine learning methods. This chapter introduces the implementation of these steps.
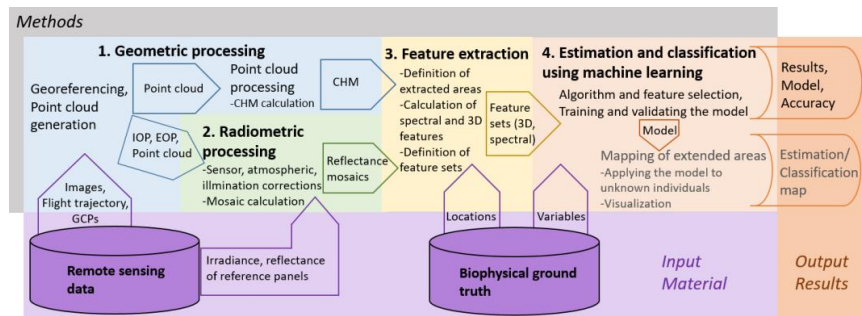
Figure 4. Thematic summary of the method's workflow, including the four main steps: 1. geometric processing, 2. radiometric processing, 3. feature extraction and 4. estimation and classification. The arrows describe the data flow between steps, starting from inputs, i.e. remote sensing and biophysical ground truth materials, and ending with the outputs, i.e. estimating and classifying the results, models and accuracy. If these models are also used to classify or estimate also unknown individuals, a result can be also classification maps, such as spruce health maps in publications I and II. GCPs: ground control points; IOP: interior orientation parameters; EOP: exterior orientation parameters; CHM: canopy height model.

4.1 Geometric processing

The aim of geometric processing is to georeference the image data and collect the photogrammetric 3D information about the object. Accurate geometric pro-cessing is crucial, especially when integrating data from different platforms, dates and sensors. Geometric processing can be divided into steps: georeferenc-ing and point cloud generation and processing (Figure 4).

In georeferencing, image exterior and sensor interior orientation parameters are estimated, allowing the positioning of the data in the object coordinate frame and its use for the 3D reconstruction of the object. Exterior orientation parameters (EOP) include the position (3 parameters) and orientation (3 pa-

rameters) of the camera at the time of exposure. The interior orientation parameters (IOPs) of the camera often comprise the principal distance, principal point coordinates and lens distortion parameters. The EOPs can be measured by GNSS and IMU systems onboard the drone, and the accuracy level will depend on the quality of the systems utilized as well as on external conditions. In the case where such a system does not exist, the estimation of the EOPs will rely on the photogrammetric bundle block adjustment (BBA) process, and the absolute georeferencing to a geographic coordinate system will require the use of GCPs. For the IOP estimation, the most common approaches are pre-estimation of the parameters in the laboratory or field or the estimation simultaneously with EOPs in the BBA. The BBA uses tie points (i.e. points that have been extracted and matched in multiple overlapping images) as the observations to solve IOPs and EOPs, and it can be supported with GCPs and the initial values of IOPs and EOPs.

In all publications, IOPs and EOPs were solved in BBA, and it was supported with GCPs in publications II–V. Coordinates of GCPs were measured during the field campaign using a GNSS receiver and artificial targets in publications III–V, and GCPs coordinates of natural targets were measured from open national datasets in Publication II (Table 6). Additionally, image position (X, Y and h) was calculated from the onboard GNSS trajectory and used as initial observations in the BBA. The RGB images and three or four spectral bands selected from the FPI cameras had their EOPs estimated using Agisoft PhotoScan Professional software in publications I and III–V, and using SocetGXP for aircraft data in Publication II. For the remaining bands of the FPI hyperspectral images, in publications I and II, the band alignment was carried out using affine 2D image transformation (Honkavaara et al., 2013); and in publications III–V, EOPs were determined via a 3D band-matching approach (Honkavaara et al., 2017).

After estimating the camera parameters, 3D dense point clouds were generated by Agisoft Photoscan using the RGB and FPI data in Publication III. Dense point clouds were generated with the original images (quality setting in Photoscan: ultra high), doubled (high) or 4-times (medium) pixel size (Table 6). The root-mean-square errors (RMSEs) of the residuals in the image coordinates (reprojection errors in Agisoft) were estimated with less than 1.6-pixel error for all datasets in all studies (Table 6).

In the point cloud processing step, canopy (or crop) height models (CHM) were created. CHM is the difference between the digital surface model (DSM) and the digital terrain model (DTM). The DSMs were calculated by interpolating the 3D point cloud to a regular grid. DTM was determined from open national laser scanning data in the forest-related studies (I, II and V). In agricultural studies, DTM extraction was more critical because the height of a crop is low compared to trees in forests, meaning that the uncertainty of the DTM accumulates rapidly in the CHM. Furthermore, in agriculture areas, the terrain level is affected by farming activities, such as tillage, thus the open national datasets are not up-to-date in most cases. Therefore, the DTM was extracted from the photogrammetric point cloud itself using the 'classify ground points' tool of Agisoft PhotoScan, as described by Viljanen et al. (2018).

Table 6. Summary of geometric processing. Quality setting parameter refers to a parameter used in photoscan dense matching: Ultrahigh: images with original pixel size, High: doubled pixel size, Medium: 4-times pixel size.

	Software	Ground control points	Reprojection error (pix)	Quality setting parameter in dense matching
Publication I	PhotoScan	No	<0.6	High-Medium
Publication II	SocetGXP, PhotoScan	Natural	<1.3	High-Medium
Publication III	PhotoScan	Artificial	<1.6	Ultrahigh
Publication IV	PhotoScan	Artificial	<1.3	High
Publication V	PhotoScan	Artificial	<0.6	High

4.2 Radiometric processing

The aim of radiometric processing is to create accurate reflectance orthomosaics. Several physical conditions during data collection, such as atmospheric effects, variable weather conditions, sensor non-uniformities and illumination geometry affect the values measured by the image sensor. In radiometric processing, these effects are minimized so that the variation in the orthomosaics is only caused by the object itself.

The radiometric processing of the FPI-based spectral cameras followed the approach developed by Honkavaara et al. (2013; Honkavaara and Khoramshahi, 2018). The approach can be divided into four parts: (1) sensor correction, (2) relative correction due to the illumination changes, (3) anisotropic corrections using the bidirectional reflectance distribution function (BRDF), and (4) absolute reflectance transformation.

First, sensor correction—including a photon response non-uniformity (PRNU) and dark signal correction—was carried out using methods provided by the VTT as a developer of the sensor (Mäkynen et al., 2011). Besides, the effect of different wavelengths in the centre and border of the frame (i.e. the spectral smile) can be corrected in the sensor correction phase by combining data from different bands. Next, relative and anisotropic correction parameters were solved using the radiometric block adjustment (RadBA) in-house software (Honkavaara et al., 2013; Honkavaara and Khoramshahi, 2018). The algorithm considers pixel values of the same object area observed from multiple overlapping images (radiometric tie point) and estimates the radiometric model parameters by minimizing the differences between observed and modelled values. The relative model parameter concerns the changes in illumination between data cubes. Irradiance measurements during the flight are measuring the same phenomena and they can be given as a priori value for adjustment. Irradiance measurements were collected from drones with wide-bandwidth relative irradiance sensors integrated into spectral cameras and from the ground with ASD spectroradiometer. Different surfaces reflect the light in different ways, depending on the direction of incoming light from the sun and outgoing direction to the sensor in passive remote sensing. BRDF is a function that models this phenomenon. RadBA uses the radiometric tie point observations to solve the parameters of the BRDF model developed by Walthall et al. (1985). Finally, the absolute reflectance transformation was done using the reflectance reference panels and

applying the empirical line method (Smith and Milton, 1999), which is a commonly used way to take atmospheric effects into account in low altitude mapping (Aasen et al. (2018). The model for the reflectance factor was thus:

$$R_{jk}(\theta_i, \theta_r, \varphi) = \frac{\frac{DN_{jk}}{a_{relj}} - b_{abs}}{a_{abs}} \, anif(\theta_i, \theta_r, \varphi)_j \qquad (1)$$

where $R_{jk}(\theta_i, \theta_r, \phi)$ is the hemispherical directional reflectance factor (HDRF) (Schaepman-Strub et al., 2006) of the object point k in image j; θ_i and θ_r are the incident illumination and reflected light (observation) zenith angles; ϕ is the relative azimuth angle of reflected and incident light, $DNjk$ is the grey value observed by the camera of the object point k in image j; a_{abs} and b_{abs} are the linear parameters to absolute reflectance transformation, a_{relj} is the relative correction parameter and $anif(\theta_i, \theta_r, \phi)$ is the anisotropic factor.

Radiometric processing was performed using the above-mentioned procedure in all publications with small modifications (Table 7). The weather during the data acquisition has an impact on the image data and therefore on radiometric processing strategies. In publications I–IV, the datasets were collected on both sunny and cloudy conditions, but the data collection for Publication V happened on a sunny and cloud-free day (Table 7). From the sensor corrections, PRNU and dark signal correction were applied to all FPI datasets, while a spectral smile correction was applied only to datasets used in publications I and II. Spectral smile effects are significant only on the border of the images. Therefore, due to large overlaps (over 60% of the side and 80% in forward direction) of the imagery data in publications III–V, the effect for the orthomosaics values was considered to be minimal. The use of the spectral smile correction led to a reduced number of spectral bands from the original 36 to 22 bands. The results of radiometric block adjustment were assessed visually and statistically, and the best correction strategy was chosen for all datasets. A relative correction was used especially during the cloudy and varying weather conditions, and calculation was supported in some cases by irradiance measurements (Table 7). The BRDF correction was mainly used in sunny weather and especially for agricultural targets where the variation in values is naturally lower than in forests. In publications I–III and V, absolute reflectance transformation was done manually using a reference image. Since the development of RadBA software (Honkavaara and Khoramashahi, 2018), the absolute parameters were also adjusted automatically in Publication IV (Table 7). Finally, reflectance orthomosaics were calculated by following Formula 1 and orthorectifying the images in RadBa software. The reflectance output of RadBA is HDRF (Honkavaara and Khromashahi, 2018) but is referred here simply as reflectance orthomosaic.

For the RGB camera, the orthorectification was carried using Agisoft Photoscan, and the absolute calibration using the reference panels and exponential function were performed in publications IV and V.

Table 7. A summary of radiometric processing of the spectral camera in four correction steps: sensor (PRNU: photon response non-uniformity, dark: dark signal, smile: spectral smile correction) relative (UAV/ASD irrad: parameter calculation was supported by irradiance measurements from a drone (UAV)/ground (ASD), anisotropic and absolute correction (ref: transformation was done using a reference image, adj: parameters were adjusted in RadBA).

	Correction step				
	Weather	**Sensor**	**Relative**	**Aniso-tropic**	**Absolute**
Publication I	Sunny/Cloudy	PRNU, dark, smile	Yes (UAV irrad)	Yes/No	Yes (ref)
Publication II	Sunny/Cloudy	PRNU, dark, smile	Yes (UAV irrad)	Yes/No	Yes (ref)
Publication III	Sunny/Cloudy	PRNU, dark	Yes (ASD irrad)	Yes/No	Yes (ref)
Publication IV	Sunny/Cloudy	PRNU, dark	Yes (UAV irrad)	Yes/No	Yes (adj)
Publication V	Sunny	PRNU, dark	No	No	Yes (ref)

4.3   Feature extraction

Feature extraction was the third step in the method's workflow (Figure 4). The aim of feature extraction is to calculate features from the remote sensing data for the estimation and classification process. The inputs for feature extraction were reflectance orthomosaics and CHMs, and the outputs were numerical feature sets, such as average, percentiles, maximum and minimum reflectances, and vegetation indices or heights. The values were computed from regions defined in the orthomosaics and CHMs, which corresponded to a group of pixels in a window (m x m) or the values within a certain diameter from the centre coordinate. The feature extraction process was divided into three steps (Figure 4). Firstly, the area of interest was defined, including the location and dimension. Secondly, the extracted values were used to calculate the interested features. Thirdly, extracted features were organized into one or multiple feature sets to be used in the estimation and classification phase.

The location of the biophysical ground truth samples was defined during the data collection, but the dimensions were not necessarily defined (Section 3.1). The object, such as a tree, consists of multiple observations since the GSDs of the remote sensing data were significantly smaller than the site of the objects. In Publication I, the area was defined as a circle, 1m in diameter, centred at the top of the tree. In Publication II, the GSD of spectral images collected from aircraft was 0.5 m, and the features were computed from a 3 x 3 –pixel area. In Publication V, the trees were delineated by selecting pixels above 5 m ground level based on the CHM to extract features. In agricultural-related studies, the size of the extracted areas in remote sensing data followed similar dimensions of the area where the field sample was collected to calculate the biophysical ground truth. The plots of experimental grass sites (Publications III and IV) were clear-bounded and digitized directly to the orthomosaics.

In publications I and II, features were extracted for the same trees of the ground truth samples and also for other trees in order to produce tree health maps of the entire study area. Individual trees were automatically detected in both studies. In the case of drone data, tree crowns were segmented based on a

watershed segmentation algorithm (Hyyppä et al., 2001). Input data for the algorithm was the CHM, which was produced using DSM and DTM as described in section 4.1. First, CHM was filtered (smoothed) and then the treetops were extracted based on local maxima. The method is called watershed segmentation due to the analogy of the last step to water flows; if CHM is turned upside down, one segment is formed from pixels from where water would flow to the same local minima (a tree top). For the aircraft spectral data, the reflectance orthomosaics were used for detecting individual trees. The method takes advantage of the fact that treetops are the brightest pixels in the orthomosaics and includes classification and filtering steps before the treetop is defined based on the local maxima.

The values of pixels inside the defined area built the set of numbers from which different descriptive statistics were then calculated to be used as features. The arithmetic mean (i.e. average) was calculated in all publications. In the agricultural-related publications III and IV, it was the only statistical feature for spectral data (Table 8). In forest-related studies, the variation of reflectance values is high, especially in sunny illumination, causing a bright and dark side for treetops, which might mean that the average is not the optimal statistic to be used as a feature. Thus, in publications I and II, the average of the six brightest pixels was calculated. And in Publication V, the average of the brightest 25% and 50% and the standard deviation were calculated.

The spectral features were calculated from all spectral bands and for each of them in all publications. In addition, vegetation indexes were calculated in publications I–IV. The development of vegetation indices has a long tradition in remote sensing, and the combination of two or more spectral bands can improve the sensitivity to the vegetation properties and reduce the effects of radiometric calibration uncertainties and other disturbances. In publications I and II, vegetation indices were calculated following the well-known formula for the NDVI. In publications III and IV both FPI2012b-based and RGB-based indices were calculated and selected based on the earlier literature. (Formulas can be found in Publications I-IV.) Indices were not used in Publication V. Instead, different numbers of principal components were calculated in order to reduce the dimensions of the spectral data (Table 8).

3D features correspond to the structure of the object; they were calculated from the RGB-based CHM in publications III–V and also from the FPI2012b-based CHM in Publication III. In publications III and IV, eight features were calculated: average, minimum, maximum, standard deviation and 50th, 70th, 80th and 90th percentiles. In Publication V, the 29 calculated features included percentiles, canopy densities and the proportions of vegetation points. The selection of extracted 3D features was made based on the application and the earlier literature. For instance, agricultural biomass is already directly linked to crop height (Bendig et al., 2014), but not for tree species and accordingly 3D features were selected to better describe the shape of the canopy than the actual height.

Table 8. Summary of extracted features. Calculated features: avg: average, 6_bright: average of 6 brightest pixels, std: standard deviation, avg50: average of the brightest 50% pixels, avg25: average of the brightest 25% pixels. Number of spectral features calculated from bands, indices and principal components (PC). No. 3D features: Number of calculated 3D features. No. all features: Number of all features together. *In addition to 11 hyperspectral indices, 4 multispectral indices were calculated. **Different numbers of principal components were extracted for radiometrically not-corrected and corrected.

	Camera	Calculated spectral features	Number of Spectral features			No. 3D features	No. all features
			Bands	Indices	PC		
Publication I	FPI2012b	avg, 6_bright	22	3	-	-	50
Publication II	FPI2012b	avg, 6_bright	24	3	-	-	54
Publication III	FPI2012b	avg	36	11	-	8	55
	RGB	avg	3	2	-	8	13
Publication IV	FPI2012b	avg	35	11 (+4)*	-	-	50
	RGB	avg	3	8		8	19
Publication V	FPI Rikola VNIR	avg, std, avg50, avg25	36	-	9, 17**	-	180, 212**
	FPI SWIR	avg, std, avg50, avg25	24	-	12, 15**	-	144, 156**
	RGB	avg, std, avg50, avg25	3	-	-	30	33

The extracted features were then organized into multiple feature sets (Table 9). The use of multiple feature sets allows for a comparison of the effects of different data measurement parameters on estimation or classification accuracy (Objective 3). Feature sets were selected separately in all studies based on the data and aims of the study. In publications I and II, FPI2010b-based spectral bands and indices form the sets; in Publication II, they were organized separately based on two different spatial resolutions (9 cm and 50 cm). Various spatial resolutions were also compared in Publication III. The effects of radiometric correction were studied in publications III and V, forming the feature sets with and without radiometric calibration. The performance of different spectral sensors was in publications III–V (Table 9). Spectral and 3D features were also integrated into the same feature sets and compared to performance when only one of them was used in publications III–V.

Table 9. The summary of feature sets according to the objective of the study effect on different data measurement parameters (Objective 3).

	Radiometric processing	Spectral sensor	Spatial resolution	Integration of spectral and 3D data	Number of feature sets
Publication I					2
Publication II			x		4
Publication III	x	x	x	x	21
Publication IV		x		x	5
Publication V	x	x		x	14

4.4   Estimation and classification using machine learning

Machine learning is the last step in the method workflow. It takes the remote sensing features sets and biophysical ground truth variables as input in order to produce estimation and classification models and validate them as the output results (Figure 4). Indeed, the approach is supervised learning. For the categorical parameters, the machine learning task was classification and for continuous parameters the task was estimation (Table 10). Algorithms were selected individually in the context of the study in all publications.

The k-nearest neighbour algorithm (k-NN), which has already been used for decades in remote sensing, was the selected algorithm for Publication I and an alternative algorithm in Publication V. K-NN is a simple algorithm. When used in classification, it will select the class-based on the k closest (meaning here the Euclidean distance) training samples in the feature space. The performance of K-NN was calculated with many values of k, and the best selected was 3–4 in both publications. Feature sets in Publication V consisted of hundreds of features, so feature selection was necessary. The genetic algorithm (Broadhurst et al., 1997) was used there for feature selection by searching for a subset of variables that maximize overall classification accuracy.

The Support Vector Machine (SVM) algorithm (Boser et al. 1992) was applied for the classification task in Publication II. SVM attempts to determine the optimal separation line (or hyperplane in high-dimensional spaces) by maximizing the gap between classes. The radial basis function was used as a kernel to handle nonlinearities, and its parameters were optimized by applying a cross-validation search. The biophysical variables in Publication II were health classes of spruce (healthy, infested and dead), but the number of observations was not equal. Especially the infested class was in the minority, i.e., the data was imbalanced. This could lead to an underestimation of this important class for the application because, in basic mode, SVM maximizes the overall accuracy. For that reason, the classifications were also done with a modified cost function in order to have an equal total cost for each class. SVM is also sensitive to the scale of different features. Although the reflectance and indices used as features in this study were already within the limited range, they were also scaled individually to the same range. The implementation was done in Matlab using the LibSVM tool (Chang and Lin, 2011).

The random forest (RF) algorithm (Breiman, 2001) was applied in publications III–V. RF is based on a large number of decision trees that are trained independently on a random subset of data. When RF is used to classify, the output class is the mode of all the individual decision trees. For estimating continuous variables, the output prediction is the average prediction of all the trees. This means that RF cannot extrapolate, i.e., predict values higher or lower than the range in the training data. The advantages of RF (compared to SVM, for example) are that RF requires relatively lower optimization of parameters, the range of features can vary, and the feature selection is not crucial; but in contrast, it provides knowledge about feature importance (Belgiu and Drăguţ 2016). The RF implementation in Weka software, mainly via python scripts, was used in publications III and IV. And the randomForest package in the R statistical software was used in Publication V.

Linear regression models were also used in publications III and IV, in order to form a reference method to demonstrate the predictive power of RF in comparison to classical linear methods. A simple linear regression (SLR) model was used in Publication III by selecting the variables with the highest correlation coefficient to the explanatory variables. In Publication IV, multilinear regression (MLR) models implemented in Weka software were used, and multiple features were selected, based on backward elimination and the Akaike information criterion (Akaike, 1974).

The accuracy of algorithms was assessed using the common method, called leave-one-out cross-validation (LOOCV), in all publications (Table 10). In LOOCV, one observation is used as testing data and the rest for training data, and the process is repeated for all observations. LOOCV is well-suitable particularly also when only few samples are available, and generally provides slightly optimally biased results (Varma and Simon, 2006). LOOCV assesses the specific model built with specific data but it does not necessarily indicate whether the model is generalizable enough to be used in other conditions. Indeed, the hold-out method was used in publications II and IV. In Publication II, the hold-out method was applied to study the smaller subset from a limited geographical area as training data sufficient to build accurate classifiers and a model sensible to different spatial resolution. In Publication V, hold-out was used to learn if the model was general enough to be used in other similar type of grass field.

In the classification tasks, general statistics were calculated based on the confusion matrix that included the overall accuracy, Cohen's kappa (Cohen, 1968) and the producer's and user's accuracy in individual classes. In the estimation tasks, the Pearson correlation coefficient (PCC), root mean square error (RMSE) and normalized RMSE using the average of reference values (RMSE%) were calculated.

Table 10. Summary of machine learning algorithms and accuracy assessment methods. LOOCV: Leave-one-out cross-validation, HO: hold-out.

	Task	Algorithms	Accuracy assessment
Publication I	Classification	K-nearest neighbour (k-NN)	LOOCV
Publication II	Classification	Support vector machine (SVM)	LOOCV, HO
Publication III	Estimation	Random forest (RF), Single linear regression (SLR)	LOOCV
Publication IV	Estimation	Random forest (RF), Multilinear regression (MLR)	LOOCV, HO with independent test data
Publication V	Classification	Random forest (RF), K-nearest neighbour (k-NN)	LOOCV

5. Results

This chapter is divided into three sections that present the results related to each objective defined in Section 1.2. Section 5.1 presents the main results considering the classification of health status and species of individual trees (Objective 1). Section 5.2 introduces the estimation results of agricultural crop parameters (Objective 2). Finally, Section 5.3 presents the effects of radiometric processing, spectral and spatial resolution, and the integration of spectral and 3D data on classification and estimation accuracy (Objective 3).

5.1 Classification of health status and species of individual trees

The developed workflow (Figure 4) was employed to detect individual trees and classify them based on health status in publications I and II and based on species and genera in Publication V. The health status of mature spruces were successfully classified into three classes that present different colonization phases of the outbreak caused by European spruce bark beetles. The K-NN method achieved an overall accuracy of 76% (kappa: 0.60) and an SVM overall accuracy of 81% (kappa: 0.70) when 78 spruces were classified as 'healthy', 'infested' or dead, using the spectral features from the drone data. This result was achieved using three indices, which were formed from five spectral bands (551, 627, 726, 773 and 794 nm) selected by analysis of variance within the health classes). When the 330 spruces were classified using spectral features from small manned aircraft, the best observed overall accuracy assessed with LOOCV was 79% (kappa: 0.54). The overall accuracy was still at the same level (80%, kappa: 0.51) when only the features from the 78 spruces inside the area covered by the drone flight were used to train the model and 252 were used as testing data. This indicates that ground truth observations can also be collected only from smaller representative areas. Even more interestingly, the overall accuracy remained at the same level (81%, kappa: 0.51) when applying the classifier model estimated from the drone data (78 spruce area) to classify the trees on the aircraft data. This means that the estimated classifier was not sensitive to spatial resolution (GSD: 9cm from drone vs 50cm from aircraft) or the time difference of three weeks between the two data collections.

The classification of spruce health status was also calculated for entire test areas based on automatically detected trees and classification models. These results were visualized to spruce health maps, which may be used to detect hotspot areas of the infestation (Figure 5).

The classification of 26 tree species from 14 different genera was studied in Publication V. Integrating spectral features extracted from novel FPI-based VNIR and SWIR cameras and photogrammetric 3D features led to the highest classification accuracy. K-NN supported with GA feature selection achieved an overall accuracy of 82% (kappa: 0.81) and RF 78% (kappa: 0.76) for species and 84% (kappa: 0.87) and 82% (kappa: 0.78) for genus, respectively. Coniferous trees were typically well-discriminated considering the genus, but the confusion of species within the same genus appeared. The genus of broadleaved trees was typically more confused than that of coniferous trees. However, the situation was the opposite when considering species because the broad-leaved tree genera were mainly represented by only one species, while the coniferous genera were represented by seven species.
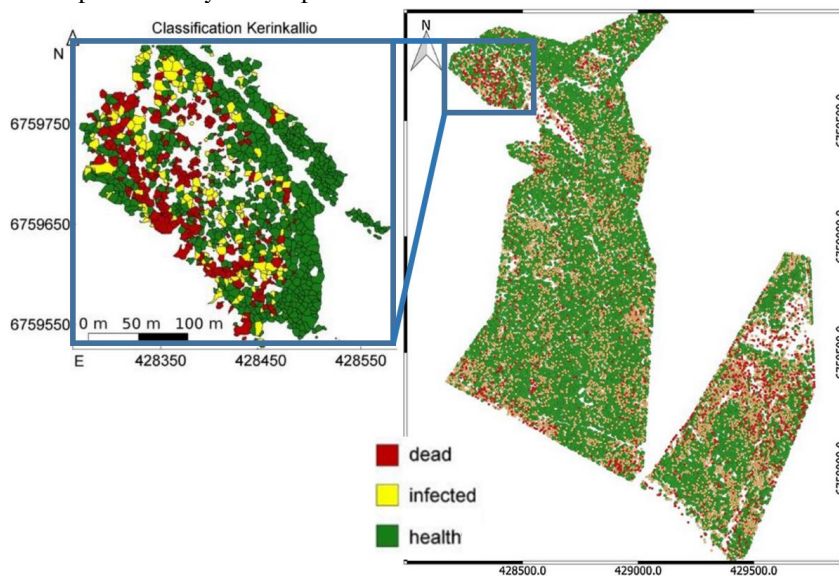
Figure 5. Visualized spruce health maps. (Modified figures from Publications I and II)

5.2 Estimation of agricultural parameters

Various crop parameters of barley and grass for silage were estimated in publications III and IV. Crop parameters were estimated using variable feature sets. Table 11 summarizes the results considering the models which combine the spectral features with the highest spectral resolution (FPI) and 3D features with the highest spatial resolution (RGB).

Above-ground biomass is the fundamental parameter to measure the quantity of the agricultural yield. Both the fresh yield (FY) and the dry matter yield (DMY) were estimated in all study areas. In general, the estimation accuracy was similar for both biomass variables, which was expected since they are highly correlated to each other. However, the accuracies differ among the datasets. For barley fresh biomass, the RF outperformed the SLR classifier, with an RMSE% of 31% and a PCC of 0.96. For Vihti grass dataset biomass estimation, SLR led to better accuracy with an RMSE% of 1.6% and a PCC of 0.85. The ground truth

of the Vihti grass dataset consists of only 8 samples with a low standard deviation, meaning that RF was not able to create a stable model with so few samples. For the Jokioinen datasets, RF and MLR led to similar results. The best accuracy was obtained with an MLR for the FY of primary growth (RMSE%: 12%, PCC: 0.98). The Jokioinen datasets consist of about 100 multitemporal samples with a high standard deviation, which explains the higher RMSE% than in the Vihti dataset.

Both the nitrogen uptake (NU)—the amount of nitrogen in the biomass (kg/m^2 in Publication III and kg/ha in Publication IV)—and the nitrogen concentration (Ncont; (10g/kg DM in Publication III and g/kg DM in Publication IV) were estimated for the Vihti barley and Jokinen grass datasets. For barley, the RF outperformed the SLR classifier, with RMSE% of 21.6% and PCC of 0.96 for NU. For the Jokioinen grass datasets, the RMSE% varied from 10.6% to 20.4% and the PCC from 0.84 to 0.96, depending on the stage of growth and classifier (Table 11).

The feeding quality parameters describe the quality of grass swards considering the nutrition process of animals, particularly ruminants. Various feeding quality parameters were estimated for the Jokioinen datasets separated for primary and regrowth. This separation was done in the regrowing season due to differences in crop properties after the harvesting of the first yield, primary growth. Digestibility of organic matter (D-value) describes the available energy in the forage dry matter; this is a feeding-quality parameter, which reduces quickly in the Nordic countries, especially during the primary growth stage. RF- and MLR-based estimators provided similar estimation accuracies for the D-value. The RMSE% (1.7–2.1%) and PCC (0.93–0.95) of the primary growth were slightly better than in the regrowth phase (Table 11). Similar results were obtained also for other feeding quality parameters, neutral detergent fibre (NDF), indigestible neutral detergent fibre (iNDF) and water-soluble carbohydrates (WSC).

Table 11. The normalized root-mean-square errors (RMSE%) and Pearson correlation coefficient (PCC) of estimated crop parameters (FY: fresh yield; DMY: dry matter yield; D-value: digestible organic matter in dry matter; iNDF: indigestible neutral detergent fibre; NDF: neutral detergent fibre; WSC: water-soluble carbohydrates; Ncont: nitrogen concentration; NU: nitrogen uptake) using FPI-based spectral features and RGB-based 3D features and Random Forest (RF) and Single linear regression (SLR) for the Vihti datasets, and RF and Multiple linear regression (MLR) for the Jokioinen datasets. The accuracy was assessed based on leave-one-out cross-validation (LOOCV).

Study area, crop	Crop parameter	RF		SLR/MLR	
		RMSE%	PCC	RMSE%	PCC
Vihti, barley	FY	31.0	0.96	39.1	0.94
	DMY	33.2	0.95	41.4	0.92
	Ncont	35.6	0.91	52.5	0.80
	NU	21.6	0.96	28.8	0.94
Vihti, grass	FY	4.8	0.49	4.5	0.71
	DMY	2.3	0.67	1.6	0.85
Jokioinen, grass, primary growth	FY	13.4	0.98	12.0	0.98
	DMY	14.7	0.97	15.6	0.97
	D-value	2.1	0.93	1.7	0.95
	iNDF	20.7	0.92	16.4	0.95
	NDF	3.5	0.94	3.2	0.95
	WSC	12.4	0.91	12.0	0.92
	Ncont	10.6	0.84	13.2	0.93
	NU	13.6	0.96	14.7	0.96
Jokioinen, grass, regrowth	FY	17.2	0.96	12.9	0.96
	DMY	16.1	0.94	13.1	0.96
	D-value	2.5	0.86	2.6	0.86
	iNDF	24.8	0.84	25.7	0.83
	NDF	4.7	0.81	5.1	0.79
	WSC	22.0	0.88	19.3	0.91
	Ncont	12.9	0.84	11.2	0.89
	NU	20.4	0.90	18.3	0.92

In Publication IV, the models estimated from the training datasets were applied in independent test area datasets to verify if the models could be generalized to estimate with sufficient accuracy the crop parameters of other areas of the same kind of grass fields. Multitemporal models, based on the data collection of 3–4 dates, were also compared to models that were trained separately for each date. Figure 6 presents the results of these two experiments for DMY, D-value and NDF.

Models based on individual dates provided RMSEs of 125–498 kg/ha and a multitemporal RMSE of 389 kg/ha for the DMY training data in the primary growth stage (Figure 6). Similar findings of accuracy for multitemporal and individual date-based models were also observed for the regrowth phase and the D-value. Since the performance of multitemporal models was yielding an accuracy similar to the individual date-based models, this indicates that remote sensing features collected on different dates were comparable enough to build stable estimators for these parameters. Overall, when machine learning models are tested with independent test data, the accuracy reduces compared to training accuracy.

In the case of primary growth, the RMSE values of the testing data for the DMY and D-value were 1.3–1.5 higher than for the training data and 1.9–2.3 in the case of regrowth. The estimation results of NDF were not as consistent as the estimation of the DMY and D-value.
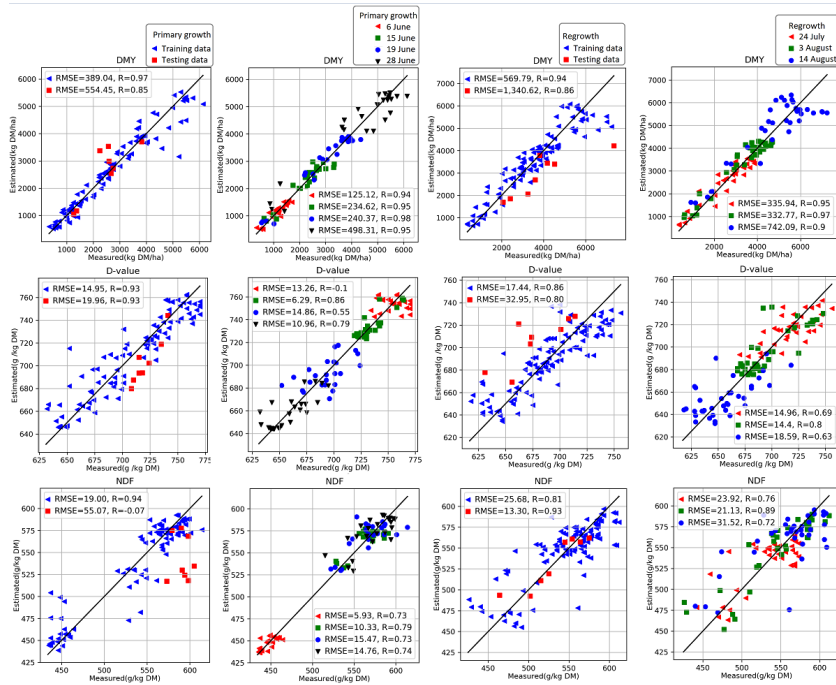

Figure 6. Estimated and measured reference values for the training and testing data for the primary (1 column) and regrowth (3 column) phase and for models for each date (2 and 4 column) using FPI-based spectral and RGB-based 3D features and RF estimator. DMY: dry matter yield; D-value: digestible organic matter in dry matter; NDF: neutral detergent fibre; RMSE: absolute root mean square error; R: Pearson correlation coefficient. (Modified figure from Publication IV).

5.3 Effects of measurement parameters on classification and estimation accuracies

5.3.1 Radiometric processing

The effect of radiometric processing on estimation and classification accuracies was studied in publications III and V. The average RMSE% of biomass and nitrogen parameters were respectively 19% and 27% lower when relative and anisotropic corrections were applied than when such corrections were not applied (Figure 7). An absolute radiometric correction yielded an improvement of 3–11% compared to the uncorrected data for the classification accuracy of the tree species and genus with FPI Rikola VNIR and FPI SWIR cameras. The improvement was greater in species classification than in genus classification and greater with the FPI SWIR camera than with the Rikola VNIR camera.
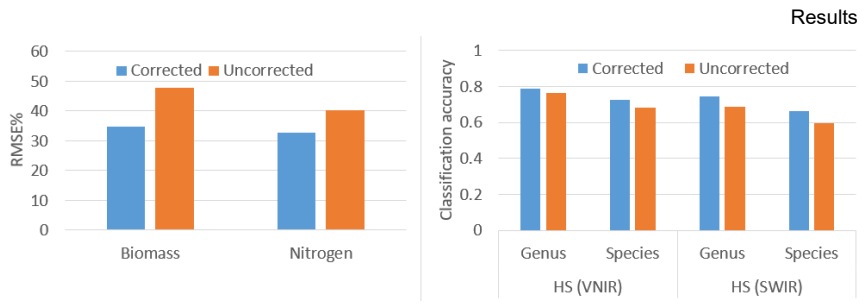
Figure 7. Left: Average RMSE% of biomass and nitrogen estimation using radiometrically corrected and uncorrected data. Right: Overall classification accuracy of tree species and genus using hyperspectral VNIR and SWIR sensors with and without radiometric correction.

5.3.2 Spectral sensor

In publications III–V, the performance of spectral sensors was compared (Section 3.2). Hyperspectral (HS) cameras performed 12–14% better than RGB when comparing the average RMSE% in biomass and nitrogen estimation (Figure 8). A similar improvement between RGB and hyperspectral cameras in the VNIR range also occurred in tree species and genus classification experiments. The SWIR range hyperspectral camera data achieved approximately 10% better classification accuracy than RGB but 3% worse than the VNIR camera (Figure 8). The combination of spectral features from the SWIR and VNIR camera did not significantly improve the classification accuracy compared to the use of only VNIR-based spectral features.

Figure 8. Left: Average RMSE% of biomass and nitrogen estimation using hyperspectral (HS) and RGB sensors. Right: Overall classification accuracy of tree species and genus using RGB, hyperspectral VNIR and SWIR sensors.
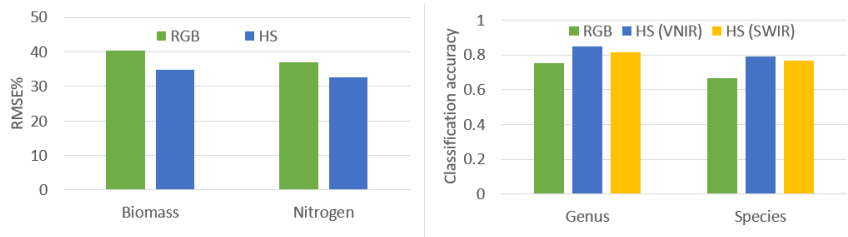
In addition to RGB and hyperspectral cameras, a simulated multispectral camera—consisting of the RGB and one NIR band from FPI camera—was conducted to evaluate the performance of the spectral resolution in grass quantity and quality parameter estimation. As expected, the RMSE% decreased when the spectral resolution increased from 3 wide RGB bands from the visible spectral range to 36 relatively narrow hyperspectral bands from the VNIR range when the estimator was assessed and trained for both quantity and quality parameters as well as for the primary and regrowth phases (Figure 9). When models were tested with independent datasets, the RGB models still presented the highest RMSE%, while the lowest RMSEs% were obtained with MS in quality parameters estimation for both primary and regrowth and also for the quantity parameter estimation in the regrowth phase. This hints that machine learning models based on MS features were more generalizable for these feature sets than models based on HS features.

Figure 9. The average RMSE% of grass biomass (FY and DMY) and feeding quality (D-value, iNDF, NDF, WSC, Ncont, NU) parameter estimations using RGB, MS (multispectral) and HS hyperspectral features. The results are shown separately for the primary and regrowth phase and for training and testing data.

5.3.3 Spatial resolution

The effect of spatial resolution on classification and estimation accuracy was studied in publications II and III. Spruce health status was estimated with an overall accuracy of 0.81, using spectral features with a spatial resolution of 9 cm and an accuracy of 0.73 when using a spatial resolution of 50cm (Figure 10). However, when spectral features were used for biomass estimation in the barley field, the spatial resolution did not significantly affect the RMSE%, especially with RF estimators. For 3D features, in the case of the spatial resolutions of 3.7 cm and 5 cm, the difference in flying height was remarkable enough (140 m and 450 m) to affect the CHM quality, which reflected the RMSE% being 30% better with a GSD of 3.7 cm than with a GSD of 5cm. Interestingly, a GSD of 10 cm resulted in a similar or better estimation accuracy than 5 cm, depending on the estimator (Figure 10).
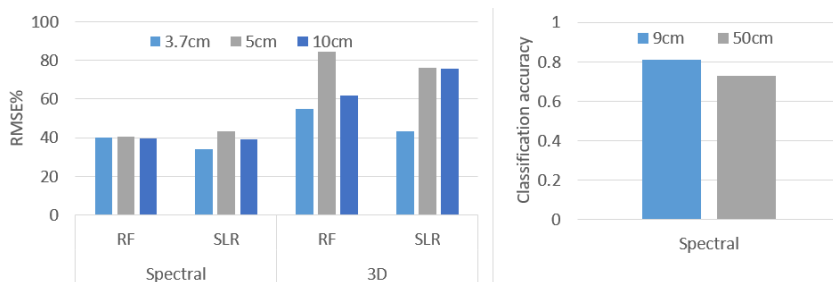
Figure 10. Left: Normalized root mean squared (RMSE%) of biomass estimation using RGB-based spectral and 3D features, RF and SLR classifiers and spatial resolutions of 3.7 cm, 5 cm and 10 cm. Right: Classification accuracy of spruce health status with spatial resolution of 9 cm and 50 cm.

5.3.4 Integration of spectral and 3D features

Integration of spectral and 3D features was investigated in publications III–V. Overall, the classification accuracy was 0.78 for the tree genus and 0.74 for the tree species when using only spectral features (Figure 11). The combination of both spectral and 3D features resulted in overall accuracies of 0.84 and 0.81, meaning that the addition of 3D features improved the accuracy by approximately 8%. The integration of both feature sets also improved biomass and nitrogen estimation accuracies of barley by 24–41% compared to only 3D features, and 8–12% compared to only spectral features (Figure 11).
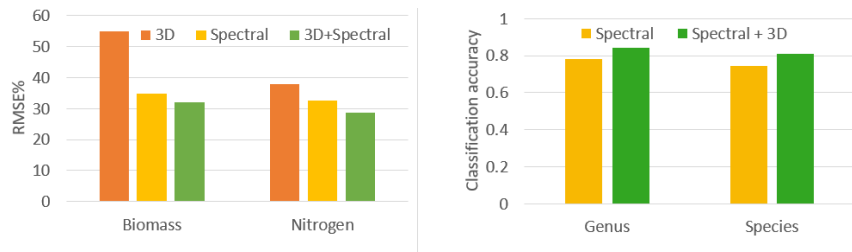
Figure 11. Left: The average RMSE% of barley biomass and nitrogen parameter estimation using RGB-based 3D, FPI-based spectral and a combination of both. Right: Classification accuracy of tree genus and species using spectral and a combination of spectral and 3D features.

When both feature sets were combined to estimate quantity parameters of grass in primary growth, the RMSE% in the training data was smaller than when using only spectral or 3D features (Figure 12). For the quality parameters in primary and regrowth, and for the quantity parameters in the regrowth phase, the inclusion of 3D features did not improve the estimation accuracy significantly. However, the RMSE% reduced less with 3D features when the primary growth quantity model was assessed in the independent test area, indicating that 3D features were more stable than spectral features in this estimation case. The quality parameters did not improve with the inclusion of 3D features, based on the RMSE% of the testing data.
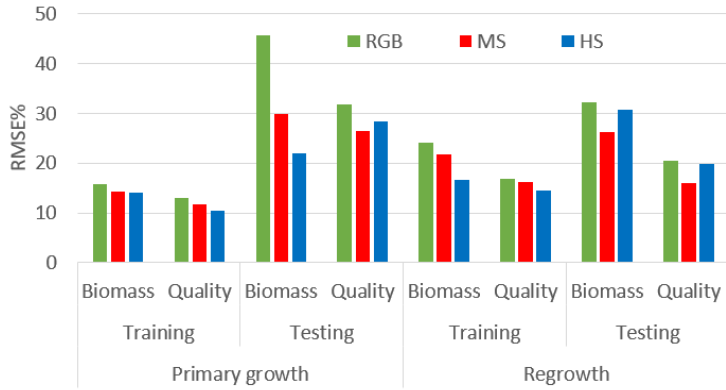

Figure 12. The average RMSE% of grass biomass (FY and DMY) and feeding quality (D-value, iNDF, NDF, WSC, Ncont, NU) parameter estimations using RGB-based 3D, FPI-based spectral and a combination of both. The results are shown separately for the primary and regrowth phase and for training and testing data.

6. Discussion

This chapter is divided into two sections. First, the scientific and practical implications concerning each objective are discussed. Secondly, the limitations and recommendations for future research are presented.

6.1   Scientific and practical implications

Objective 1: To develop drone-based 3D and spectral remote sensing techniques for classifying the health status and species of an individual tree

Remote sensing workflows to evaluate individual tree health status were developed in publications I and II. Spruces in a forest suffering from bark beetle invasion were classified based on their health status (healthy, infested or dead) with an overall accuracy of 81% using drone-based hyperspectral imaging. The spectra of dead spruce clearly differ from other classes, but the difference between the spectra of healthy and infested spruce was small, resulting in the producer's accuracy for the infested class being lower than for the healthy and dead classes. For instance, Abdullah et al. (2018a) reported that VNIR range spectra of needles from infested and healthy spruces differ statistically due to changes of in needle biochemical properties, such as chlorophyll and foliar nitrogen concentrations. Publications I and II showed that this difference is possible to detect also from a drone at tree level. In particular, forest health mapping using drone-based hyperspectral imaging at the individual tree level was demonstrated for the first time in Publication I. Other studies, which use hyperspectral sensors from drones for detecting insect damage, are still rare. But in China, they have been employed for mapping damage by the pine shoot beetle (Tomicus spp) (Lin et al., 2019; Liu et al., 2020) and by d. tabulaeformis (Zhang et al., 2018).

After publications I and II, drone-based mapping of damage caused by the European spruce bark beetle has been investigated—especially in the Czech Republic for reasons mentioned in the introduction—with multispectral sensors in the VNIR range (Klouček et al., 2019; Minarik et al., 2020; Brovkina et al., 2018). For instance, Klouček et al. (2019) collected multispectral time series and classified the healthy and infested trees with the Maximum Likelihood classifier for an overall accuracy of 78–96%, which is similar to the results in publications I and II. An interesting approach employing only RGB images with a CNN was conducted in Russia, where the mapping of an invasion caused by another bark beetle (*Polygraphus proximus*) in a fir forest (*Abies sibirica*) was studied

(Safonova et al., 2019). They first detected the tree crowns and then classified them into four health classes and reported the accuracies of classes from 92.0% to 98.8%.

Tree species and genus recognition were studied in Publication V, where the capability of two novel FPI-based sensors operating in the VNIR and SWIR range was comprehensively demonstrated for the first time in a forest environment. The description of the same dataset was earlier published by Näsi et al. (2016) and in a preliminary analysis by Tuominen et al. (2017). The best overall classification accuracy obtained was 82.3% for 26 species and 86.9% for 14 genera, respectively, in a species-rich arboretum. The comparison of several studies involving drone-based spectral imaging for tree species classification published in the literature is not straightforward due to a significant difference in the number of tree species, biomes and natural or managed forests. Such features affect the performance of classifications tasks. Nevalainen (2017) reported a classification of four species in a boreal forest with an overall accuracy of 95% using multilayer perceptron and RF classifiers. Later, the same dataset (but using only three out of the four species) was studied by Nezami et al. (2020) employing a CNN-based deep learning approach. They reported an overall accuracy of 98.3% using point cloud, hyperspectral and RGB layers and, interestingly, an overall accuracy of 96% using only RGB data. Drones and FPI-based hyperspectral sensors have also been used to classify tree species in Brazil (Sothe et al., 2019; 2020, Miyoshi et al., 2020a and 2020b). Sothe et al. (2019) reported a maximum overall accuracy of 72.4% when structural features from the photogrammetric point cloud and spectral features were considered to classify 12 tree species using the SVM classifier. Miyoshi et al. (2020a) used similar spectral data and RF algorithms and reported an overall accuracy of 50% for the classification of eight emergent tree species in a highly complex regeneration area in the Brazilian Atlantic forest. From a machine learning perspective, these studies were closer to the experiments in Publication V than to studies with only a few tree species in a boreal forest since the number of tree species was high and the analysis methods were similar, yielding quite similar results. However, even more recently, CNN-based deep learning methods were reported to further improve the classification results (Miyoshi et al., 2020b; Sothe et al., 2020).

Before the development of drone and sensor technology, the area- or pixelbased method was mostly used in mapping bark beetle damage (e.g. Lausch et al., 2013; Fassnact et al., 2014). Fine spatial resolution enables the individual tree-based approach, which provides a new level for forestry management purposes. The information about tree species or infested trees could even be distributed directly to forest harvesters for logging operations to avoid the spread of damage. In the proposed approach, individual trees were also detected based on collected remote sensing data but, in the operational system, basic forest inventory attributes, such as the location of trees, species and height, can already exist in the context of precision forestry (Holopainen et al., 2014). Various efficient remote sensing technologies, such as aerial, terrestrial and mobile laser scanning (ALS, TLS, MLS), can provide this information (e.g., White et al., 2016; Kaartinen et al., 2012; Liang et al., 2016; Jaakkola et al., 2010). However, dronebased photogrammetric point clouds have been employed especially for individual tree-height estimation (Mikita et al., 2016, Guerra-Hernández et al., 2017, Moe et al., 2020) and spectral imaging for species classification (Lisien et al., 2015, Nevalainen et al., 2017). The basic forest inventory attributes are relatively

stable. On the other hand, forest health can change rapidly, particularly during a bark beetle invasion. Accordingly, drone-based spectral imaging is a great tool for flexible and continuous monitoring of forest health at the individual tree level, especially on a local scale. In addition, the mapping coverage potential of drones is continuously increasing (Stöcker et al., 2017; Shakhatreh et al., 2019). In Publication II, 3000 ha of urban forests were covered by a small, manned aircraft. Currently, the same area could also be efficiently collected using drones, for example, with fixed wings operating beyond-visual-line-of-sight (BVLOS). However, for regional mapping, satellite-based remote sensing is a more efficient tool, but drones have been seen to fill the gap from terrestrial and satellite-based observations (Abdullah et al., 2019a; Senf et al., 2017). Publication II showed that drone-based spectra (GSD 10 cm) can be used as a reference for data with 50 cm of GSD collected from an aircraft. This is a promising result considering the shifting of the scale from local individual tree level to regional scale covered by high-resolution satellites. However, further analysis is needed to study the advantages with lower-resolution satellites such as Sentinel 2. Stakeholders have also seen the advantages of the technology. For example, in Finland, big companies in the wood industry and the Finnish Forest Centre, which collects and shares forest-related data and enforces forestry legislation, have begun to employ drone-based mapping of bark beetle damage (Stora Enso, 2020; Metsäkeskus, 2019).

Objective 2: To develop drone-based 3D and spectral remote sensing and machine learning methods for agricultural crop parameter estimation

Drone-based remote sensing methods to estimate agricultural crop parameters were developed employing spectral and photogrammetric 3D data and machine learning algorithms in publications III and IV. In the biomass estimations, RMSE% were at a level of 31–33% for barley and 12–15% for grass in both fresh and dry biomass, respectively. Although various case studies involving drone-based spectral imaging for agricultural biomass estimation have been published, most of them utilize only spectral data and single linear regressions (Liu et al., 2019; Jenal et al., 2020). However, Karunaratne et al. (2020) conducted a similar approach, combining multispectral and 3D features to estimate the biomass of grass pasture with RF. Their result, a normalized RMSE of 16.6% for dry biomass, was at the same level (12–15%) as in Publication IV. Castro et al. (2020) proposed CNN-based deep learning methods for grass biomass estimation and reports a mean absolute error of 13%. It should be noted that the comparison of case studies is not straightforward since the various aspects, such as variability of the data and different units (Berger et al., 2020a), affect estimation accuracies, and there are different practices to report them.

Concerning the estimation of biochemical parameters, the nitrogen uptake (N kg/ha) was estimated for barley in Publication III, with an RMSE% of 21.6% and a nitrogen concentration (g N/kg in dry matter) for grass in Publication IV with an RMSE% of 11% (PCC: 0.88–0.96, R2: 0.77–0.92). In the context of feeding quality, the crude protein is usually calculated by multiplying the nitrogen concentration by 6.25, known as the factor of Jones (1931); thus, the results are comparable to studies that estimated crude protein with drone-based imaging, such as Capolupo et al. (2015), Michez et al. (2020), Barnetson et al. (2020)

reporting R^2 of 0.54-0.76 and Wijesingha et al. (2020) with a normalized RMSE of 10.6%. Another important feeding quality parameter, the D-value, was estimated with an RMSE% of 1.7–2.1% and PCC of 0.93–0.95 (R^2: 0.86-0.9) for the primary growth of grass in Publication IV. For this parameter, Michez et al. (2020) achieved an R^2 of 0.83 with a multispectral sensor, and Capolupo et al. (2015) achieved an R^2 of 0.8 for metabolic energy (ME) to which the D-value is directly related. However, the models of the above-mentioned studies related to digestibility were not tested in independent test areas, such as in Publication IV, to prove if the models are also relevant in other similar grass fields. For instance, Michez et al. (2020) stated that their models cannot be directly used at other sites due to differences in site properties and uncertainties of radiometric calibration.

As a flexible and low-cost technology, drone-based imaging has raised crop monitoring for precision agriculture to a new level (Maes and Steppe, 2019; Tsouros et al., 2019). As the idea of crop monitoring is to support management decisions to improve the sustainability of agricultural production, it is important to discuss the usefulness of drone-based crop monitoring in those management decisions, such as in planning optimal fertilizing rates and harvesting times. The study by Kaivosoja et al. (2019) showed that drone-based monitoring provided very suitable input material compared to satellite- and tractor-based monitoring to generate additional fertilization tasks in the barley field studied in Publication III. With precision fertilizing, nutrients such as nitrogen are spread based on the needs of the crop in furthering sustainable agriculture principles in the context of both the environment by reducing the runoff of nutrients to water bodies and economically by increasing the productivity of crops. Optimizing the harvesting time for silage-making is an important task especially in the Nordic countries, where the feeding quality of grass swards decreases rapidly while the biomass is increasing. The achieved accuracies of the biomass and D-value means that the optimal harvesting day is possible to find to an accuracy of 2–3 days. This accuracy can be seen as suitable for practical purposes. In comparison to other methods of evaluating the D-value in the field—such as cutting and analysing the samples in the laboratory and typically providing a single value for the field—the advantage of drone-based imaging is the ability to map the spatial heterogeneity within the field. This can facilitate the optimal use of silage by categorizing it based on feeding quality. Even though drone-based imaging is already widely applied in precision agriculture, the significance of user-friendly tools is highlighted when the technology is expanded to even wider use.

Objective 3: To assess the effects of different measurement parameters on classification and estimation accuracy

Radiometry is a basis for passive spectral remote sensing, and the importance of radiometric calibration has been known for decades (Slater, 1980). However, the effects of different radiometric processing levels in drone-based remote sensing on classification and estimation accuracies in agricultural and forestry applications has not been studied much. The relative and anisotropic corrections conducted in this work improved the biomass and nitrogen estimation accuracy in a barley field by 19–27%, and absolute calibration using the empirical

line method improved the tree species and genus classification accuracies by 3–11% (Figure 7). These results emphasize the importance of radiometric calibration in actual applications.

Assmann et al. (2018) reported that different aspects considering the radiometric calibration accumulated +-10% uncertainty to NDVI values at tundra field sites. Honkavaara et al. (2013) even reported a 40% improvement in wheat biomass estimation accuracy with radiometric calibration. However, the importance and complexity of the radiometric calibration depends of the circumstances of data acquisition. For instance, the relative calibration of individual images is very important in variable lighting conditions, absolute calibration in multitemporal data campaigns, and BRDF correction in sunny weather. The empirical line method with two or more reference panels was used to compensate for the atmospheric effects on above-canopy reflectance values. This method requires that conditions over the panels and the target of interest are equal, which is usually a relevant assumption if the panels are located in open area far from obstacles, such as trees, that can cause scattered light to the panels (Aasen et al. 2018). In the Publication V, the panels were located in relatively open areas far from a dense forest, and few individual trees were about 10 meters far from panels meaning that scattered light could cause only minor effects. In addition to these radiometric processing options in reflectance mosaic calculation, the various aspects related to sensor non-uniformities affect radiometric quality (Hakala et al., 2018; Kokka et al., 2019). Recently, the radiometric calibration of the FPI-based spectral camera has been further improved so that at-sensor radiance and irradiance can be used in direct reflectance transformation (Suomalainen et al. 2021).

In general, the increase in spectral resolution and spectral range improved the estimation and classification accuracies (Figures 8-9). Hyperspectral features with the VNIR range outperformed the RGB features by 10–14% in tree species and barley parameter estimation. However, when machine learning models for grass quantity and quality were tested with independent datasets, the multispectral features mostly outperformed the hyperspectral features, meaning that models based on multispectral features were more generalizable for these than models based on hyperspectral features. The reason for this can be related to many aspects such as the Hughes phenomenon (Hughes 1968) or differences in image quality within the bands of the hyperspectral sensor used (FPI2012b) (Honkavaara et al., 2013; Hakala et al.,2018). The related literature focusing on comparing the spectral resolution from drones mainly supports these findings. For example, Mozgeris et al. (2016) reported that hyperspectral features provided 3% better tree species classification accuracy than multispectral features. In a study by Maimaitijiang et al. (2017), multispectral features in the VNIR range outperformed RGB features for nitrogen estimation, but for biomass, they provided similar results. Michez et al. (2020) report that RGB provided relatively similar results as a multispectral camera in estimating the heterogeneity of grass-feeding quality in a field.

Hyperspectral sensors characterized the spectral properties in more detail than multispectral or RGB cameras (Figure 3). However, the spectral resolution and data collection costs are always a tradeoff; thus, it is important to understand the spectral requirements in different applications. The spectral properties of vegetation are strongly related to biophysical and biochemical parameters (Curran, 1980), which means that changes in spectra are ultimately based

on their changes. For instance, the invasion of bark beetles affects the chlorophyll and nitrogen concentration of needles (leaves) because the tree aims to breakdown their pigments under the stress (Carter and Knapp, 2001; Abdullah et al., 2018a). Thus, it is not surprising that wavelengths, which have been detected to be most suitable to separate infested and healthy needles using field spectrometers, are similar to the absorption bands of chlorophylls (Foster et al., 2017; Abdullah et al., 2018a). In addition to needle spectra, many other aspects—such as the structure of the needles, spectral properties of woody parts, atmosphere and viewing geometry—affect the observed canopy spectra (Rautiainen et al., 2018). Therefore, the requirement of spatial resolution is highly dependent on the application and the biochemical and biophysical properties behind the application.

The effect of spatial resolution on classification and estimation accuracies were studied in forestry and agricultural case studies. Concerning the spectral features, the spatial resolution affected the classification accuracy of the forestry application but not the estimation accuracy of the agricultural crop parameters (Figure 10). The reason for this difference can be related to the nature of the studied object and the feature extraction strategy adopted: the sampling plot size of the barley field was clearly larger than the GSD, and the object is relatively homogeneous, which indicates that a different GSD does not affect the average spectra. Instead, a GSD of 50cm was only slightly smaller than an individual treetop, and pixels at the top are brighter than the surrounding pixels, increasing the variability of the spectral sample collected.

The spatial resolution combined with other parameters—for instance, the measuring geometry (flight parameters and camera parameters), geometric distortions related to errors interior and exterior parameters, relief, and object textures, among others (Remondino et al., 2014; Tu, et al., 2020)—can affect the quality of the photogrammetric point cloud (used in this study to generate DSM, DTM and CHM). Consequently, the estimations based on 3D data features demonstrated the effects of the data geometric properties and not only from the spatial resolution. The results were consistent with the CHM quality that was evaluated based on in situ height measurements since the RMSE values for the GSD of 3.7cm, 5cm and 10cm were 7cm, 10cm and 10 cm, respectively (Publication III). Karunaratne et al. (2020) compared the performance of four flying altitudes (25–100 m) in grass parameter estimation using both spectral and 3D features. In their experiments, the importance of 3D features was lower at 25 m than at other flying heights.

In general, the integration of spectral and photogrammetric CHM-based 3D features improved the classification and estimation accuracies over the employment of only one of them. For example, the addition of 3D features improved the accuracy by approximately 8% in tree species classification. Similar findings have also been concluded in other tree species classification studies. For instance, Sothe et al. (2019) reported that by including the photogrammetric CHM features in the spectral features, the overall accuracy increased by 4.2%. Also, 3D features that have been extracted from LiDAR (Light Detection And Ranging) data and added to the hyperspectral features have improved classification performance (Jones et al., 2010; Piiroinen et al., 2017). The integration of 3D and spectral features has also been shown to be an advantage in studies related to forest health monitoring (Shendryk et al., 2016; Lin et al., 2019).

In agricultural crop parameter estimation, the spectral features mostly out-performed the 3D features, but the integration of both of them did not increase accuracy in all cases (Figures 11-12). In particular, the estimation of grass-feeding quality parameters did not gain from the 3D features. A reason for this can be that, even though the leaf/stem ratio is in relation to feeding quality parameters (Van Soest, 1994), the extracted 3D features were not able to describe such small scale structural details. Although 3D structure is only indirectly linked to nitrogen concentration, integration of spectral and 3D features improved slightly the estimation accuracy in the case of barley field (Figure 12). A similar finding was also reported by Grüner et al. (2020), who stated that especially textural 3D features gained the nitrogen estimation accuracy in grass mixtures. In the biomass estimation of grass, the CHM-based 3D features were noted to be more stable than the spectral features. The great performance of 3D features for biomass estimation is consistent with expectations since the CHM has been proved to measure crop height directly and thus it correlates strongly with the biomass (Bendig et al., 2015; Viljanen et al., 2018; Wijesingha et al., 2019). Findings that the integration of photogrammetric 3D and spectral features to estimate agricultural yield, i.e. above-ground-biomass improves estimation accuracy, have been widely proven, as stated in a review by Poley and McDermic (2020).

6.2   Limitations and future research

Detection of bark beetle damage as early as possible benefits forest management. In publications I and II, the class 'infested' refers to the yellow-attack phase and therefore to the identification of early detection, i.e. a green-attack phase was not studied because the green-attack phase was not part of the dataset. The green-attack phase has been detected at the regional level from satellites, for example in middle Europe from Sentinel-2 (Abdullah et al., 2018b, Huo et al., 2021, Fernandez-Carrillo et al, 2020). These studies were conducted in area-based plots, where almost all trees were in the green-attack phase, which is not a typical situation in the Nordic countries, where damages are distributed due to local conditions (Blomqvist et al., 2018). Thus, there is a need to detect bark beetle damage at the individual tree level. In Klouček et al. (2019) and Honkavaara et al. (2020), multitemporal spectral remote sensing data by drone was collected to study the detection of the green-attack phase. In Klouček et al. (2019), drone data was collected four times, and they reported that damage was in the green-attack phase in the first two attacks, when an overall classification accuracy of 10 infested and 40 healthy trees was 0.78—0.84, the user's accuracy was 0.47—0.56 and the producer's accuracy was 0.90 for infested trees. In the study by Honkavaara et al. (2020a), the infestation stayed at the green-attack level during seven dates when data was collected, except for one tree. In addition to bark beetle damage, the detection of spruces suffering from root-rot was studied. The best overall accuracy was 0.55 within the classes of 'bark beetle green attack', 'root-rot' and 'healthy' using a hyperspectral dataset, even though mul-

tispectral data resulted in a nearly similar performance. The user's and producer's accuracies for the green-attack class were 0.62–0.64, which is a similar level as in the study by Klouček et al. (2019). Although these results are promising, they were conducted with a small number of test trees (fewer than 55). Thus, more comprehensive studies are still needed to find optimal sensors and analytical approaches for drone-based green-attack detection. In particular, the recent drone studies have been limited to visible and near-infrared spectral ranges, but earlier results from the laboratory or satellite measurements suggested that other spectral ranges, particularly the SWIR or thermal ranges (Hais and Kučera, 2008; Foster et al., 2017; Abdullah et al., 2019a and 2019b), are of high interest when considering the mapping of bark beetle damage. An interesting approach could be flying under the canopy (Hyyppä et al., 2020), where early signs of bark beetles in tree trunks could be observed. In addition, further development of the method by Junttila et al. (2019) can be considered, wherein dual-wavelength terrestrial laser scanning data was used to detect the green-attack phase via leaf water content measurements. In general, it is not expected that the on-going, fast development of drones and sensors is decelerating. Consequently, new drones and sensors can enhance the accuracy and efficiency of drone-based mapping further. Thus, future research is needed to compare and evaluate their performance and optimal balance between spectral and spatial resolution in different applications.

The popularity of deep learning methods, such as convolutional neural networks (CNN), autoencoders (AE) and recurrent neural networks (RNN), has been growing quickly in vegetation remote sensing during recent years, CNN being the most popular among them (Ma et al., 2019; Kattenborn et al., 2021). In contrast to conventional machine learning methods, such as k-NN, RF and SVM used in publications I–V, CNN does not require hand-engineered feature extraction. Instead, the algorithm learns directly from input training images (2D-CNN). CNN benefits especially from high spatial resolution, but spectral resolution has also improved classification performance. Accordingly, it is not surprising that drones have been the most-used platform and RGB the most-used camera for vegetation remote sensing studies using CNN (Kattenborn et al., 2021). For instance, Mäyrä et al. (2021) and Sothe et al. (2020) reported that the classification accuracy of tree species increased by 5% and 22–26%, respectively, using CNN in comparison to conventional machine learning methods (SVM, RF) when only spectral features were used. However, Sothe et al. (2020) showed that with careful and enormous feature extraction including spectral indices, CHM and point cloud features, conventional machine learning can provide almost as good results as CNN, being faster and less sensitive to changes in the dataset. Furthermore, CNN has yielded promising results in insect damage mapping (Safonova et al., 2019). In agricultural-related studies, CNN has been mainly adopted for classification tasks; however, Nevavuori et al. (2019) achieved promising results with CNN in crop yield estimation. Thus, it is more likely that adopting deep learning methods instead of conventional machine learning methods would most probably improve the gain classification and estimation procedures found in publications I–V, presuming that enough training samples would be available.

Considering the usability of the developed machine learning models in practical situations, it would be highly beneficial if they can be applied at other sites without the additional ground truth collection that increases costs significantly.

Discussion

In this context, the validation experiments at individual tests sites are highly relevant. The results from bark beetle experiments showed that a smaller subset from a limited geographical area as training data was enough to build an accurate model for the entire area, even if the training data was collected with a different spatial resolution (GSD: 9–50cm). In grass experiments, the RMSE% of independent test areas was higher than in the training field but was still at an acceptable level for the requirements of the application (Figures 6, 9 and 12). These independent test fields were similar in second-year timothy-meadow mixtures as in the training field. A preliminary study showed that when RGB-based models trained in the same field were tested in another grass field located 450 km north of it and the data was collected using a different RGB camera, this did not lead to an acceptable performance, which highlights the importance of further work towards more generalized models (Honkavaara et al., 2020b). Keeping in mind that the concept of machine learning is a data-driven, empirical approach, there are several practices to improve their performance in the context of spectral imaging. The first is to collect a huge amount of training data that covers a wide range of both the biophysical variable to be studied and the conditions during data collection, such as the imaging geometry and illumination conditions. The second option is to improve the quality of spectral measurement in order to make them as standardized as possible. Both of these options will increase the knowledge of physically-based modelling of remote sensing signals. For instance, radiative transfer models (e.g. PROSPECT; Jacquemoud and Baret, 1990) can be used to simulate more training data for machine learning models (Verger, et al., 2011; Berger et al., 2020b; Annala et al., 2020). In this context, the understanding of spectral properties and spectral libraries plays a key role (Hovi et al., 2017; Forsström et al., 2021). An option is to downscale drone-based spectral characterization to the branch or leaf level instead of the current canopy level. In this situation, the compatibility of spectral and structural measures is highlighted, and approaches where both of them are characterized simultaneously are beneficial (Aasen et al., 2018; Oliveira et al., 2019). To conclude, in the development of machine learning, particularly deep learning, the understanding of the nature of remote sensing signals needs more attention, not only to collected data itself.

7. Conclusions

Drones have taken their place as flexible and low-cost remote sensing plat-forms between terrestrial and other aerial platforms, such as manned aircraft and satellites. Lightweight spectral sensors offer applicable information about plant's spectral properties. In addition, photogrammetric point clouds are a cost-efficient way to collect information about the 3D or structural properties of plants. Drone-based spectral imaging is a revolutionary tool to monitor forest health at the individual tree level and to estimate agricultural crop parameters. Optimal sensors, data collection and processing methods highly depend on the accuracy requirements of the different applications. Machine learning methods are efficient in estimating and classifying variables related to forestry and agri-culture based on drone-based remote sensing data. The combination of stand-ardized remote sensing workflows, an understanding of the physics of remote sensing signals and data, which covers the whole range of biophysical variables, are crucial when the goal is to build generalizable machine learning models for wide use. Fast and continuous development of drones, sensors and machine learning methods are expected to continue improving the efficiency, accuracy - and therefore the popularity - of drone-based remote sensing methods in for-estry and agricultural applications further.

References

Aasen, H., Burkart, A., Bolten, A., & Bareth, G. (2015). Generating 3D hyperspectral information with lightweight UAV snapshot cameras for vegetation monitoring: From camera calibration to quality assurance. ISPRS Journal of Photogrammetry and Remote Sensing, 108, 245-259.

Aasen, H., Honkavaara, E., Lucieer, A., & Zarco-Tejada, P. J. (2018). Quantitative remote sensing at ultra-high resolution with UAV spectroscopy: a review of sensor technology, measurement procedures, and data correction workflows. Remote Sensing, 10(7), 1091.

Abdullah, H., Darvishzadeh, R., Skidmore, A. K., Groen, T. A., & Heurich, M. (2018a). European spruce bark beetle (Ips typographus, L.) green attack affects foliar reflectance and biochemical properties. International journal of applied earth observation and geoinformation, 64, 199-209.

Abdullah, H., Skidmore, A. K., Darvishzadeh, R., & Heurich, M. (2018b). Sentinel-2 accurately maps green-attack stage of European spruce bark beetle (Ips typographus, L.) compared with Landsat-8. Remote sensing in ecology and conservation, 5(1), 87-106.

Abdullah, H., Skidmore, A. K., Darvishzadeh, R., & Heurich, M. (2019a). Timing of red-edge and shortwave infrared reflectance critical for early stress detection induced by bark beetle (Ips typographus, L.) attack. International Journal of Applied Earth Observation and Geoinformation, 82, 101900.

Abdullah, H., Darvishzadeh, R., Skidmore, A. K., & Heurich, M. (2019b). Sensitivity of Landsat-8 OLI and TIRS data to foliar properties of early stage bark beetle (Ips typographus, L.) infestation. Remote sensing, 11(4), 398.

Agisoft (2019) Agisoft Metashape User Manual: Professional Edition, Version 1.5. Available: https://www.agisoft.com/pdf/metashape-pro_1_5_en.pdf. Accessed: 28.2.2021.

Akaike, H. (1974). A new look at the statistical model identification. IEEE transactions on automatic control, 19(6), 716-723.

Ali, I., Cawkwell, F., Dwyer, E., & Green, S. (2016). Modeling managed grassland biomass estimation by using multitemporal remote sensing data—A machine learning approach. IEEE Journal of Selected Topics in Applied Earth Observations and Remote Sensing, 10(7), 3254-3264.

Annala, L., Honkavaara, E., Tuominen, S., & Pölönen, I. (2020). Chlorophyll Concentration Retrieval by Training Convolutional Neural Network for Stochastic Model of Leaf Optical Properties (SLOP) Inversion. Remote Sensing, 12(2), 283.

Assmann, J. J., Kerby, J. T., Cunliffe, A. M., & Myers-Smith, I. H. (2018). Vegetation monitoring using multispectral sensors—Best practices and lessons learned from high latitudes. Journal of Unmanned Vehicle Systems, 7(1), 54-75.

Barnetson, J., Phinn, S., & Scarth, P. (2020). Estimating Plant Pasture Biomass and Quality from UAV Imaging across Queensland's Rangelands. AgriEngineering, 2(4), 523-543.

Bauer, M. E., & Cipra, J. E. (1973). Identification of agricultural crops by computer processing of ERTS MSS data. In Symposium on significant results obtained from the Earth Resources Technology Satellite-1 (Vol. 1, pp. 205-212).

Belgiu, M., & Drăguţ, L. (2016). Random forest in remote sensing: A review of applications and future directions. ISPRS journal of photogrammetry and remote sensing, 114, 24-31.

Bendig, J., Bolten, A., Bennertz, S., Broscheit, J., Eichfuss, S., & Bareth, G. (2014). Estimating biomass of barley using crop surface models (CSMs) derived from UAV-based RGB imaging. Remote sensing, 6(11), 10395-10412.

Bendig, J., Yu, K., Aasen, H., Bolten, A., Bennertz, S., Broscheit, J., ... & Bareth, G. (2015). Combining UAV-based plant height from crop surface models, visible, and near infrared vegetation indices for biomass monitoring in barley. International Journal of Applied Earth Observation and Geoinformation, 39, 79-87.

Berger, K., Verrelst, J., Féret, J. B., Wang, Z., Wocher, M., Strathmann, M., ... & Hank, T. (2020a). Crop nitrogen monitoring: Recent progress and principal developments in the context of imaging spectroscopy missions. Remote Sensing of Environment, 242, 111758.

Berger, K., Verrelst, J., Féret, J. B., Hank, T., Wocher, M., Mauser, W., & Camps-Valls, G. (2020b). Retrieval of aboveground crop nitrogen content with a hybrid machine learning method. International Journal of Applied Earth Observation and Geoinformation, 92, 102174.

Berni, J. A., Zarco-Tejada, P. J., Suárez, L., & Fereres, E. (2009). Thermal and narrowband multispectral remote sensing for vegetation monitoring from an unmanned aerial vehicle. IEEE Transactions on geoscience and Remote Sensing, 47(3), 722-738.

Bhatti, A. U., Mulla, D. J., & Frazier, B. E. (1991). Estimation of soil properties and wheat yields on complex eroded hills using geostatistics and thematic mapper images. Remote Sensing of Environment, 37(3), 181-191.

Blaschke, T. (2010). Object based image analysis for remote sensing. ISPRS journal of photogrammetry and remote sensing, 65(1), 2-16.

Blomqvist, M., Kosunen, M., Starr, M., Kantola, T., Holopainen, M., & Lyytikäinen-Saarenmaa, P. (2018). Modelling the predisposition of Norway spruce to Ips typographus L. infestation by means of environmental factors in southern Finland. European Journal of Forest Research, 137(5), 675-691.

Boser, B. E., Guyon, I. M., & Vapnik, V. N. (1992, July). A training algorithm for optimal margin classifiers. In Proceedings of the fifth annual workshop on Computational learning theory (pp. 144-152).

Breiman, L. (2001). Random forests. Machine learning, 45(1), 5-32.

Broadhurst, D., Goodacre, R., Jones, A., Rowland, J. J., & Kell, D. B. (1997). Genetic algorithms as a method for variable selection in multiple linear regression and partial least squares regression, with applications to pyrolysis mass spectrometry. Analytica Chimica Acta, 348(1-3), 71-86.

Brovkina, O., Cienciala, E., Surový, P., & Janata, P. (2018). Unmanned aerial vehicles (UAV) for assessment of qualitative classification of Norway spruce in temperate forest stands. Geo-spatial information science, 21(1), 12-20.

Burkart, A., Cogliati, S., Schickling, A., & Rascher, U. (2013). A novel UAV-based ultra-light weight spectrometer for field spectroscopy. IEEE sensors journal, 14(1), 62-67.

Candiago, S., Remondino, F., De Giglio, M., Dubbini, M., & Gattelli, M. (2015). Evaluating multispectral images and vegetation indices for precision farming applications from UAV images. Remote sensing, 7(4), 4026-4047.

Capolupo, A., Kooistra, L., Berendonk, C., Boccia, L., & Suomalainen, J. (2015). Estimating plant traits of grasslands from UAV-acquired hyperspectral images: a comparison of statistical approaches. ISPRS International Journal of Geo-Information, 4(4), 2792-2820.

Carneggie, D. M., & Lauer, D. T. (1966). Uses of multiband remote sensing in forest and range inventory. Photogrammetria, 21(4), 115-141.

Carter, G. A., & Knapp, A. K. (2001). Leaf optical properties in higher plants: linking spectral characteristics to stress and chlorophyll concentration. American journal of botany, 88(4), 677-684.

Castro, W., Marcato Junior, J., Polidoro, C., Osco, L. P., Gonçalves, W., Rodrigues, L., ... & Matsubara, E. (2020). Deep learning applied to phenotyping of biomass in forages with UAV-based RGB imagery. Sensors, 20(17), 4802.

Chang, C. C., & Lin, C. J. (2011). LIBSVM: a library for support vector machines. ACM transactions on intelligent systems and technology (TIST), 2(3), 1-27.

Chlingaryan, A., Sukkarieh, S., & Whelan, B. (2018). Machine learning approaches for crop yield prediction and nitrogen status estimation in precision agriculture: A review. Computers and electronics in agriculture, 151, 61-69.

Clevers, J. G., Kooistra, L., & Van den Brande, M. M. (2017). Using Sentinel-2 data for retrieving LAI and leaf and canopy chlorophyll content of a potato crop. Remote Sensing, 9(5), 405.

Cohen, J. (1968). Weighted kappa: nominal scale agreement provision for scaled disagreement or partial credit. Psychological bulletin, 70(4), 213.

Colomina, I., & Molina, P. (2014). Unmanned aerial systems for photogrammetry and remote sensing: A review. ISPRS Journal of photogrammetry and remote sensing, 92, 79-97.

Curran, P. (1980). Multispectral remote sensing of vegetation amount. Progress in physical geography, 4(3), 315-341.

Dasgupta, P. (2021). The economics of biodiversity: the Dasgupta review. Available: https://www.gov.uk/government/publications/final-report-the-economics-of-biodiversity-the-dasgupta-review. Accessed: 28.2.2021

Dash, J. P., Watt, M. S., Pearse, G. D., Heaphy, M., & Dungey, H. S. (2017). Assessing very high resolution UAV imagery for monitoring forest health during a simulated disease outbreak. ISPRS Journal of Photogrammetry and Remote Sensing, 131, 1-14.

Decruyenaere, V., Lecomte, P., Demarquilly, C., Aufrere, J., Dardenne, P., Stilmant, D., & Buldgen, A. (2009). Evaluation of green forage intake and digestibility in ruminants using near infrared reflectance spectroscopy (NIRS): Developing a global calibration. Animal Feed Science and Technology, 148(2-4), 138-156.

Delloye, C., Weiss, M., & Defourny, P. (2018). Retrieval of the canopy chlorophyll content from Sentinel-2 spectral bands to estimate nitrogen uptake in intensive winter wheat cropping systems. Remote Sensing of Environment, 216, 245-261.

EC (2020), European Commission: Farm to Fork Strategy for a fair, healthy and environmentally-friendly food system, Communication from the Commission to the European Parliament, the European Council, the Council, the European Economic And Social Committee and the Committee of the Regions, COM/2020/381 final, https://eur-lex.europa.eu/legal-content/EN/TXT/?qid=1590404602495&uri=CELEX%3A52020DC0381 Accessed: 28.2.2021

Eisenbeiß, H. (2009). UAV photogrammetry (Doctoral dissertation, ETH Zurich). Available: https://www.research-collection.ethz.ch/bitstream/handle/20.500.11850/20976/eth-498-02.pdf?sequence=2. Accessed 28.2.2021

Fassnacht, F. E., Latifi, H., Ghosh, A., Joshi, P. K., & Koch, B. (2014). Assessing the potential of hyperspectral imagery to map bark beetle-induced tree mortality. Remote Sensing of Environment, 140, 533-548.

Fassnacht, F. E., Latifi, H., Stereńczak, K., Modzelewska, A., Lefsky, M., Waser, L. T., ... & Ghosh, A. (2016). Review of studies on tree species classification from remotely sensed data. Remote Sensing of Environment, 186, 64-87.

Fernandez-Carrillo, A., Patočka, Z., Dobrovolný, L., Franco-Nieto, A., & Revilla-Romero, B. (2020). Monitoring bark beetle forest damage in Central Europe. A

remote sensing approach validated with field data. Remote Sensing, 12(21), 3634.

Forsström, P. R., Hovi, A., Ghielmetti, G., Schaepman, M. E., & Rautiainen, M. (2021). Multi-angular reflectance spectra of small single trees. Remote Sensing of Environment, 255, 112302.

Foster, A. C., Walter, J. A., Shugart, H. H., Sibold, J., & Negron, J. (2017). Spectral evidence of early-stage spruce beetle infestation in Engelmann spruce. Forest Ecology and Management, 384, 347-357.

Franklin, S. E. (2018). Pixel-and object-based multispectral classification of forest tree species from small unmanned aerial vehicles. Journal of Unmanned Vehicle Systems, 6(4), 195-211.

Geipel, J., Link, J., Wirwahn, J. A., & Claupein, W. (2016). A programmable aerial multispectral camera system for in-season crop biomass and nitrogen content estimation. Agriculture, 6(1), 4.

González-Jorge, H., Martínez-Sánchez, J., & Bueno, M. (2017). Unmanned aerial systems for civil applications: A review. Drones, 1(1), 2.

Grüner, E., Astor, T., & Wachendorf, M. (2020). Prediction of Biomass and N Fixation of Legume–Grass Mixtures Using Sensor Fusion. Frontiers in plant science, 11.

Guerra-Hernández, J., González-Ferreiro, E., Monleón, V. J., Faias, S. P., Tomé, M., & Díaz-Varela, R. A. (2017). Use of multi-temporal UAV-derived imagery for estimating individual tree growth in Pinus pinea stands. Forests, 8(8), 300.

Hais, M., & Kučera, T. (2008). Surface temperature change of spruce forest as a result of bark beetle attack: remote sensing and GIS approach. European Journal of Forest Research, 127(4), 327-336.

Hakala, T., Markelin, L., Honkavaara, E., Scott, B., Theocharous, T., Nevalainen, O., ... & Fox, N. (2018). Direct reflectance measurements from drones: Sensor absolute radiometric calibration and system tests for forest reflectance characterization. Sensors, 18(5), 1417.

Hall, R. J., Castilla, G., White, J. C., Cooke, B. J., & Skakun, R. S. (2016). Remote sensing of forest pest damage: a review and lessons learned from a Canadian perspective. The Canadian Entomologist, 148(S1), S296-S356.

Hirschmuller, H. (2008). Stereo processing by semiglobal matching and mutual information. IEEE Transactions on pattern analysis and machine intelligence, 30(2), 328-341.

Hlásny, T., Krokene, P., Liebhold, A., Montagné-Huck, C., Müller, J., Qin, H., ... & Viiri, H. (2019). Living with bark beetles: impacts, outlook and management options (No. 8). European Forest Institute.

Hoffmeister, D., Waldhoff, G., Curdt, C., Tilly, N., Bendig, J., & Bareth, G. (2013). Spatial variability detection of crop height in a single field by terrestrial laser scanning. In Precision agriculture'13 (pp. 267-274). Wageningen Academic Publishers, Wageningen.

Holmgren, J., & Persson, Å. (2004). Identifying species of individual trees using airborne laser scanner. Remote Sensing of Environment, 90(4), 415-423.

Holopainen, M., Vastaranta, M., & Hyyppä, J. (2014). Outlook for the next generation's precision forestry in Finland. Forests, 5(7), 1682-1694.

Honkavaara, E., Saari, H., Kaivosoja, J., Pölönen, I., Hakala, T., Litkey, P., ... & Pesonen, L. (2013). Processing and assessment of spectrometric, stereoscopic imagery collected using a lightweight UAV spectral camera for precision agriculture. Remote Sensing, 5(10), 5006-5039.

Honkavaara, E., Eskelinen, M. A., Pölönen, I., Saari, H., Ojanen, H., Mannila, R., ... & Pulkkanen, M. (2016). Remote sensing of 3-D geometry and surface moisture of a peat production area using hyperspectral frame cameras in visible to short-wave infrared spectral ranges onboard a small unmanned airborne vehicle (UAV). IEEE Transactions on Geoscience and Remote Sensing, 54(9), 5440-5454.

Honkavaara, E., Rosnell, T., Oliveira, R., & Tommaselli, A. (2017). Band registration of tuneable frame format hyperspectral UAV imagers in complex scenes. ISPRS Journal of Photogrammetry and Remote Sensing, 134, 96-109.

Honkavaara, E., & Khoramshahi, E. (2018). Radiometric correction of close-range spectral image blocks captured using an unmanned aerial vehicle with a radiometric block adjustment. Remote Sensing, 10(2), 256.

Honkavaara, E., Näsi, R., Oliveira, R., Viljanen, N., Suomalainen, J., Khoramshahi, E., ... & Haataja, L. (2020a). Using multitemporal hyper-and multispectral UAV imaging for detecting bark beetle infestation on norway spruce. The International Archives of the Photogrammetry, Remote Sensing and Spatial Information Sciences, Volume XLIII-B3-2020, 2020.

Honkavaara, E., Näsi, R., Oliveira, R. A., Niemeläinen, O., Viljanen, N., Hakala, T., & Kaivosoja, J. (2020b). Precision agriculture in practice–utilisation of novel remote sensing technologies in grass silage production. In Meeting the future demands for grassland production (p. 583).

Hovi, A., Korhonen, L., Vauhkonen, J., & Korpela, I. (2016). LiDAR waveform features for tree species classification and their sensitivity to tree-and acquisition related parameters. Remote sensing of environment, 173, 224-237.

Hovi, A., Raitio, P., & Rautiainen, M. (2017). A spectral analysis of 25 boreal tree species. Silva Fenn, 51(51), 4.

Hughes, G. (1968). On the mean accuracy of statistical pattern recognizers. IEEE transactions on information theory, 14(1), 55-63.

Hunt, E. R., Hively, W. D., Fujikawa, S. J., Linden, D. S., Daughtry, C. S., & McCarty, G. W. (2010). Acquisition of NIR-green-blue digital photographs from unmanned aircraft for crop monitoring. Remote Sensing, 2(1), 290-305.

Huo, L., Persson, H. J., & Lindberg, E. (2021). Early detection of forest stress from European spruce bark beetle attack, and a new vegetation index: Normalized distance red & SWIR (NDRS). Remote Sensing of Environment, 255, 112240.

Hyyppä, J., Kelle, O., Lehikoinen, M., & Inkinen, M. (2001). A segmentation-based method to retrieve stem volume estimates from 3-D tree height models produced by laser scanners. IEEE Transactions on Geoscience and remote Sensing, 39(5), 969-975.

Hyyppä, E., Hyyppä, J., Hakala, T., Kukko, A., Wulder, M. A., White, J. C., ... & Kaartinen, H. (2020). Under-canopy UAV laser scanning for accurate forest field measurements. ISPRS Journal of Photogrammetry and Remote Sensing, 164, 41-60.

Immitzer, M., Vuolo, F., & Atzberger, C. (2016). First experience with Sentinel-2 data for crop and tree species classifications in central Europe. Remote sensing, 8(3), 166.

ISPA (2019). International Society for Precision Agriculture. Available: https://www.ispag.org/about/definition. Accessed: 28.2.2021

Jaakkola, A., Hyyppä, J., Kukko, A., Yu, X., Kaartinen, H., Lehtomäki, M., & Lin, Y. (2010). A low-cost multi-sensoral mobile mapping system and its feasibility for tree measurements. ISPRS journal of Photogrammetry and Remote Sensing, 65(6), 514-522.

Jacquemoud, S., & Baret, F. (1990). PROSPECT: A model of leaf optical properties spectra. Remote sensing of environment, 34(2), 75-91.

Jenal, A., Bareth, G., Bolten, A., Kneer, C., Weber, I., & Bongartz, J. (2019). Development of a VNIR/SWIR multispectral imaging system for vegetation monitoring with unmanned aerial vehicles. Sensors, 19(24), 5507.

Jenal, A., Lussem, U., Bolten, A., Gnyp, M. L., Schellberg, J., Jasper, J., ... & Bareth, G. (2020). Investigating the Potential of a Newly Developed UAV-based VNIR/SWIR Imaging System for Forage Mass Monitoring. PFG–Journal of Photogrammetry, Remote Sensing and Geoinformation Science, 88(6), 493-507.

Jetz, W., McGeoch, M. A., Guralnick, R., Ferrier, S., Beck, J., Costello, M. J., ... & Turak, E. (2019). Essential biodiversity variables for mapping and monitoring species populations. Nature ecology & evolution, 3(4), 539-551.

Jones, D. B. (1931). Factors for converting percentages of nitrogen in foods and feeds into percentages of protein. USDA Circ., 183, 1-21.

Jones, T. G., Coops, N. C., & Sharma, T. (2010). Assessing the utility of airborne hyperspectral and LiDAR data for species distribution mapping in the coastal Pacific Northwest, Canada. Remote Sensing of Environment, 114(12), 2841-2852.

Junttila, S., Holopainen, M., Vastaranta, M., Lyytikäinen-Saarenmaa, P., Kaartinen, H., Hyyppä, J., & Hyyppä, H. (2019). The potential of dual-wavelength terrestrial lidar in early detection of Ips typographus (L.) infestation−Leaf water content as a proxy. Remote Sensing of Environment, 231, 111264.

Kaartinen, H., Hyyppä, J., Yu, X., Vastaranta, M., Hyyppä, H., Kukko, A., ... & Wu, J. C. (2012). An international comparison of individual tree detection and extraction using airborne laser scanning. Remote Sensing, 4(4), 950-974.

Kaivosoja, J., Näsi, R., Hakala, T., Viljanen, N., & Honkavaara, E. (2019). Different remote sensing data in relative biomass determination and in precision fertilization task generation for cereal crops. In International Conference on Information and Communication Technologies in Agriculture, Food & Environment (pp. 164-176). Springer, Cham.

Kantola, T., Vastaranta, M., Yu, X., Lyytikainen-Saarenmaa, P., Holopainen, M., Talvitie, M., ... & Hyyppa, J. (2010). Classification of defoliated trees using tree-level airborne laser scanning data combined with aerial images. Remote Sensing, 2(12), 2665-2679.

Karjalainen, M., Kaartinen, H., & Hyyppä, J. (2008). Agricultural monitoring using Envisat alternating polarization SAR images. Photogrammetric Engineering & Remote Sensing, 74(1), 117-126.

Karunaratne, S., Thomson, A., Morse-McNabb, E., Wijesingha, J., Stayches, D., Copland, A., & Jacobs, J. (2020). The fusion of spectral and structural datasets derived from an airborne multispectral sensor for estimation of pasture dry matter yield at paddock scale with time. Remote Sensing, 12(12), 2017.

Kattenborn, T., Leitloff, J., Schiefer, F., & Hinz, S. (2021). Review on Convolutional Neural Networks (CNN) in vegetation remote sensing. ISPRS Journal of Photogrammetry and Remote Sensing, 173, 24-49.

Klouček, T., Komárek, J., Surový, P., Hrach, K., Janata, P., & Vašíček, B. (2019). The use of UAV mounted sensors for precise detection of bark beetle infestation. Remote Sensing, 11(13), 1561.

Knipling, E. B. (1970). Physical and physiological basis for the reflectance of visible and near-infrared radiation from vegetation. Remote sensing of environment, 1(3), 155-159.

Kokka, A., Pulli, T., Honkavaara, E., Markelin, L., Kärhä, P., & Ikonen, E. (2019). Flat-field calibration method for hyperspectral frame cameras. Metrologia, 56(5), 055001.

Korpela, I. S., & Tokola, T. E. (2006). Potential of aerial image-based monoscopic and multiview single-tree forest inventory: A simulation approach. Forest Science, 52(2), 136-147.

Korpela, I., Ørka, H. O., Maltamo, M., Tokola, T., & Hyyppä, J. (2010). Tree species classification using airborne LiDAR−effects of stand and tree parameters, downsizing of training set, intensity normalization, and sensor type. Silva Fennica, 44(2), 319-339.

Kotsiantis, S. B., Zaharakis, I., & Pintelas, P. (2007). Supervised machine learning: A review of classification techniques. Emerging artificial intelligence applications in computer engineering, 160(1), 3-24.

Laasasenaho, J. (1982). Taper curve and volume functions for pine, spruce and birch. Communications Instituti Forestalis Fenniae, Finland, Vantaa: Finnish Forest Research Institute, pp. 74-74, 1982.

Lary, D. J., Alavi, A. H., Gandomi, A. H., & Walker, A. L. (2016). Machine learning in geosciences and remote sensing. Geoscience Frontiers, 7(1), 3-10.

Lausch, A., Heurich, M., Gordalla, D., Dobner, H. J., Gwillym-Margianto, S., & Salbach, C. (2013). Forecasting potential bark beetle outbreaks based on spruce forest vitality using hyperspectral remote-sensing techniques at different scales. Forest Ecology and Management, 308, 76-89.

Lehmann, J. R. K., Nieberding, F., Prinz, T., & Knoth, C. (2015). Analysis of unmanned aerial system-based CIR images in forestry—A new perspective to monitor pest infestation levels. Forests, 6(3), 594-612.

Lelong, C. C., Burger, P., Jubelin, G., Roux, B., Labbé, S., & Baret, F. (2008). Assessment of unmanned aerial vehicles imagery for quantitative monitoring of wheat crop in small plots. Sensors, 8(5), 3557-3585.

Li, W., Niu, Z., Chen, H., Li, D., Wu, M., & Zhao, W. (2016). Remote estimation of canopy height and aboveground biomass of maize using high-resolution stereo images from a low-cost unmanned aerial vehicle system. Ecological Indicators, 67, 637-648.

Liang, X., Kankare, V., Hyyppä, J., Wang, Y., Kukko, A., Haggrén, H., ... & Vastaranta, M. (2016). Terrestrial laser scanning in forest inventories. ISPRS Journal of Photogrammetry and Remote Sensing, 115, 63-77.

Lin, Q., Huang, H., Wang, J., Huang, K., & Liu, Y. (2019). Detection of pine shoot beetle (PSB) Stress on pine forests at individual tree level using UAV-based hyperspectral imagery and lidar. Remote Sensing, 11(21), 2540.

Lindner, M., Maroschek, M., Netherer, S., Kremer, A., Barbati, A., Garcia-Gonzalo, J., ... & Marchetti, M. (2010). Climate change impacts, adaptive capacity, and vulnerability of European forest ecosystems. Forest ecology and management, 259(4), 698-709.

Liu, Y., Cheng, T., Zhu, Y., Tian, Y., Cao, W., Yao, X., & Wang, N. (2016). Comparative analysis of vegetation indices, non-parametric and physical retrieval methods for monitoring nitrogen in wheat using UAV-based multispectral imagery. In 2016 IEEE International Geoscience and Remote Sensing Symposium (IGARSS) (pp. 7362-7365). Ieee.

Liu, H., Dahlgren, R. A., Larsen, R. E., Devine, S. M., Roche, L. M., O'Geen, A. T., ... & Jin, Y. (2019). Estimating rangeland forage production using remote sensing data from a small unmanned aerial system (sUAS) and planetscope satellite. Remote Sensing, 11(5), 595.

Liu, M., Zhang, Z., Liu, X., Yao, J., Du, T., Ma, Y., & Shi, L. (2020). Discriminant Analysis of the Damage Degree Caused by Pine Shoot Beetle to Yunnan Pine Using UAV-Based Hyperspectral Images. Forests, 11(12), 1258.

Lisein, J., Michez, A., Claessens, H., & Lejeune, P. (2015). Discrimination of deciduous tree species from time series of unmanned aerial system imagery. PLoS One, 10(11), e0141006.

Lumme, J., Karjalainen, M., Kaartinen, H., Kukko, A., Hyyppä, J., Hyyppä, H., ... & Kleemola, J. (2008). Terrestrial laser scanning of agricultural crops. Int. Arch. Photogramm. Remote Sens. Spat. Inf. Sci, 37, 563-566.

Ma, L., Liu, Y., Zhang, X., Ye, Y., Yin, G., & Johnson, B. A. (2019). Deep learning in remote sensing applications: A meta-analysis and review. ISPRS journal of photogrammetry and remote sensing, 152, 166-177.

Maes, W. H., & Steppe, K. (2019). Perspectives for remote sensing with unmanned aerial vehicles in precision agriculture. Trends in plant science, 24(2), 152-164.

MAFF, D. (1975). Energy allowances and feeding systems for ruminants. Technical Bulletin (London), 33.

Maimaitijiang, M., Ghulam, A., Sidike, P., Hartling, S., Maimaitiyiming, M., Peterson, K., ... & Fritschi, F. (2017). Unmanned Aerial System (UAS)-based phenotyping of soybean using multi-sensor data fusion and extreme learning machine. ISPRS Journal of Photogrammetry and Remote Sensing, 134, 43-58.

Manfreda, S., McCabe, M. F., Miller, P. E., Lucas, R., Pajuelo Madrigal, V., Mallinis, G., ... & Toth, B. (2018). On the use of unmanned aerial systems for environmental monitoring. Remote sensing, 10(4), 641.

Maxwell, A. E., Warner, T. A., & Fang, F. (2018). Implementation of machine-learning classification in remote sensing: An applied review. International Journal of Remote Sensing, 39(9), 2784-2817.

Metsäkeskus (2019). Drone kerää ketterästi tietoa metsästä. Available (in finnish): https://www.metsakeskus.fi/uutiset/drone-keraa-ketterasti-tietoa-metsasta. Accessed: 28.2.2021.

Michez, A., Piégay, H., Lisein, J., Claessens, H., & Lejeune, P. (2016). Classification of riparian forest species and health condition using multi-temporal and hyperspatial imagery from unmanned aerial system. Environmental monitoring and assessment, 188(3), 146.

Michez, A., Philippe, L., David, K., Sébastien, D., Christian, D., & Bindelle, J. (2020). Can Low-Cost Unmanned Aerial Systems Describe the Forage Quality Heterogeneity? Insight from a Timothy Pasture Case Study in Southern Belgium. Remote Sensing, 12(10), 1650.

Mikhail, E. M., Bethel, J. S., & McGlone, J. C. (2001). Introduction to modern photogrammetry. New York, 19.

Mikita, T., Janata, P., & Surový, P. (2016). Forest stand inventory based on combined aerial and terrestrial close-range photogrammetry. Forests, 7(8), 165.

Minařík, R., Langhammer, J., & Lendzioch, T. (2020). Automatic Tree Crown Extraction from UAS Multispectral Imagery for the Detection of Bark Beetle Disturbance in Mixed Forests. Remote Sensing, 12(24), 4081.

Miyoshi, G. T., Imai, N. N., Tommaselli, A. M. G., Moraes, M. V., & Honkavaara, E. (2020a). Evaluation of hyperspectral multitemporal information to improve tree species identification in the highly diverse Atlantic forest. Remote Sensing, 12(2), 244.

Miyoshi, G. T., Arruda, M. D. S., Osco, L. P., Marcato Junior, J., Gonçalves, D. N., Imai, N. N., ... & Gonçalves, W. N. (2020b). A novel deep learning method to identify single tree species in UAV-based hyperspectral images. Remote Sensing, 12(8), 1294.

Moe, K. T., Owari, T., Furuya, N., & Hiroshima, T. (2020). Comparing individual tree height information derived from field surveys, LiDAR and UAV-DAP for high-value timber species in Northern Japan. Forests, 11(2), 223.

Mozgeris, G., Gadal, S., Jonikavičius, D., Straigytė, L., Ouerghemmi, W., & Juodkienė, V. (2016, August). Hyperspectral and color-infrared imaging from ultralight aircraft: Potential to recognize tree species in urban environments. In 2016 8th Workshop on Hyperspectral Image and Signal Processing: Evolution in Remote Sensing (WHISPERS) (pp. 1-5). IEEE.

Mulla, D. J. (2013). Twenty five years of remote sensing in precision agriculture: Key advances and remaining knowledge gaps. Biosystems engineering, 114(4), 358-371.

Mäkynen, J., Holmlund, C., Saari, H., Ojala, K., & Antila, T. (2011, October). Unmanned aerial vehicle (UAV) operated megapixel spectral camera. In Electro-Optical Remote Sensing, Photonic Technologies, and Applications V (Vol. 8186, p. 81860Y). International Society for Optics and Photonics.

Mäyrä, J., Keski-Saari, S., Kivinen, S., Tanhuanpää, T., Hurskainen, P., Kullberg, P., ... & Vihervaara, P. (2021). Tree species classification from airborne hyperspectral and LiDAR data using 3D convolutional neural networks. Remote Sensing of Environment, 256, 112322.

Nevalainen, O., Honkavaara, E., Tuominen, S., Viljanen, N., Hakala, T., Yu, X., ... & Tommaselli, A. M. (2017). Individual tree detection and classification with UAV-based photogrammetric point clouds and hyperspectral imaging. Remote Sensing, 9(3), 185.

Nevavuori, P., Narra, N., & Lipping, T. (2019). Crop yield prediction with deep convolutional neural networks. Computers and electronics in agriculture, 163, 104859.

Nex, F., & Remondino, F. (2014). UAV for 3D mapping applications: a review. Applied geomatics, 6(1), 1-15.

Nezami, S., Khoramshahi, E., Nevalainen, O., Pölönen, I., & Honkavaara, E. (2020). Tree species classification of drone hyperspectral and RGB imagery with deep learning convolutional neural networks. Remote Sensing, 12(7), 1070.

Näsi, R., Honkavaara, E., Tuominen, S., Saari, H., Pölönen, I., Hakala, T., ... & Reinikainen, J. (2016). UAS based tree species identification using the novel FPI based hyperspectral cameras in visible, NIR and SWIR spectral ranges. International archives of the photogrammetry, remote sensing and spatial information sciences; Volume XLI-B1.

Oliveira, R. A., Tommaselli, A. M., & Honkavaara, E. (2016). Geometric calibration of a hyperspectral frame camera. The Photogrammetric Record, 31(155), 325-347.

Oliveira, R. A., Tommaselli, A. M., & Honkavaara, E. (2019). Generating a hyperspectral digital surface model using a hyperspectral 2D frame camera. ISPRS Journal of Photogrammetry and Remote Sensing, 147, 345-360.

Pajares, G. (2015). Overview and current status of remote sensing applications based on unmanned aerial vehicles (UAVs). Photogrammetric Engineering & Remote Sensing, 81(4), 281-330.

Pereira, H. M., Ferrier, S., Walters, M., Geller, G. N., Jongman, R. H. G., Scholes, R. J., ... & Wegmann, M. (2013). Essential biodiversity variables. Science, 339(6117), 277-278.

Persson, M., Lindberg, E., & Reese, H. (2018). Tree species classification with multi-temporal Sentinel-2 data. Remote Sensing, 10(11), 1794.

Piiroinen, R., Heiskanen, J., Maeda, E., Viinikka, A., & Pellikka, P. (2017). Classification of tree species in a diverse African agroforestry landscape using imaging spectroscopy and laser scanning. Remote Sensing, 9(9), 875.

Poley, L. G., & J McDermid, G. (2020). A Systematic Review of the Factors Influencing the Estimation of Vegetation Aboveground Biomass Using Unmanned Aerial Systems. Remote Sensing, 12(7).

Potterf, M., Nikolov, C., Kočická, E., Ferenčík, J., Mezei, P., & Jakuš, R. (2019). Landscape-level spread of beetle infestations from windthrown-and beetle-killed trees in the non-intervention zone of the Tatra National Park, Slovakia (Central Europe). Forest Ecology and Management, 432, 489-500.

Pullanagari, R. R., Yule, I. J., Tuohy, M. P., Hedley, M. J., Dynes, R. A., & King, W. M. (2012). In-field hyperspectral proximal sensing for estimating quality parameters of mixed pasture. Precision Agriculture, 13(3), 351-369.

Puliti, S., Ørka, H. O., Gobakken, T., & Næsset, E. (2015). Inventory of small forest areas using an unmanned aerial system. Remote Sensing, 7(8), 9632-9654.

Rautiainen, M., Lukeš, P., Homolova, L., Hovi, A., Pisek, J., & Mõttus, M. (2018). Spectral properties of coniferous forests: A review of in situ and laboratory measurements. Remote Sensing, 10(2), 207.

Remondino, F., Spera, M. G., Nocerino, E., Menna, F., & Nex, F. (2014). State of the art in high density image matching. The photogrammetric record, 29(146), 144-166.

Rock, B. N., Vogelmann, J. E., Williams, D. L., Vogelmann, A. F., & Hoshizaki, T. (1986). Remote detection of forest damage. Bioscience, 36(7), 439-445.

Rouse, J. W., Haas, R. H., Schell, J. A., & Deering, D. W. (1974). Monitoring vegetation systems in the Great Plains with ERTS. NASA special publication, 351(1974), 309.

Saari, H., Pellikka, I., Pesonen, L., Tuominen, S., Heikkilä, J., Holmlund, C., ... & Antila, T. (2011). Unmanned Aerial Vehicle (UAV) operated spectral camera system for forest and agriculture applications. In Remote Sensing for Agriculture, Ecosystems, and Hydrology XIII (Vol. 8174, p. 81740H). International Society for Optics and Photonics.

Safonova, A., Tabik, S., Alcaraz-Segura, D., Rubtsov, A., Maglinets, Y., & Herrera, F. (2019). Detection of fir trees (Abies sibirica) damaged by the bark beetle in unmanned aerial vehicle images with deep learning. Remote sensing, 11(6), 643.

Schaepman-Strub, G., Schaepman, M. E., Painter, T. H., Dangel, S., & Martonchik, J. V. (2006). Reflectance quantities in optical remote sensing—Definitions and case studies. Remote sensing of environment, 103(1), 27-42.

Seidl, R., Thom, D., Kautz, M., Martin-Benito, D., Peltoniemi, M., Vacchiano, G., ... & Reyer, C. P. (2017). Forest disturbances under climate change. Nature climate change, 7(6), 395-402.

Senf, C., Seidl, R., & Hostert, P. (2017). Remote sensing of forest insect disturbances: Current state and future directions. International Journal of Applied Earth Observation and Geoinformation, 60, 49-60.

Shakhatreh, H., Sawalmeh, A. H., Al-Fuqaha, A., Dou, Z., Almaita, E., Khalil, I., ... & Guizani, M. (2019). Unmanned aerial vehicles (UAVs): A survey on civil applications and key research challenges. Ieee Access, 7, 48572-48634.

Shendryk, I., Broich, M., Tulbure, M. G., McGrath, A., Keith, D., & Alexandrov, S. V. (2016). Mapping individual tree health using full-waveform airborne laser scans and imaging spectroscopy: A case study for a floodplain eucalypt forest. Remote Sensing of Environment, 187, 202-217.

Siebert, S., & Teizer, J. (2014). Mobile 3D mapping for surveying earthwork projects using an Unmanned Aerial Vehicle (UAV) system. Automation in construction, 41, 1-14.

Slater, P. N. (1980). Remote sensing: optics and optical systems. Reading.

Smith, G. M., & Milton, E. J. (1999). The use of the empirical line method to calibrate remotely sensed data to reflectance. International Journal of remote sensing, 20(13), 2653-2662.

Smith, C., Karunaratne, S., Badenhorst, P., Cogan, N., Spangenberg, G., & Smith, K. (2020). Machine learning algorithms to predict forage nutritive value of in situ perennial ryegrass plants using hyperspectral canopy reflectance data. Remote Sensing, 12(6), 928.

Sommerfeld, A., Senf, C., Buma, B., D'Amato, A. W., Després, T., Díaz-Hormazábal, I., ... & Seidl, R. (2018). Patterns and drivers of recent disturbances across the temperate forest biome. Nature communications, 9(1), 1-9.

Sothe, C., De Almeida, C. M., Schimalski, M. B., La Rosa, L. E. C., Castro, J. D. B., Feitosa, R. Q., ... & Tommaselli, A. M. G. (2020). Comparative performance of convolutional neural network, weighted and conventional support vector machine and random forest for classifying tree species using hyperspectral and photogrammetric data. GIScience & Remote Sensing, 57(3), 369-394.

Stora Enso (2020). Drone pilots scanned thousands of trees: insect damages identified from the air. Available: https://www.storaenso.com/en/newsroom/news/2020/6/drone-pilots-scanned-thousands-of-trees-insect-damages-identified-from-the-air. Accessed: 28.2.2021.

Stöcker, C., Bennett, R., Nex, F., Gerke, M., & Zevenbergen, J. (2017). Review of the current state of UAV regulations. Remote sensing, 9(5), 459.

Suomalainen, J., Oliveira, R. A., Hakala, T., Koivumäki, N., Markelin, L., Näsi, R., & Honkavaara, E. (2021). Direct reflectance transformation methodology for

drone-based hyperspectral imaging. Remote Sensing of Environment, 266, 112691.

Suratno, A., Seielstad, C., & Queen, L. (2009). Tree species identification in mixed coniferous forest using airborne laser scanning. ISPRS Journal of Photogrammetry and Remote Sensing, 64(6), 683-693.

Swain, K. C., Thomson, S. J., & Jayasuriya, H. P. (2010). Adoption of an unmanned helicopter for low-altitude remote sensing to estimate yield and total biomass of a rice crop. Transactions of the ASABE, 53(1), 21-27.

Thenkabail, P. S. (2003). Biophysical and yield information for precision farming from near-real-time and historical Landsat TM images. International Journal of Remote Sensing, 24(14), 2879-2904.

Tilly, N., Hoffmeister, D., Cao, Q., Huang, S., Lenz-Wiedemann, V., Miao, Y., & Bareth, G. (2014). Multitemporal crop surface models: accurate plant height measurement and biomass estimation with terrestrial laser scanning in paddy rice. Journal of Applied Remote Sensing, 8(1), 083671.

Torresan, C., Berton, A., Carotenuto, F., Di Gennaro, S. F., Gioli, B., Matese, A., ... & Wallace, L. (2017). Forestry applications of UAVs in Europe: A review. International Journal of Remote Sensing, 38(8-10), 2427-2447.

Toth, C., & Jóźków, G. (2016). Remote sensing platforms and sensors: A survey. ISPRS Journal of Photogrammetry and Remote Sensing, 115, 22-36.

Toth, D., Maitah, M., Maitah, K., & Jarolínová, V. (2020). The impacts of calamity logging on the development of spruce wood prices in czech forestry. Forests, 11(3), 283.

Tremblay, N., Wang, Z., Ma, B. L., Belec, C., & Vigneault, P. (2009). A comparison of crop data measured by two commercial sensors for variable-rate nitrogen application. Precision Agriculture, 10(2), 145-161.

Tsouros, D. C., Bibi, S., & Sarigiannidis, P. G. (2019). A review on UAV-based applications for precision agriculture. Information, 10(11), 349.

Tu, Y. H., Phinn, S., Johansen, K., Robson, A., & Wu, D. (2020). Optimising drone flight planning for measuring horticultural tree crop structure. ISPRS Journal of Photogrammetry and Remote Sensing, 160, 83-96.

Tuominen, S., Näsi, R., Honkavaara, E., Balazs, A., Hakala, T., Viljanen, N., ... & Reinikainen, J. (2017). Tree species recognition in species rich area using UAV-borne hyperspectral imagery and stereo-photogrammetric point cloud. International archives of the photogrammetry, remote sensing and spatial information sciences; Volume XLII-3/W3.

Ustin, S. L., & Gamon, J. A. (2010). Remote sensing of plant functional types. New Phytologist, 186(4), 795-816.

Van Cleemput, E., Vanierschot, L., Fernández-Castilla, B., Honnay, O., & Somers, B. (2018). The functional characterization of grass-and shrubland ecosystems using hyperspectral remote sensing: trends, accuracy and moderating variables. Remote Sensing of Environment, 209, 747-763.

Van Soest, P. J. (1994). Nutritional ecology of the ruminant. Cornell university press.

Varma, S., & Simon, R. (2006). Bias in error estimation when using cross-validation for model selection. BMC bioinformatics, 7(1), 1-8.

Verger, A., Baret, F., & Camacho, F. (2011). Optimal modalities for radiative transfer-neural network estimation of canopy biophysical characteristics: Evaluation over an agricultural area with CHRIS/PROBA observations. Remote Sensing of Environment, 115(2), 415-426.

Verrelst, J., Malenovský, Z., Van der Tol, C., Camps-Valls, G., Gastellu-Etchegorry, J. P., Lewis, P., ... & Moreno, J. (2019). Quantifying vegetation biophysical variables from imaging spectroscopy data: a review on retrieval methods. Surveys in Geophysics, 40(3), 589-629.

Vihervaara, P., Auvinen, A. P., Mononen, L., Törmä, M., Ahlroth, P., Anttila, S., ... & Virkkala, R. (2017). How essential biodiversity variables and remote sensing can

help national biodiversity monitoring. Global Ecology and Conservation, 10, 43-59.

Viljanen, N., Honkavaara, E., Näsi, R., Hakala, T., Niemeläinen, O., & Kaivosoja, J. (2018). A novel machine learning method for estimating biomass of grass swards using a photogrammetric canopy height model, images and vegetation indices captured by a drone. Agriculture, 8(5), 70.

Walsh, S. J. (1980). Coniferous tree species mapping using Landsat data. Remote Sensing of Environment, 9(1), 11-26.

Walthall, C. L., Norman, J. M., Welles, J. M., Campbell, G., & Blad, B. L. (1985). Simple equation to approximate the bidirectional reflectance from vegetative canopies and bare soil surfaces. Applied Optics, 24(3), 383-387.

Weiss, M., Jacob, F., & Duveiller, G. (2020). Remote sensing for agricultural applications: A meta-review. Remote Sensing of Environment, 236, 111402.

Wermelinger, B. (2004). Ecology and management of the spruce bark beetle Ips typographus—a review of recent research. Forest ecology and management, 202(1-3), 67-82.

White, J. C., Coops, N. C., Wulder, M. A., Vastaranta, M., Hilker, T., & Tompalski, P. (2016). Remote sensing technologies for enhancing forest inventories: A review. Canadian Journal of Remote Sensing, 42(5), 619-641.

Wijesingha, J., Moeckel, T., Hensgen, F., & Wachendorf, M. (2019). Evaluation of 3D point cloud-based models for the prediction of grassland biomass. International Journal of Applied Earth Observation and Geoinformation, 78, 352-359.

Wijesingha, J., Astor, T., Schulze-Brüninghoff, D., Wengert, M., & Wachendorf, M. (2020). Predicting forage quality of grasslands using UAV-borne imaging spectroscopy. Remote Sensing, 12(1), 126.

Wu, C. (2013). Towards linear-time incremental structure from motion. In 2013 International Conference on 3D Vision-3DV 2013 (pp. 127-134). IEEE.

Wulder, M. A., Dymond, C. C., White, J. C., Leckie, D. G., & Carroll, A. L. (2006). Surveying mountain pine beetle damage of forests: A review of remote sensing opportunities. Forest Ecology and management, 221(1-3), 27-41.

Yue, J., Yang, G., Li, C., Li, Z., Wang, Y., Feng, H., & Xu, B. (2017). Estimation of winter wheat above-ground biomass using unmanned aerial vehicle-based snapshot hyperspectral sensor and crop height improved models. Remote Sensing, 9(7), 708.

Zarco-Tejada, P. J., González-Dugo, V., & Berni, J. A. (2012). Fluorescence, temperature and narrow-band indices acquired from a UAV platform for water stress detection using a micro-hyperspectral imager and a thermal camera. Remote sensing of environment, 117, 322-337.

Zarco-Tejada, P. J., Hornero, A., Hernández-Clemente, R., & Beck, P. S. A. (2018). Understanding the temporal dimension of the red-edge spectral region for forest decline detection using high-resolution hyperspectral and Sentinel-2a imagery. ISPRS Journal of Photogrammetry and Remote Sensing, 137, 134-148.

Zhang, N., Zhang, X., Yang, G., Zhu, C., Huo, L., & Feng, H. (2018). Assessment of defoliation during the Dendrolimus tabulaeformis Tsai et Liu disaster outbreak using UAV-based hyperspectral images. Remote Sensing of Environment, 217, 323-339.

Suomen Geodeettisen laitoksen julkaisut:
Veröffentlichungen des Finnischen Geodätischen Institutes:
Publications of the Finnish Geodetic Institute:

1. Y. VÄISÄLÄ: Tafeln für geodätische Berechnungen nach den Erddimensionen von Hayford. Helsinki 1923. 30 S.
2. Y. VÄISÄLÄ: Die Anwendung der Lichtinterferenz zu Längenmessungen auf grösseren Distanzen. Helsinki 1923. 22 S.
3. ILMARI BONSDORFF, Y. LEINBERG, W. HEISKANEN: Die Beobachtungsergebnisse der südfinnischen Triangulation in den Jahren 1920-1923. Helsinki 1924. 235 S.
4. W. HEISKANEN: Untersuchungen über Schwerkraft und Isostasie. Helsinki 1924. 96 S. 1 Karte.
5. W. HEISKANEN: Schwerkraft und isostatische Kompensation in Norwegen. Helsinki 1926. 33 S. 1 Karte.
6. W. HEISKANEN: Die Erddimensionen nach den europäischen Gradmessungen. Helsinki 1926. 26 S.
7. ILMARI BONSDORFF, V.R. ÖLANDER, Y. LEINBERG: Die Beobachtungsergebnisse der südfinnischen Triangulation in den Jahren 1924-1926. Helsinki 1927. 164 S. 1 Karte.
8. V.R. ÖLANDER: Ausgleichung einer Dreieckskette mit Laplaceschen Punkten. Helsinki 1927. 49 S. 1 Karte.
9. U. PESONEN: Relative Bestimmungen der Schwerkraft auf den Dreieckspunkten der südfinnischen Triangulation in den Jahren 1924-1925. Helsinki 1927. 129 S.
10. ILMARI BONSDORFF: Das Theorem von Clairaut und die Massenverteilung im Erdinnern. Helsinki 1929. 10 S.
11. ILMARI BONSDORFF, V.R. ÖLANDER, W. HEISKANEN, U. PESONEN: Die Beobachtungsergebnisse der Triangulationen in den Jahren 1926-1928. Helsinki 1929. 139 S. 1 Karte.
12. W. HEISKANEN: Über die Elliptizität des Erdäquators. Helsinki 1929. 18 S.
13. U. PESONEN: Relative Bestimmungen der Schwerkraft in Finnland in den Jahren 1926-1929. Helsinki 1930. 168 S. 1 Karte.
14. Y. VÄISÄLÄ: Anwendung der Lichtinterferenz bei Basismessungen. Helsinki 1930. 47 S.
15. M. FRANSSILA: Der Einfluss der den Pendel umgebenden Luft auf die Schwingungszeit beim v. Sterneckschen Pendelapparat. Helsinki 1931. 23 S.
16. Y. LEINBERG: Ergebnisse der astronomischen Ortsbestimmungen auf den finnischen Dreieckspunkten. Helsinki 1931. 162 S.
17. V.R. ÖLANDER: Über die Beziehung zwischen Lotabweichungen und Schwereanomalien sowie über das Lotabweichungssystem in Süd-Finnland. Helsinki 1931. 23 S.
18. PENTTI KALAJA, UUNO PESONEN, V.R. ÖLANDER, Y. LEINBERG: Beobachtungsergebnisse. Helsinki 1933. 240 S. 1 Karte.
19. R.A. HIRVONEN: The continental undulations of the geoid. Helsinki 1934. 89 pages. 1 map.
20. ILMARI BONSDORFF: Die Länge der Versuchsbasis von Helsinki und Längenveränderungen der Invardrähte 634-637. Helsinki 1934. 41 S.
21. V.R. ÖLANDER: Zwei Ausgleichungen des grossen südfinnischen Dreieckskranzes. Helsinki 1935. 66 S. 1 Karte.
22. U. PESONEN, V.R. ÖLANDER: Beobachtungsergebnisse. Winkelmessungen in den Jahren 1932-1935. Helsinki 1936. 148 S. 1 Karte.
23. R.A. HIRVONEN: Relative Bestimmungen der Schwerkraft in Finnland in den Jahren 1931, 1933 und 1935. Helsinki 1937. 151 S.
24. R.A. HIRVONEN: Bestimmung des Schwereunterschiedes Helsinki-Potsdam im Jahre 1935 und Katalog der finnischen Schwerestationen. Helsinki 1937. 36 S. 1 Karte.
25. T.J. KUKKAMÄKI: Über die nivellitische Refraktion. Helsinki 1938. 48 S.
26. Finnisches Geodätisches Institut 1918-1938. Helsinki 1939. 126 S. 2 Karten.
27. T.J. KUKKAMÄKI: Formeln und Tabellen zur Berechnung der nivellitischen Refraktion. Helsinki 1939. 18 S.
28. T.J. KUKKAMÄKI: Verbesserung der horizontalen Winkelmessungen wegen der Seitenrefraktion. Helsinki 1939. 18 S.
29. ILMARI BONSDORFF: Ergebnisse der astronomischen Ortsbestimmungen im Jahre 1933. Helsinki 1939. 47 S.
30. T. HONKASALO: Relative Bestimmungen der Schwerkraft in Finnland im Jahre 1937. Helsinki 1941. 78 S.
31. PENTTI KALAJA: Die Grundlinienmessungen des Geodätischen Institutes in den Jahren 1933-1939 nebst Untersuchungen über die Verwendung der Invardrähte. Helsinki 1942. 149 S.
32. U. PESONEN, V.R. ÖLANDER: Beobachtungsergebnisse. Winkelmessungen in den Jahren 1936-1940. Helsinki 1942. 165 S. 1 Karte.
33. PENTTI KALAJA: Astronomische Ortsbestimmungen in den Jahren 1935-1938. Helsinki 1944. 142 S.
34. V.R. ÖLANDER: Astronomische Azimutbestimmungen auf den Dreieckspunkten in den Jahren 1932-1938; Lotabweichungen und Geoidhöhen. Helsinki 1944. 107 S. 1 Karte.
35. U. PESONEN: Beobachtungsergebnisse. Winkelmessungen in den Jahren 1940-1947. Helsinki 1948. 165 S. 1 Karte.
36. Professori Ilmari Bonsdorffille hänen 70-vuotispäivänään omistettu juhlajulkaisu. Publication dedicated to Ilmari Bonsdorff on the occasion of his 70th anniversary. Helsinki 1949. 262 pages. 13 maps.
37. TAUNO HONKASALO: Measuring of the 864 m-long Nummela standard base line with the Väisälä light interference comparator and some investigations into invar wires. Helsinki 1950. 88 pages.
38. V.R. ÖLANDER: On the geoid in the Baltic area and the orientation of the Baltic Ring. Helsinki 1950. 26 pages.
39. W. HEISKANEN: On the world geodetic system. Helsinki 1951. 25 pages.
40. R.A. HIRVONEN: The motions of Moon and Sun at the solar eclipse of 1947 May 20th. Helsinki 1951. 36 pages.
41. PENTTI KALAJA: Catalogue of star pairs for northern latitudes from 55° to 70° for astronomic determination of latitudes by the Horrebow-Talcott method. Helsinki 1952. 191 pages.
42. ERKKI KÄÄRIÄINEN: On the recent uplift of the Earth's crust in Finland. Helsinki 1953. 106 pages. 1 map.
43. PENTTI KALAJA: Astronomische Ortsbestimmungen in den Jahren 1946-1948. Helsinki 1953. 146 S.
44. T.J. KUKKAMÄKI, R.A. HIRVONEN: The Finnish solar eclipse expeditions to the Gold Coast and Brazil 1947. Helsinki 1954. 71 pages.
45. JORMA KORHONEN: Einige Untersuchungen über die Einwirkung der Abrundungsfehler bei Gross-Ausgleichungen. Neu-Ausgleichung des südfinnischen Dreieckskranzes. Helsinki 1954. 138 S. 3 Karten.

46. Professori Weikko A. Heiskaselle hänen 60-vuotispäivänään omistettu juhlajulkaisu. Publication dedicated to Weikko A. Heiskanen on the occasion of his 60th anniversary. Helsinki 1955. 214 pages.
47. Y. VÄISÄLÄ: Bemerkungen zur Methode der Basismessung mit Hilfe der Lichtinterferenz. Helsinki 1955. 12 S.
48. U. PESONEN, TAUNO HONKASALO: Beobachtungsergebnisse der finnischen Triangulationen in den Jahren 1947-1952. Helsinki 1957. 91 S.
49. PENTTI KALAJA: Die Zeiten von Sonnenschein, Dämmerung und Dunkelheit in verschiedenen Breiten. Helsinki 1958. 63 S.
50. V.R. ÖLANDER: Astronomische Azimutbestimmungen auf den Dreieckspunkten in den Jahren 1938-1952. Helsinki 1958. 90 S. 1 Karte.
51. JORMA KORHONEN, V.R. ÖLANDER, ERKKI HYTÖNEN: The results of the base extension nets of the Finnish primary triangulation. Helsinki 1959. 57 pages. 5 appendices. 1 map.
52. V.R. ÖLANDER: Vergleichende Azimutbeobachtungen mit vier Instrumenten. Helsinki 1960. 48 pages.
53. Y. VÄISÄLÄ, L. OTERMA: Anwendung der astronomischen Triangulationsmethode. Helsinki 1960. 18 S.
54. V.R. ÖLANDER: Astronomical azimuth determinations on trigonometrical stations in the years 1955-1959. Helsinki 1961. 15 pages.
55. TAUNO HONKASALO: Gravity survey of Finland in years 1945-1960. Helsinki 1962. 35 pages. 3 maps.
56. ERKKI HYTÖNEN: Beobachtungsergebnisse der finnischen Triangulationen in den Jahren 1953-1962. Helsinki 1963. 59 S.
57. ERKKI KÄÄRIÄINEN: Suomen toisen tarkkavaaituksen kiintopisteluettelo I. Bench mark list I of the Second Levelling of Finland. Helsinki 1963. 164 pages. 2 maps.
58. ERKKI HYTÖNEN: Beobachtungsergebnisse der finnischen Triangulationen in den Jahren 1961-1962. Helsinki 1963. 32 S.
59. AIMO KIVINIEMI: The first order gravity net of Finland. Helsinki 1964. 45 pages.
60. V.R. ÖLANDER: General list of astronomical azimuths observed in 1920-1959 in the primary triangulation net. Helsinki 1965. 47 pages. 1 map.
61. ERKKI KÄÄRIÄINEN: The second levelling of Finland in 1935-1955. Helsinki 1966. 313 pages. 1 map.
62. JORMA KORHONEN: Horizontal angles in the first order triangulation of Finland in 1920-1962. Helsinki 1966. 112 pages. 1 map.
63. ERKKI HYTÖNEN: Measuring of the refraction in the Second Levelling of Finland. Helsinki 1967. 18 pages.
64. JORMA KORHONEN: Coordinates of the stations in the first order triangulation of Finland. Helsinki 1967. 42 pages. 1 map.
65. Geodeettinen laitos - The Finnish Geodetic Institute 1918-1968. Helsinki 1969. 147 pages. 4 maps.
66. JUHANI KAKKURI: Errors in the reduction of photographic plates for the stellar triangulation. Helsinki 1969. 14 pages.
67. PENTTI KALAJA, V.R. ÖLANDER: Astronomical determinations of latitude and longitude in 1949-1958. Helsinki 1970. 242 pages. 1 map.
68. ERKKI KÄÄRIÄINEN: Astronomical determinations of latitude and longitude in 1954-1960. Helsinki 1970. 95 pages. 1 map.
69. AIMO KIVINIEMI: Niinisalo calibration base line. Helsinki 1970. 36 pages. 1 sketch appendix.
70. TEUVO PARM: Zero-corrections for tellurometers of the Finnish Geodetic Institute. Helsinki 1970. 18 pages.
71. ERKKI KÄÄRIÄINEN: Astronomical determinations of latitude and longitude in 1961-1966. Helsinki 1971. 102 pages. 1 map.
72. JUHANI KAKKURI: Plate reduction for the stellar triangulation. Helsinki 1971. 38 pages.
73. V.R. ÖLANDER: Reduction of astronomical latitudes and longitudes 1922-1948 into FK4 and CIO systems. Helsinki 1972. 40 pages.
74. JUHANI KAKKURI AND KALEVI KALLIOMÄKI: Photoelectric time micrometer. Helsinki 1972. 53 pages.
75. ERKKI HYTÖNEN: Absolute gravity measurement with long wire pendulum. Helsinki 1972. 142 pages.
76. JUHANI KAKKURI: Stellar triangulation with balloon-borne beacons. Helsinki 1973. 48 pages.
77. JUSSI KÄÄRIÄINEN: Beobachtungsergebnisse der finnischen Winkelmessungen in den Jahren 1969-70. Helsinki 1974. 40 S.
78. AIMO KIVINIEMI: High precision measurements for studying the secular variation in gravity in Finland. Helsinki 1974. 64 pages.
79. TEUVO PARM: High precision traverse of Finland. Helsinki 1976. 64 pages.
80. R.A. HIRVONEN: Precise computation of the precession. Helsinki 1976. 25 pages.
81. MATTI OLLIKAINEN: Astronomical determinations of latitude and longitude in 1972-1975. Helsinki 1977. 90 pages. 1 map.
82. JUHANI KAKKURI AND JUSSI KÄÄRIÄINEN: The Second Levelling of Finland for the Aland archipelago. Helsinki 1977. 55 pages.
83. MIKKO TAKALO: Suomen Toisen tarkkavaaituksen kiintopisteluettelo II. Bench mark list II of the Second Levelling of Finland. Helsinki 1977. 150 sivua.
84. MATTI OLLIKAINEN: Astronomical azimuth determinations on triangulation stations in 1962-1970. Helsinki 1977. 47 pages. 1 map.
85. MARKKU HEIKKINEN: On the tide-generating forces. Helsinki 1978. 150 pages.
86. PEKKA LEHMUSKOSKI AND JAAKKO MÄKINEN: Gravity measurements on the ice of Bothnian Bay. Helsinki 1978. 27 pages.
87. T.J. KUKKAMÄKI: Väisälä interference comparator. Helsinki 1978. 49 pages.
88. JUSSI KÄÄRIÄINEN: Observing the Earth Tides with a long water-tube tiltmeter. Helsinki 1979. 74 pages.
89. Publication dedicated to T.J. Kukkamäki on the occasion of his 70th anniversary. Helsinki 1979. 184 pages.
90. B. DUCARME AND J. KÄÄRIÄINEN: The Finnish Tidal Gravity Registrations in Fennoscandia. Helsinki 1980. 43 pages.
91. AIMO KIVINIEMI: Gravity measurements in 1961-1978 and the results of the gravity survey of Finland in 1945-1978. Helsinki 1980. 18 pages. 3 maps.
92. LIISI OTERMA: Programme de latitude du tube zénithal visuel de l'observatoire Turku-Tuorla systéme amélioré de 1976. Helsinki 1981. 18 pages.
93. JUHANI KAKKURI, AIMO KIVINIEMI AND RAIMO KONTTINEN: Contributions from the Finnish Geodetic Institute to the Tectonic Plate Motion Studies in the Area between the Pamirs and Tien-Shan Mountains. Helsinki 1981. 34 pages.
94. JUSSI KÄÄRIÄINEN: Measurement of the Ekeberg baseline with invar wires. Helsinki 1981. 17 pages.
95. MATTI OLLIKAINEN: Astronomical determinations of latitude and longitude in 1976-1980. Helsinki 1982. 90 pages. 1 map.
96. RAIMO KONTTINEN: Observation results. Angle measurements in 1977-1978. Helsinki 1982. 29 pages.

97. G.P. ARNAUTOV, YE N. KALISH, A. KIVINIEMI, YU F. STUS, V.G. TARASIUK, S.N. SCHEGLOV: Determination of absolute gravity values in Finland using laser ballistic gravimeter. Helsinki 1982. 18 pages.

98. LEENA MIKKOLA (EDITOR): Mean height map of Finland. Helsinki 1983. 3 pages. 1 map.

99. MIKKO TAKALO AND JAAKKO MÄKINEN: The Second Levelling of Finland for Lapland. Helsinki 1983. 144 pages.

100. JUSSI KÄÄRIÄINEN: Baseline Measurements with invar wires in Finland 1958-1970. Helsinki 1984. 78 pages.

101. RAIMO KONTTINEN: Plate motion studies in Central Asia. Helsinki 1985. 31 pages.

102. RAIMO KONTTINEN: Observation results. Angle measurements in 1979-1983. Helsinki 1985. 30 pages.

103. J. KAKKURI, T.J. KUKKAMÄKI, J.-J. LEVALLOIS ET H. MORITZ: Le 250ᵉ anniversaire de la mesure de l'arc du meridien en Laponie. Helsinki 1986. 60 pages.

104. G. ASCH, T. JAHR, G. JENTZSCH, A. KIVINIEMI AND J. KÄÄRIÄINEN: Measurements of Gravity Tides along the "Blue Road Geotraverse" in Fennoscandia. Helsinki 1987. 57 pages.

105. JUSSI KÄÄRIÄINEN, RAIMO KONTTINEN, LU QIANKUN AND DU ZONG YU: The Chang Yang Standard Baseline. Helsinki 1986. 36 pages.

106. E.W. GRAFAREND, H. KREMERS, J. KAKKURI AND M. VERMEER: Adjusting the SW Finland Triangular Network with the TAGNET 3-D operational geodesy software. Helsinki 1987. 60 pages.

107. MATTI OLLIKAINEN: Astronomical determinations of latitude and longitude in 1981-1983. Helsinki 1988. 37 pages.

108. MARKKU POUTANEN: Observation results. Angle measurements in 1967-1973. Helsinki 1988. 35 pages.

109. JUSSI KÄÄRIÄINEN, RAIMO KONTTINEN AND ZSUZSANNA NÉMETH: The Gödöllö Standard Baseline. Helsinki 1988. 66 pages.

110. JUSSI KÄÄRIÄINEN AND HANNU RUOTSALAINEN: Tilt measurements in the underground laboratory Lohja 2, Finland, in 1977-1987. Helsinki 1989. 37 pages.

111. MIKKO TAKALO: Lisäyksiä ja korjauksia Suomen tarkkavaaitusten linjastoon 1977-1989. Helsinki 1991. 98 sivua.

112. RAIMO KONTTINEN: Observation results. Angle measurements in the Pudasjärvi loop in 1973-1976. Helsinki 1991. 42 pages.

113. RAIMO KONTTINEN, JORMA JOKELA AND LI QUAN: The remeasurement of the Chang Yang Standard Baseline. Helsinki 1991. 40 pages.

114. JUSSI KÄÄRIÄINEN, RAIMO KONTTINEN AND MARKKU POUTANEN: Interference measurements of the Nummela Standard Baseline in 1977, 1983, 1984 and 1991. Helsinki 1992. 78 pages.

115. JUHANI KAKKURI (EDITOR): Geodesy and geophysics. Helsinki 1993. 200 pages.

116. JAAKKO MÄKINEN, HEIKKI VIRTANEN, QIU QI-XIAN AND GU LIANG-RONG: The Sino-Finnish absolute gravity campaign in 1990. Helsinki 1993. 49 pages.

117. RAIMO KONTTINEN: Observation results. Geodimeter observations in 1971-72, 1974-80 and 1984-85. Helsinki 1994. 58 pages.

118. RAIMO KONTTINEN: Observation results. Angle measurements in 1964-65, 1971, 1984 and 1986-87. Helsinki 1994. 67 pages.

119. JORMA JOKELA: The 1993 adjustment of the Finnish First-Order Terrestrial Triangulation. Helsinki 1994. 137 pages.

120. MARKKU POUTANEN (EDITOR): Interference measurements of the Taoyuan Standard Baseline. Helsinki 1995. 35 pages.

121. JORMA JOKELA: Interference measurements of the Chang Yang Standard Baseline in 1994. Kirkkonummi 1996. 32 pages.

122. OLLI JAAKKOLA: Quality and automatic generalization of land cover data. Kirkkonummi 1996. 39 pages.

123. MATTI OLLIKAINEN: Determination of orthometric heights using GPS levelling. Kirkkonummi 1997. 143 pages.

124. TIINA KILPELÄINEN: Multiple Representation and Generalization of Geo-Databases for Topographic Maps. Kirkkonummi 1997. 229 pages.

125. JUSSI KÄÄRIÄINEN AND JAAKKO MÄKINEN: The 1979-1996 gravity survey and the results of the gravity survey of Finland 1945-1996. Kirkkonummi 1997. 24 pages. 1 map.

126. ZHITONG WANG: Geoid and crustal structure in Fennoscandia. Kirkkonummi 1998. 118 pages.

127. JORMA JOKELA AND MARKKU POUTANEN: The Väisälä baselines in Finland. Kirkkonummi 1998. 61 pages.

128. MARKKU POUTANEN: Sea surface topography and vertical datums using space geodetic techniques. Kirkkonummi 2000. 158 pages

129. MATTI OLLIKAINEN, HANNU KOIVULA AND MARKKU POUTANEN: The Densification of the EUREF Network in Finland. Kirkkonummi 2000. 61 pages.

130. JORMA JOKELA, MARKKU POUTANEN, ZHAO JINGZHAN, PEI WEILI, HU ZHENYUAN AND ZHANG SHENGSHU: The Chengdu Standard Baseline. Kirkkonummi 2000. 46 pages.

131. JORMA JOKELA, MARKKU POUTANEN, ZSUZSANNA NÉMETH AND GÁBOR VIRÁG: Remeasurement of the Gödöllö Standard Baseline. Kirkkonummi 2001. 37 pages.

132. ANDRES RÜDJA: Geodetic Datums, Reference Systems and Geodetic Networks in Estonia. Kirkkonummi 2004. 311 pages.

133. HEIKKI VIRTANEN: Studies of Earth Dynamics with the Superconducting Gravimeter. Kirkkonummi 2006. 130 pages.

134. JUHA OKSANEN: Digital elevation model error in terrain analysis. Kirkkonummi 2006. 142 pages. 2 maps.

135. MATTI OLLIKAINEN: The EUVN-DA GPS campaign in Finland. Kirkkonummi 2006. 42 pages.

136. ANNU-MAARIA NIVALA: Usability perspectives for the design of interactive maps. Kirkkonummi 2007. 157 pages.

137. XIAOWEI YU: Methods and techniques for forest change detection and growth estimation using airborne laser scanning data. Kirkkonummi 2007. 132 pages.

138. LASSI LEHTO: Real-time content transformations in a WEB service-based delivery architecture for geographic information. Kirkkonummi 2007. 150 pages.

139. PEKKA LEHMUSKOSKI, VEIKKO SAARANEN, MIKKO TAKALO AND PAAVO ROUHIAINEN: Suomen Kolmannen tarkkavaaituksen kiintopisteluettelo. Bench Mark List of the Third Levelling of Finland. Kirkkonummi 2008. 220 pages.

140. EIJA HONKAVAARA: Calibrating digital photogrammetric airborne imaging systems using a test field. Kirkkonummi 2008. 139 pages.

141. MARKKU POUTANEN, EERO AHOKAS, YUWEI CHEN, JUHA OKSANEN, MARITA PORTIN, SARI RUUHELA, HELI SUURMÄKI (EDITORS): Geodeettinen laitos – Geodetiska Institutet – Finnish Geodetic Institute 1918–2008. Kirkkonummi 2008. 173 pages.

142. MIKA KARJALAINEN: Multidimensional SAR Satellite Images – a Mapping Perspective. Kirkkonummi 2010. 132 pages.
143. MAARIA NORDMAN: Improving GPS time series for geodynamic studies. Kirkkonummi 2010. 116 pages.
144. JORMA JOKELA AND PASI HÄKLI: Interference measurements of the Nummela Standard Baseline in 2005 and 2007. Kirkkonummi 2010. 85 pages.
145. EETU PUTTONEN: Tree Species Classification with Multiple Source Remote Sensing Data. Kirkkonummi 2012. 162 pages.
146. JUHA SUOMALAINEN: Empirical Studies on Multiangular, Hyperspectral, and Polarimetric Reflectance of Natural Surfaces. Kirkkonummi 2012. 144 pages.
147. LEENA MATIKAINEN: Object-based interpretation methods for mapping built-up areas. Kirkkonummi 2012. 210 pages.
148. LAURI MARKELIN: Radiometric calibration, validation and correction of multispectral photogrammetric imagery. Kirkkonummi 2013. 160 pages.
149. XINLIAN LIANG: Feasibility of Terrestrial Laser Scanning for Plotwise Forest Inventories. Kirkkonummi 2013. 150 pages.
150. EERO AHOKAS: Aspects of accuracy, scanning angle optimization, and intensity calibration related to nationwide laser scanning. Kirkkonummi 2013. 124 pages.
151. LAURA RUOTSALAINEN: Vision-Aided Pedestrian Navigation for Challenging GNSS Environments. Kirkkonummi 2013. 180 pages.
152. HARRI KAARTINEN: Benchmarking of airborne laser scanning based feature extraction methods and mobile laser scanning system performance based on high-quality test fields. Kirkkonummi 2013. 346 pages.
153. ANTERO KUKKO: Mobile Laser Scanning – System development, performance and applications. Kirkkonummi 2013. 247 pages.
154. JORMA JOKELA: Length in Geodesy – On Metrological Traceability of a Geospatial Measurand. Kirkkonummi 2014. 240 pages.
155. PYRY KETTUNEN: Analysing landmarks in nature and elements of geospatial images to support wayfinding. Kirkkonummi 2014. 281 pages.
156. MARI LAAKSO: Improving Accessibility for Pedestrians with Geographic Information. Kirkkonummi 2014. 129 pages.

The name of the series has changed the 1st of January in 2015.

FGI Publications:

157. LINGLI ZHU: A pipeline of 3D scene reconstruction from point clouds. Kirkkonummi 2015. 208 pages.
158. ROBERT E. GUINNESS: Context Awareness for Navigation Applications. Kirkkonummi 2015. 244 pages.
159. HANNU KOIVULA: Finnish permanent GNSS network FinnRef. Helsinki 2019. 141 pages.
160. PAULIINA KRIGSHOLM: Towards a future cadastral system: An exploration of the Finnish case. Helsinki 2020. 110 pages.
161. VEIKKO SAARANEN, PEKKA LEHMUSKOSKI, MIKKO TAKALO, PAAVO ROUHIAINEN: The Third Precise Levelling of Finland. Helsinki 2021. 307 pages.
162. JUHANI KAKKURI: Muistelmia geodeettien maailmasta = Memoirs From the World of Geodesy. Kirkkonummi 2021. 125 pages.
163. MIRJAM BILKER-KOIVULA: Geoid and postglacial rebound related gravity change in Finland. Helsinki 2021. 84 pages.
164. MATTI LEHTOMÄKI: Detection and Recognition of Objects from Mobile Laser Scanning Point Clouds: Case studies in a road environment and power line corridor. Helsinki 2021. 89 pages.
165. ROOPE NÄSI: Drone-based spectral and 3D remote sensing applications for forestry and agriculture. Helsinki 2021.78 pages.